NASA CONTRACTOR REPORT

NASA CR-

NASA CR-803

DISCRETE-ELEMENT METHODS FOR THE PLASTIC ANALYSIS OF STRUCTURES

by G. Isakson, H. Armen, Jr., and A. Pifko

Prepared by
GRUMMAN AIRCRAFT ENGINEERING CORPORATION
Bethpage, N. Y.
for Langley Research Center

NATIONAL AERONAUTICS AND SPACE ADMINISTRATION • WASHINGTON, D. C. • OCTOBER 1967

NASA CR-803

DISCRETE-ELEMENT METHODS FOR THE PLASTIC ANALYSIS OF STRUCTURES

By G. Isakson, H. Armen, Jr., and A. Pifko

Issued by Originator as Report RE-287

Prepared under Contract No. NAS 1-5040 by
GRUMMAN AIRCRAFT ENGINEERING CORPORATION
Bethpage, N.Y.

for Langley Research Center

NATIONAL AERONAUTICS AND SPACE ADMINISTRATION

For sale by the Clearinghouse for Federal Scientific and Technical Information
Springfield, Virginia 22151 – CFSTI price $3.00

FOREWORD

This report was prepared by the Grumman Aircraft Engineering Corporation, Bethpage, New York, under Contract NAS 1-5040, entitled, "A Research Study for the Development of a Digital Method of Analysis of Supersonic Transport Aircraft Structures in the Plastic Range." The work was performed by the Research Department of Grumman Aircraft Engineering Corporation, with support from the Structural Mechanics Section of Engineering.

The authors wish to acknowledge the valuable contributions of the following individuals: Mr. Paul W. Hornack and Miss Eloise M. Turner for digital computer programming, Mr. Francis J. Nolan for consultation on computing problems and for preparation of a special eigenvalue subroutine, Dr. Warner Lansing and Mr. Philip W. Mason of the Structural Mechanics Section for valuable counsel concerning discrete-element methods, Messrs. William R. Jensen, William E. Falby, Henry H. Loshigian, and Theodore Balderes of the Structural Mechanics Section for conducting analyses which generated the linear elastic properties of the sample structures, and, in the case of Mr. Balderes, for helpful advice concerning the plate buckling problem, Mrs. Ellen Konz for technical aid and typing, and Miss Catherine O'Regan for drafting services.

The present volume is devoted to a presentation of the methods that have been developed and of results obtained in the application of these methods to some sample structures. The digital computer programs that have been devised for implementation of these methods are presented in a separate report, NASA CR- 66364, "Computer Programs for the Plastic Analysis of Structures using Discrete-Element Methods," by H. Armen, Jr. and A. Pifko.

ABSTRACT

This study deals with the extension of finite-element methods to provide analytical means for determining the failure loads of aeronautical structures. Two areas are considered as related to predicting failure loads, inelastic stress analysis in the presence of load cycling and plastic buckling of the bifurcation type.

Finite element inelastic stress analysis methods are extended to take into account the Bauschinger effect for biaxial stress states using a plasticity theory based on Ziegler's modification to Prager's kinematic hardening theory. The application of this methodology is made to several structures representative of aeronautical construction, including a notched plate, a shear lag specimen and a swept wing. Good correlation is obtained between analytical and experimental results for the strains at the root of the notched plate subjected to load cycling in the plastic range.

Finite element buckling methods are also extended to consider plastic buckling using Stowell's formulation for implementing a deformation plasticity theory into the buckling theory. Sample calculations are carried out for the plastic buckling of a flat plate with various geometries and edge conditions.

DISCRETE-ELEMENT METHODS FOR THE PLASTIC ANALYSIS OF STRUCTURES

By G. Isakson, H. Armen, Jr. and A. Pifko

Grumman Research Department

SUMMARY

The present report is concerned with the development of discrete-element methods for the plastic analysis of complex, highly redundant structures, such as aircraft structures. These methods fall into two categories, those applicable to stable structures and useful in the prediction of failure associated with excessive plastic straining, and those applicable to the determination of buckling loads.

In the development of methods falling into the former category, particular attention is given to the case of intermittently applied loads causing successive excursions into the plastic range, including reversals of stress into the plastic range. In order to accommodate this case and to take the Bauschinger effect into account, the plasticity theory selected for use is the kinematic hardening theory of Prager.

The methods in this category are based on the application of two matrix relations coming out of a linear elastic analysis of the structure and involving the concept of initial strain. Plastic effects are introduced by interpreting plastic strains as initial strains. Solutions are effected by the application of incremental procedures of two types. In one, which is termed a predictor procedure, the initial strains introduced in any step are estimated values based on values of plastic strain computed in the

preceding step. The other is a stepwise linearization procedure in which a linear relationship between plastic strain increments and stress increments, coming out of the flow theory used, is introduced into the governing matrix relation, which may then be solved directly.

These procedures were programmed for digital computation and applied to three different sample structures. These are: 1) a plate subjected to concentrated loads applied through tapered stiffeners; 2) a notched bar loaded in tension or compression; 3) a simplified swept wing structure. Cyclic loads were applied to all three structures and, in the case of the notched bar, the results obtained are compared with available experimental results and show good agreement.

Consideration is given to the problem of failure associated with excessive plastic straining. In this connection, criteria for plastic collapse are established. These criteria may be applied in the course of computations using the procedures discussed above, and serve to test whether, at any point in the loading process, a collapse state has been reached.

The problem of plastic buckling is treated as a bifurcation phenomenon, with attention concentrated on flat rectangular plates. A previously developed discrete-element method for elastic buckling analysis is extended to take into account the effect of plastic deformation. It is based on the matrix displacement method of structural analysis. A deformation theory of plasticity, used previously in a plastic buckling analysis of plates on a continuum basis and found to yield results in substantial agreement with experiment, is incorporated into the present method. Plate buckling results are presented for various geometries, edge loadings and boundary conditions.

A brief review of the literature on temperature effects in the plastic behavior of structures is presented. A heuristic approach to the introduction of such effects is tentatively proposed.

The computer programs developed in the present study are presented in a separate report, NASA CR- 66364.

TABLE OF CONTENTS

Item		Page
1.	Introduction	1
2.	Plasticity Relations	10
3.	Discrete-Element Methods of Plastic Analysis of Stable Structures	16
	Stress Method	27
	Predictor procedure	28
	Stepwise linearization procedure	29
	Strain Method	31
	Predictor procedure	33
	Stepwise linearization procedure	34
4.	Application of Plastic Analysis Methods for Stable Structures	36
	Stiffened Panel	38
	Notched Bar	47
	Swept Multicell Box Beam	52
5.	Failure Criteria — Plastic Collapse	54
6.	Plastic Buckling	66
	Discrete-Element Buckling Formulation	68
	Discussion of the Stowell-Ilyushin Theory of Plastic Buckling	72
	Development of the Element Stiffness Matrices	78
7.	Discussion of Results from the Discrete-Element Buckling Analysis	82
8.	Thermal Effects on Plastic Deformation	91
9.	Concluding Remarks	98

Item	Page
Appendix A - A Discussion of Some Pertinent Plasticity Theories	103
Appendix B - Multiaxial Perfect Plasticity Criteria	121
Appendix C - Development of Some Matrix Relations Used in Section 3	123
Appendix D - Relations Between the Linear Influence Coefficient Matrices Associated with the Stress and Strain Methods	127
Appendix E - A Procedure to Compute the Load Level Necessary to Cause Yielding from an Elastic State	130
Appendix F - A Yield Condition for the Notched Bar	134
Appendix G - Residual Stresses and Strains	136
Appendix H - Plastic Collapse of Continuous Media with Limited Strain-Hardening Properties	139
Appendix I - Rectangular Finite Element Stiffness Matrices	142
References	144

1. INTRODUCTION

The present report is concerned with the development of methods for predicting the strength of aircraft structures on a more realistic basis than has hitherto been practicable. The greater realism is associated with the analysis of the plastic behavior of the structure prior to, and accompanying, failure.

Two main types of failure are considered. One is associated with the attainment of a failure state without the necessity of significant geometry changes. Failure occurs when the plastic strain reaches a level at which the material ruptures or when the deformations become excessive from a functional standpoint. It may occur as the cumulative effect of several successive loadings, possibly involving reversals of stress into the plastic range. Prediction of such failure requires a method of analysis capable of determining stresses and deformations in a stable highly-redundant structure stressed into the plastic range. The method should have the capability of taking into account the Bauschinger effect, which, in the simple case of uniaxial stress, takes the form of a reduction in compressive yield stress due to prior tensile yielding, and vice versa.

The other type of failure is characterized by buckling of the structure, that is, by instability in which geometry changes play an essential role. In the present work, we are primarily concerned with buckling which occurs at loads that give rise to stresses in the plastic range in the prebuckling configuration.

It has been the purpose of the present study to develop methods of analysis appropriate to both types of failure. To permit the analysis of complex structures of arbitrary shape, these

methods have been based on an extension of the discrete-element methods of structural analysis to provide the desired capability.

Inclusion of plastic effects in a discrete-element analysis of stable structures has been considered in a number of studies. In some, only uniaxial stresses are considered (Refs. 1-4). In others, specific consideration is given to the presence of multiaxial stress (Refs. 5-14), usually on the basis of the Lévy-Mises criterion for yield and the Prandtl-Reuss flow relations. Such a treatment assumes the plastic flow to leave the material isotropic and thus precludes inclusion of the Bauschinger effect.

The mathematical techniques that have been used in the discrete-element methods in effecting a solution to the nonlinear problem associated with plastic behavior fall into two main categories, namely, the incremental and the iterative. In the former approach, the loading is applied incrementally and the plastic behavior is introduced in the form of a relation between plastic strain increments and stress increments (Refs. 1, 6-13). This permits the use of a flow theory of plasticity.

In the iterative approach, the entire load may be applied at once and a solution is effected by application of a Newton-Raphson type of iterative technique (Ref. 3). In this procedure, a deformation theory of plasticity must be applied. If the more generally applicable flow theory is to be used, the loading must be applied incrementally and the iteration carried out within each increment. As the computations associated with the iteration are formidable, the whole process can become very lengthy. Other procedures involving iteration within a basically incremental procedure are presented in Refs. 10 and 15.

In most of the work performed up to the present on the development of discrete-element methods of plastic analysis, and in all

the references cited above, the assumption of geometric linearity is made. That is, it is assumed that changes in geometry can be treated as being infinitesimal. A study in which geometric nonlinearity and inelasticity are considered simultaneously is reported in Ref. 16. It is concerned specifically with the problem of buckling and does not take multiaxial stresses into account.

The present work is based on the assumption of geometric linearity in the plastic analysis of stable structures. The methods developed are applicable to complex built-up structures subjected to biaxial membrane stress. The extension to triaxial stress, while not treated, is straightforward. Attention is concentrated on incremental methods. Application of the developed procedures is made to three different sample structures and results are presented. Consideration is given to the problem of establishing failure criteria, with attention concentrated on the phenomenon of plastic collapse.

The status of the plastic buckling problem is at present somewhat confused. While the plastic buckling phenomenon is well understood in the case of columns, the same cannot be said of plates and shells. The essential difference is that in the former the stresses are uniaxial, whereas in the latter they are biaxial and may assume a substantially different distribution among components during buckling than exists prior to buckling. This makes an analytical solution quite sensitive to the type of plasticity theory that is used (Refs. 17 and 18). An additional factor appears to be a marked sensitivity of plastic buckling of plates and shells to small initial imperfections (Refs. 19 and 20).

The treatment of buckling by discrete-element methods has until now been limited to stressing within the elastic range and to framed structures or flat plates. While both the matrix force

method (Ref. 21) and the matrix displacement method (Refs. 22-24) have been applied to this problem, the latter is more appealing in that it permits a more direct approach.

Specific treatment of the buckling problem by this means has until now been as a bifurcation phenomenon; that is, the geometry of the structure is assumed to remain unaffected by loading prior to buckling. The method is, however, basically capable of taking geometric nonlinearity into account, and, consequently, treating buckling of the "top-of-the-knee" variety. The magnitude of the undertaking is then much greater.

In the present investigation, the displacement method, as applied to bifurcation buckling analysis, has been extended to treat the problem of plastic buckling. Attention has been concentrated on initially flat rectangular plates with various types of loading and boundary conditions. While only simple loading conditions, giving rise to statically determinate stress distributions, have been considered, the method is capable of treating more complex stress distributions. The stress distribution just prior to buckling may be determined by the methods developed for the plastic analysis of stable structures. The buckling analysis serves to determine when these stresses reach a critical state.

LIST OF SYMBOLS

a	length of plate
b	width of plate
c	hardening coefficient
D	elastic flexural rigidity of plate, $Eh^3/12(1 - \nu^2)$
D'	plastic flexural rigidity of plate, $E_s h^3/9$
e	total strain
e'	elastic strain
e_i	effective strain
E	Young's modulus
E_s	secant modulus
E_t	tangent modulus
f	yield or loading function
g	loading function defined in a subspace of stress space; nonisothermal yield or loading function
h	plate thickness
M_x, M_y, M_{xy}	plate bending and twisting moments
n	index in Ramberg-Osgood stress-strain relation
S	average stress in minimum cross section of notched bar; initial stress
T	temperature
w	transverse displacement of plate
x, y, z	coordinates of plate

α	stress parameter, σ_x/σ_*
α_{ij}	coordinates of center of loading surface
$\bar{\alpha}_{ij}$	coordinates of center of loading surface immediately prior to unloading
β	stress parameter, σ_y/σ_*
γ	stress parameter, τ_{xy}/σ_*; shear strain
δ	nodal generalized displacement
ϵ	plastic strain; initial strain
η	plasticity reduction factor in plate buckling, $\sigma_{cr_{plastic}}/\sigma_{cr_{elastic}}$
$d\lambda$	differential of scalar quantity appearing in flow rule, Eq. (A-9)
λ	parameter in eigenvalue problem for elastic buckling
$\bar{\lambda}$	tracer in eigenvalue problem for plastic buckling
$d\mu$	differential of scalar quantity appearing in Ziegler's hardening rule, Eq. (2.10)
ν	Poisson's ratio
σ	stress; normal stress
σ_i	effective stress
σ_o	yield stress in tension
σ_*	nominal stress; maximum stress in triangular distribution
$\sigma_{0.7}$	parameter in Ramberg-Osgood stress-strain relation
τ	shear stress
χ_1, χ_2, χ_3	curvature and twist of plate

Matrices:

$[A]$ matrix relating total strains in redundant structure to applied load

$[B]$ matrix relating stresses in redundant structure to applied load

$[C]$ matrix relating plastic strain increments to stress increments in individual strain-hardening elements

$[\searrow C \swarrow]$ diagonally partitioned matrix involving an assemblage of [C] matrices for all strain-hardening elements

$[E]$ matrix relating elastic strains to stresses in individual elements

$[\searrow E \swarrow]$ diagonally partitioned matrix involving an assemblage of [E] matrices for a group of elements

$[\bar{E}]$ matrix expressing condition of tangency of stress increment vector to yield or loading surface in an individual perfectly plastic element

$[\searrow \bar{E} \swarrow]$ diagonally partitioned matrix involving an assemblage of $[\bar{E}]$ matrices for all perfectly plastic elements

$[\tilde{E}]$ matrix expressing condition of normality of plastic strain increment vector to yield or loading surface in an individual perfectly plastic element

$[\searrow \tilde{E} \swarrow]$ diagonally partitioned matrix involving an assemblage of $[\tilde{E}]$ matrices for all perfectly plastic elements

$\{f\}$ vector of nodal generalized forces

$[G]$ matrix relating total strain in redundant structure to initial stresses

$[H]$ matrix relating stresses in redundant structure to initial strains

$[J]$ matrix relating total strains in redundant structure to initial strains

$[K]$	stiffness matrix relating nodal generalized forces to nodal generalized displacements
$[K_B]$	bending stiffness matrix
$[K_B^P]$	bending stiffness matrix as modified by plastic effects
$[K_M]$	initial stress stiffness matrix
$[\tilde{K}_M]$	initial stress stiffness matrix corresponding to a nominal stress state
$\{P\}$	vector of external loads
$[R]$	matrix relating total strain increments to stress increments in an individual strain-hardening element
$\left[\begin{smallmatrix} \searrow & \\ & \swarrow \end{smallmatrix} R \right]$	diagonally partitioned matrix involving an assemblage of [R] matrices for all the strain-hardening elements
$\{S\}$	vector of initial stresses
$[Y^{(2)}]$	matrix defined in Eq. (3.41)
$[Y^{(3)}]$	matrix defined in Eq. (3.37')
$[Z^{(2)}]$	matrix defined in Eq. (3.28)
$[Z^{(3)}]$	matrix defined in Eq. (3.25)
$\{\Delta\omega\}$	vector defined in Eq. (3.22)

Matrix Notation:

$\{\ \}$	column matrix
$[\ ]$	square or rectangular matrix
$\begin{bmatrix} \searrow & \\ & \searrow \end{bmatrix}$	diagonal matrix
$\begin{bmatrix} \searrow & \\ & \searrow \end{bmatrix}$	diagonally partitioned matrix

2. PLASTICITY RELATIONS

Because of the complexity associated with plastic deformation, the laws governing the behavior of materials in the plastic range have not, as yet, reached a level of general acceptance. Thus, any attempt to predict analytically the behavior of structures in the plastic range must begin with a choice, among the available plasticity theories, of one which successfully combines mathematical simplicity with a proper representation of experimentally observed material behavior.

In the following, plasticity relations which have been incorporated in the present investigation are presented and briefly discussed. A more thorough examination of these relations and a review of some of the currently available plasticity theories are presented in Appendix A.

As indicated by Ziegler (Ref. 25), the plastic behavior of a material can be described by specifying the following:

1) An initial yield condition, defining the elastic limit of the material

2) A flow rule, relating the plastic strain increments to the stresses and stress increments

3) A hardening rule, used to establish conditions for subsequent yield from a plastic state

Although the exact nature of the yield surface for structural metals has not yet been firmly established, there exists sufficient experimental evidence to indicate that it is a smooth surface (Refs. 26-28). Consequently, the von Mises yield function, which describes a smooth surface in stress space and is representable by a simple mathematical function, was chosen for use as the initial

yield function. With consideration limited to plane stress situations ($\sigma_z = \tau_{xz} = \tau_{yz} = 0$), the von Mises yield function is represented as an ellipsoid in stress space, given by

$$f(\sigma_{ij}) = \sigma_x^2 - \sigma_x\sigma_y + \sigma_y^2 + 3\tau_{xy}^2 - \sigma_o^2 = 0 \tag{2.1}$$

where σ_o is the yield stress in tension.

In the case of subsequent yielding from a plastic state, the function used to define the elastic limit is referred to as the subsequent yield function, or the loading function, and can be represented as

$$f(\sigma_{ij},\alpha_{ij}) = 0 \tag{2.2}$$

where α_{ij} is a measure of the degree of work hardening.

The symbolic representation of the loading function given in Eq. (2.2) can be used to specify conditions for loading and unloading from a plastic state. The total differential of $f(\sigma_{ij},\alpha_{ij})$ can be written as

$$df = \frac{\partial f}{\partial \sigma_{ij}} d\sigma_{ij} + \frac{\partial f}{\partial \alpha_{ij}} d\alpha_{ij} \tag{2.3}$$

With $f = 0$ representing a plastic state and $f < 0$ representing an elastic state, $f > 0$ not being defined, unloading from a plastic state to an elastic state will result in $df < 0$. Since we will consider unloading to be elastic, $d\alpha_{ij} = 0$, and the condition for unloading can be written as

$$\frac{\partial f}{\partial \sigma_{ij}} d\sigma_{ij} < 0 \tag{2.4}$$

If

$$\frac{\partial f}{\partial \sigma_{ij}} d\sigma_{ij} = 0 \tag{2.5}$$

and there is no accompanying plastic deformation, the condition given in Eq. (2.5) is termed neutral loading. For an ideally plastic material the yield function is a function of stress only. Consequently, if there is plastic deformation, any changes in stresses during plastic flow must satisfy Eq. (2.5). The geometric interpretation of Eq. (2.5) is that the stress increment vector is tangential to the loading surface; thus Eq. (2.5) will be referred to as the tangency condition associated with ideal, or perfect, plasticity.

When

$$\frac{\partial f}{\partial \sigma_{ij}} d\sigma_{ij} > 0 \tag{2.6}$$

there will necessarily be plastic deformation, indicating loading from one plastic state to another. This condition is termed consistent loading by Prager.

The yield and loading conditions serve to establish criteria for yielding from some elastic or plastic states, respectively. Additional information, in the form of a constitutive relation between increments of plastic strain, stress and stress increments, is required to describe the plastic behavior of a material. This constitutive relation, termed the flow rule, is based on Drucker's postulate for work-hardening materials. A discussion of this postulate and conditions necessary for its satisfaction is presented in Appendix A. The flow rule is represented as

$$d\epsilon_{ij} = d\lambda \frac{\partial f(\sigma_{ij},\alpha_{ij})}{\partial \sigma_{ij}} \tag{2.7}$$

where $d\epsilon_{ij}$ is the increment of plastic strain, and $d\lambda$ is a positive scalar quantity.

Having chosen a yield condition and flow rule, we are now left with consideration of a choice of a hardening rule to complete the description of the plastic behavior of a material. The choice of a specific hardening rule, among those currently available for our present purpose, depends upon its satisfaction of certain requirements, namely, its ability to describe cyclic plastic behavior. A discussion of these requirements, together with an appraisal of some of the hardening rules, is presented in Appendix A. This appraisal has indicated that the kinematic hardening theory due to Prager (Refs. 29 and 30) is the most applicable. The hardening behavior postulated in this theory assumes that, during plastic deformation, the loading surface, which is the geometrical representation of the loading function in stress space, translates as a rigid body, maintaining the size, shape and orientation of the yield surface.

Denoting the translation of the center of the yield surface by α_{ij}, the loading function, $f(\sigma_{ij},\alpha_{ij})$, may be represented as

$$f(\sigma_{ij} - \alpha_{ij}) = 0 \tag{2.8}$$

so that the von Mises yield condition for plane stress, Eq. (2.1), can be written as follows, to represent the subsequent yield condition,

$$\begin{aligned} f(\sigma_{ij},\alpha_{ij}) = {} & (\sigma_x - \alpha_x)^2 - (\sigma_x - \alpha_x)(\sigma_y - \alpha_y) + (\sigma_y - \alpha_y)^2 \\ & + 3(\tau_{xy} - \alpha_{xy})^2 - \sigma_o^2 = 0 \end{aligned} \tag{2.9}$$

Kinematic hardening, as set forth by Prager, predicts that the increment of translation of the loading surface in the full nine-dimensional stress space occurs in the direction of the exterior normal to the surface at the instantaneous stress state. However, inconsistencies have been shown to arise when it is applied to various subspaces of stress, that is, when the symmetry of the stress tensor or the absence of some stress components is taken into account. These inconsistencies are discussed in more detail in Appendix A.

In order to avoid the difficulty associated with the implementation of Prager's hardening rule, Ziegler (Ref. 25) has proposed a modification which assumes that the increment of translation of the loading surface is directed along the radius vector connecting the center of the loading surface to the instantaneous stress state. In this modification, the increment of translation is expressed as

$$d\alpha_{ij} = d\mu(\sigma_{ij} - \alpha_{ij}) \tag{2.10}$$

where $d\mu$, a positive scalar, is defined in Eq. (A-7) of Appendix A.

An expression for the scalar factor, $d\lambda$, associated with the flow rule, Eq. (2.7), is given in Eq. (A-9), and rewritten here as follows,

$$d\lambda = \frac{1}{c} \frac{\frac{\partial f}{\partial \sigma_{ij}} d\sigma_{ij}}{\frac{\partial f}{\partial \sigma_{mn}} \frac{\partial f}{\partial \sigma_{mn}}} \tag{A-9}$$

where c is a parameter characterizing the hardening behavior of the material. A procedure used to determine this parameter is discussed in Appendix A.

Substituting the expression for $d\lambda$ given in Eq. (A-9) into the flow rule, Eq. (2.7), yields the following equation

$$d\epsilon_{ij} = \frac{1}{c} \frac{\partial f}{\partial \sigma_{ij}} \frac{\frac{\partial f}{\partial \sigma_{k\ell}} d\sigma_{k\ell}}{\frac{\partial f}{\partial \sigma_{mn}} \frac{\partial f}{\partial \sigma_{mn}}} \tag{2.11}$$

which represents the incremental constitutive relation used in the present investigation.

Greater realism may be achieved in the description of the plastic behavior of some materials by assuming that strain hardening occurs only up to some finite limit of strain, and that the behavior beyond this limit is perfectly plastic. Such behavior may be termed "limited strain hardening." A detailed treatment of the mathematical representation of this type of behavior is presented in Appendix B.

3. DISCRETE-ELEMENT METHODS OF PLASTIC ANALYSIS OF STABLE STRUCTURES

The elastic analysis of complex, redundant structures necessarily involves a determination of the stiffness properties of the structure. The specific form of representation of these properties varies with the method of analysis chosen for use. In the discrete-element methods, influence coefficients relating applied forces to displacements in the structure, or expressing the inverse relationship, are derived. These influence coefficients are determined either by the "force" method or by the "displacement" method. In the former, a matrix of influence coefficients representing the flexibility of the structure is determined; in the latter, the influence coefficients represent the stiffness of the structure. The stiffness or flexibility matrices can be used to obtain a matrix of influence coefficients relating stresses or strains within the discrete elements of the structure to the externally applied loads.

As a consequence of the general acceptance of the discrete-element methods, there has been a continuous refinement of these methods to provide a more accurate representation of the elastic behavior of complex structures subjected to general loading conditions. As discussed in the Introduction, there have been concurrent efforts to extend these methods to include the effects of plastic deformation.

The introduction of plasticity within the framework of the methods developed for elastic analysis adds considerable complexity to the implementation of these methods. This added complexity is associated with the fact that the stiffness, or flexibility, of the structure varies with continued plastic flow.

The modifications of the elastic procedures can be carried out by either of two general approaches associated with incremental methods of solution. In the first approach, suggested in Refs. 1, 2 and 13, the effects of plasticity are introduced into the procedure used to determine the basic stiffness properties of the structure. That is, the influence coefficient matrices are recomputed in each increment of external load. This type of approach constitutes an "internal" modification of the stiffness properties of the structure. This distinguishes it from the second approach, suggested and applied in Refs. 4, 6, 9 and 12, which involves what may be termed the "external" modification technique. In this approach, the effects of plasticity are introduced without the necessity of modifying the influence coefficient matrices associated with the linear elastic properties of the structure during the course of plastic deformation. This advantage makes the external modification technique an appealing one, and it was consequently chosen for use in the development of discrete-element plastic analysis methods in the present investigation.

Basically, the external modification of the stiffness properties of the structure is effected by introducing initial strains or initial stresses into the linear matrix equation governing the behavior of the elastic structure. Initial strains are those strains which may exist in the elements if they are unloaded and imagined to be unconstrained by adjoining elements; initial stresses are those stresses necessary to eliminate the initial strains. In its present state of development, this approach is limited in application to loading conditions which cause only membrane stresses.

Most incremental inelastic analyses implementing the concept of initial strain have used estimated values of initial strain increments based on values of the plastic strain increments computed in the preceding loading step. Such a procedure may be termed a predictor procedure. As an alternative, a procedure which directly incorporates the linear incremental plastic strain-stress relation, Eq. (2.11), into the governing equations, can be set up. This second procedure, termed the stepwise linearization procedure, thus avoids the necessity of introducing estimated values of initial strain.

In the present investigation, attention is concentrated on two related methods of solution which can implement either the predictor procedure or the stepwise linearization procedure in effecting a solution to the plasticity problem. In the first method, referred to as the stress method, the governing linear matrix equation is written for the stresses in the elements, as follows,

$$\{\sigma\} = [B]\{P\} + [H]\{\epsilon\} \tag{3.1}$$

where

σ_i = element stresses

P_i = external loads

ϵ_k = initial strains

B_{ij} = i^{th} element stress in redundant structure due to j^{th} applied load

H_{ik} = i^{th} element stress in redundant structure caused by unit initial strain in the k^{th} element.

In the second method, referred to as the strain method, the linear matrix equation for the idealized structure is written for the total strains in the elements,

$$\{e\} = [A]\{P\} + [G]\{S\} \tag{3.2}$$

where

e_i = total strains in elements

S_k = initial stresses

A_{ij} = i^{th} element strain in redundant structure due to j^{th} applied load

G_{ik} = i^{th} element strain in redundant structure caused by unit initial stress in the k^{th} element.

From the definition of initial stress, the relation between initial stress and initial strain can be written as,

$$\left\{S\right\} = - \left[E\right]^{-1} \left\{\epsilon\right\} \tag{3.3}$$

where $\left[E\right]^{-1}$ is a diagonally partitioned matrix whose sub-matrices contain the elastic coefficients associated with Hooke's law as applied to a plane stress situation. The elements of a sub-matrix of $\left[E\right]^{-1}$ are given in Eq. (C-1b) of Appendix C.

If we define

$$\left[J \right] = - \left[G \right]\left[E\right]^{-1} \tag{3.4}$$

Eq. (3.2) can be written in the following form,

$$\{e\} = [A]\{P\} + [J]\{\epsilon\} \tag{3.5}$$

It should be noted that Eqs. (3.1) and (3.5) are related. Relationships between the influence coefficient matrices [B] and [A] and between [H] and [J] are given in Eqs. (D-5) and (D-11), Appendix D, and involve only the elastic properties of the structure. Consequently, Eqs. (3.1) and (3.5) are not uniquely identified with the matrix force and the matrix displacement method, respectively, since either one of these equations can be derived from the other.

By interpreting plastic strains as initial strains, Eqs. (3.1) and (3.5) can be applied to the plasticity problem, the material nonlinearity being introduced through the incremental constitutive relations from the plasticity theory. The introduction of this device into the discrete-element methods for the treatment of plastic behavior is generally credited to Padlog, Huff, and Holloway (Ref. 6), and concurrently to Argyris (Ref. 4).

The procedures used in effecting a solution are based on an incremental application of the loading. This is consistent with the kinematic hardening theory, which is an incremental theory of plasticity. Equations (3.1) and (3.5) are thus written in the form,

$$\{\Delta\sigma\} = [B]\{\Delta P\} + [H]\{\Delta\epsilon\} \tag{3.1'}$$

$$\{\Delta e\} = [A]\{\Delta P\} + [J]\{\Delta\epsilon\} \tag{3.5'}$$

respectively.

For the sake of generality, the plastic behavior is assumed to be limited strain hardening, as described in Section 2 and Appendix B. Unlimited strain hardening and perfect plasticity may then be treated as special cases of this type of behavior.

If we distinguish, by means of the following superscripts, the possible stress conditions existing within an element,

superscript (1) - elastic
superscript (2) - strain hardening
superscript (3) - perfectly plastic

the matrices in Eqs. (3.1') and (3.5') can be partitioned on this basis and the equations written, respectively, as follows,

$$\begin{Bmatrix} \Delta\sigma^{(1)} \\ \hline \Delta\sigma^{(2)} \\ \hline \Delta\sigma^{(3)} \end{Bmatrix} = \begin{bmatrix} B_1 \\ \hline B_2 \\ \hline B_3 \end{bmatrix} \Delta P + \left[\begin{array}{c|c|c} H_{11} & H_{12} & H_{13} \\ \hline H_{21} & H_{22} & H_{23} \\ \hline H_{31} & H_{32} & H_{33} \end{array}\right] \begin{Bmatrix} \Delta\epsilon^{(1)} \\ \hline \Delta\epsilon^{(2)} \\ \hline \Delta\epsilon^{(3)} \end{Bmatrix} \tag{3.6}$$

and

$$\begin{Bmatrix} \Delta e^{(1)} \\ \hline \Delta e^{(2)} \\ \hline \Delta e^{(3)} \end{Bmatrix} = \begin{bmatrix} A_1 \\ \hline A_2 \\ \hline A_3 \end{bmatrix} \Delta P + \left[\begin{array}{c|c|c} J_{11} & J_{12} & J_{13} \\ \hline J_{21} & J_{22} & J_{23} \\ \hline J_{31} & J_{32} & J_{33} \end{array}\right] \begin{Bmatrix} \Delta\epsilon^{(1)} \\ \hline \Delta\epsilon^{(2)} \\ \hline \Delta\epsilon^{(3)} \end{Bmatrix} \tag{3.7}$$

If the structure is originally free of any initial strains, that is, thermal strains or strains caused by lack of fit, there will be no initial strains in those elements which remain elastic during the loading process. Therefore, in Eqs. (3.6) and (3.7) we can set

$$\{\Delta\epsilon^{(1)}\} = 0 \tag{3.8}$$

Equation (3.6) can be expanded and written as three matrix equations, each associated with a particular stress condition, as follows,

$$\{\Delta\sigma^{(1)}\} = [\ B_1\ ]\{\Delta P\} + [\ H_{12}\ ]\{\Delta\epsilon^{(2)}\} + [\ H_{13}\ ]\{\Delta\epsilon^{(3)}\} \quad (3.9a)$$

$$\{\Delta\sigma^{(2)}\} = [\ B_2\ ]\{\Delta P\} + [\ H_{22}\ ]\{\Delta\epsilon^{(2)}\} + [\ H_{23}\ ]\{\Delta\epsilon^{(3)}\} \quad (3.9b)$$

$$\{\Delta\sigma^{(3)}\} = [\ B_3\ ]\{\Delta P\} + [\ H_{32}\ ]\{\Delta\epsilon^{(2)}\} + [\ H_{33}\ ]\{\Delta\epsilon^{(3)}\} \quad (3.9c)$$

Similarly, Eq. (3.7) can be expanded and written as

$$\{\Delta e^{(1)}\} = [\ A_1\ ]\{\Delta P\} + [\ J_{12}\ ]\{\Delta\epsilon^{(2)}\} + [\ J_{13}\ ]\{\Delta\epsilon^{(3)}\} \quad (3.10a)$$

$$\{\Delta e^{(2)}\} = [\ A_2\ ]\{\Delta P\} + [\ J_{22}\ ]\{\Delta\epsilon^{(2)}\} + [\ J_{23}\ ]\{\Delta\epsilon^{(3)}\} \quad (3.10b)$$

$$\{\Delta e^{(3)}\} = [\ A_3\ ]\{\Delta P\} + [\ J_{32}\ ]\{\Delta\epsilon^{(2)}\} + [\ J_{33}\ ]\{\Delta\epsilon^{(3)}\} \quad (3.10c)$$

The implementation of the plasticity relations and solution of the plasticity problem may now be carried out using either Eqs. (3.9) or Eqs. (3.10), the former constituting the stress method and the latter the strain method. Although Eqs. (3.9) and (3.10) are interrelated sets of matrix equations, sufficient differences arise in carrying out the required solution to warrant separate treatment. However, prior to consideration of the solution of these equations, some basic matrix relations common to both methods of solution will be presented. These matrix relations are derived for those elements that are plastic, strain-hardening or perfectly plastic.

For plastic, strain-hardening materials, the differential plastic strain-stress relation is given in tensor notation in Eq. (2.11). This equation is expanded into a set of equations for the various components of plastic strain in Eqs. (C-2) of Appendix C. If we represent $d\epsilon_{ij}$ as $\Delta\epsilon_{ij}$, and $d\sigma_{ij}$ as $\Delta\sigma_{ij}$, Eqs. (C-2) can be written in matrix form to represent the incremental plastic strain-stress relations for the plastic strain-hardening elements;

$$\left\{\Delta\epsilon^{(2)}\right\} = \left[C\right] \left\{\Delta\sigma^{(2)}\right\} \tag{3.11}$$

The construction of the submatrices of the diagonally partitioned matrix $\left[C\right]$ is shown in Eq. (C-3) of Appendix C.

In the plastically deforming elements, the increments of total strain can be decomposed into elastic and plastic parts

$$\left\{\Delta e\right\} = \left\{\Delta e'\right\} + \left\{\Delta\epsilon\right\} \tag{3.12}$$

where $\{\Delta e'\}$ is the elastic part of the strain increment and is related to the stress increment through Hooke's law,

$$\left\{\Delta e'\right\} = \left[E\right] \left\{\Delta\sigma\right\} \tag{3.13}$$

Substituting Eqs. (3.11) and (3.13) into Eq. (3.12) results in the following incremental total strain-stress relation for strain-hardening elements,

$$\left\{\Delta e^{(2)}\right\} = \left[R\right] \left\{\Delta\sigma^{(2)}\right\} \tag{3.14}$$

where

$$\left[{}^{\nu}R_{\lambda}\right] = \left[{}^{\nu}E_{\lambda}\right] + \left[{}^{\nu}C_{\lambda}\right] \tag{3.15}$$

The elements of a submatrix of $\left[{}^{\nu}R_{\lambda}\right]$ are given in Eq. (C-4) of Appendix C.

Because of the normality condition imposed upon the plastic strain increment vector, there is no unique stress increment vector corresponding to a given plastic strain increment vector. Consequently, the matrix $\left[{}^{\nu}C_{\lambda}\right]$ does not possess an inverse. However, the matrix $\left[{}^{\nu}R_{\lambda}\right]$, relating the incremental total strain to the stress increment, is a nonsingular matrix. Thus, we can write the inverse relationship,

$$\left\{\Delta\sigma^{(2)}\right\} = \left[{}^{\nu}R_{\lambda}\right]^{-1} \left\{\Delta e^{(2)}\right\} \tag{3.16}$$

An incremental relation between plastic strain and total strain can be obtained by substituting Eq. (3.16) into Eq. (3.11),

$$\left\{\Delta\epsilon^{(2)}\right\} = \left[{}^{\nu}C_{\lambda}\right] \left\{\Delta\sigma^{(2)}\right\} = \left[{}^{\nu}C_{\lambda}\right]\left[{}^{\nu}R_{\lambda}\right]^{-1} \left\{\Delta e^{(2)}\right\} \tag{3.17}$$

Consideration is now given to those elements which are in a state of perfect plasticity. As stated in Section 2, the conditions that must be satisfied for perfectly plastic behavior are:

1) The stress increment vector must be tangential to the loading surface during continued plastic deformation, and

2) The strain increment vector must remain normal to the loading surface.

Condition 1) is expressed analytically in Eq. (2.5), and is presented for the von Mises yield condition in Eq. (C-5) of Appendix C. If we again represent $d\sigma_{ij}$ as $\Delta\sigma_{ij}$, the implicit differential of Eq. (C-5) provides a linear relation among the components of stress increment in a perfectly plastic element. This linear dependence can be represented in matrix form for the j^{th} perfectly plastic element as follows,

$$\left\{\Delta\sigma^{(3)}\right\}_j = \left[\bar{E}\right] \left\{\Delta\sigma^{(3)}\right\}_j \tag{3.18}$$

If we choose to express $\Delta\sigma_x$ in terms of $\Delta\sigma_y$ and $\Delta\tau_{xy}$, the elements of the matrix $\left[\bar{E}^x\right]$ are those given in Eq. (C-6). It is seen from this equation that the first column of $\left[\bar{E}\right]$ is zero. For the whole set of perfectly plastic elements we may write the matrix relation,

$$\left\{\Delta\sigma^{(3)}\right\} = \left[\bar{E}\right] \left\{\Delta\sigma^{(3)}\right\} \tag{3.19}$$

Since the submatrices of the diagonally partitioned matrix contain only zeros in their first column, every third column of the diagonally partitioned matrix will be zero.

The second condition that must be satisfied in the case of perfectly plastic behavior is the flow law, given in Eq. (2.7) and rewritten here,

$$d\epsilon_{ij} = \frac{\partial f}{\partial \sigma_{ij}}\, d\lambda \tag{3.20}$$

Using the von Mises yield condition, we can write the above equation as Eq. (C-7) of Appendix C. If we again replace $d\epsilon_{ij}$ by $\Delta\epsilon_{ij}$, Eq. (C-7) provides a linear relation between the components of plastic strain increment in a perfectly plastic element.

Paralleling the development of Eq. (3.19), we can express Eq. (C-7) in matrix form, for all perfectly plastic elements as

$$\left\{\Delta\epsilon^{(3)}\right\} = \left[\tilde{E}\right] \left\{\Delta\epsilon^{(3)}\right\} \tag{3.21}$$

if $\Delta\epsilon_y$ and $\Delta\gamma_{xy}$ are expressed in terms of $\Delta\epsilon_x$, the elements of a submatrix of $\left[\tilde{E}\right]$ are given by Eq. (C-8). From this equation it is seen that the first column of these submatrices is the only nonzero column. Thus, only every third column of the diagonally partitioned matrix $\left[\tilde{E}\right]$ will be nonzero.

Equations (3.19) and (3.21) are the matrix representations of the two conditions which must be satisfied in the case of perfect plasticity. These matrix equations indicate that, in a perfectly plastic element, only two of the three components of stress increment, and only one of the three components of strain increment, are required to specify all the components of the increments of stress and plastic strain in that element. Therefore, for the j^{th} perfectly plastic element, we can introduce the vector,

$$\left\{\Delta\omega\right\}_j = \begin{Bmatrix} \Delta\epsilon_x \\ \Delta\sigma_y \\ \Delta\tau_{xy} \end{Bmatrix}_j \tag{3.22}$$

which, together with Eqs. (3.19) and (3.21), can be used to specify the increments of stress and plastic strain in that element. In fact, it is easily seen that, because of the special properties of $\left[\bar{E}\right]$ and $\left[\tilde{E}\right]$, Eqs. (3.19) and (3.21) can be written in the form,

$$\left\{\Delta\sigma^{(3)}\right\} = \left[\overline{E}_{\nearrow}\right] \left\{\Delta\omega\right\} \tag{3.19'}$$

and

$$\left\{\Delta\epsilon^{(3)}\right\} = \left[\tilde{E}_{\nearrow}\right] \left\{\Delta\omega\right\} \tag{3.21'}$$

respectively.

Equations (3.11), (3.17), (3.19'), and (3.21') will now be implemented in developing solutions to Eqs. (3.9) and (3.10). Consideration will first be given to the solution of the stress increment equation.

Stress Method

Substitution of Eqs. (3.19') and (3.21') into Eq. (3.9c) results in the following equation,

$$\left[\overline{E}_{\nearrow}\right] \left\{\Delta\omega\right\} = \left[B\right] \left\{\Delta P\right\} + \left[\ H_{32}\ \right] \left\{\Delta\epsilon^{(2)}\right\} + \left[\ H_{33}\ \right]\left[\tilde{E}_{\nearrow}\right] \left\{\Delta\omega\right\} \tag{3.23}$$

or

$$\left[\ Z^{(3)}\ \right] \left\{\Delta\omega\right\} = \left[\ B_3\ \right] \left\{\Delta P\right\} + \left[\ H_{32}\ \right] \left\{\Delta\epsilon^{(2)}\right\} \tag{3.24}$$

where

$$\left[\ Z^{(3)}\ \right] = \left[\overline{E}_{\nearrow}\right] - \left[\ H_{33}\ \right]\left[\tilde{E}_{\nearrow}\right] \tag{3.25}$$

A solution may now be effected by either the predictor procedure or the stepwise linearization procedure.

Predictor procedure. -

In this procedure, the load is applied in small increments and, at the end of each loading step, values for the plastic strain increment, $\Delta\epsilon^{(2)}$, equal to those determined in the preceding step are introduced into Eq. (3.24). Thus, Eq. (3.24) becomes

$$\left[Z^{(3)} \right] \left\{\Delta\omega\right\}^{(k)} = \left[B_3 \right] \left\{\Delta P\right\} + \left[H_{32} \right] \left\{\Delta\epsilon^{(2)}\right\}^{(k-1)} \qquad (3.24')$$

where the superscripts (k) and (k-1) refer to values computed at the k^{th} and $(k-1)^{th}$ load levels, respectively.

As a consequence of using estimated values of $\left\{\Delta\epsilon^{(2)}\right\}$ in Eq. (3.24'), the only remaining unknowns in this equation are the elements of the solution vector, $\left\{\Delta\omega\right\}^{(k)}$. Thus, we can write

$$\left\{\Delta\omega\right\}^{(k)} = \left[Z^{(3)} \right]^{-1} \left(\left[B_3 \right] \left\{\Delta P\right\} + \left[H_{32} \right] \left\{\Delta\epsilon^{(2)}\right\}^{(k-1)} \right) \qquad (3.26)$$

The order of the matrix, $\left[Z^{(3)} \right]$, is equal to the number of strain component increments to be solved for in all the perfectly plastic elements.

Equations (3.9a) and (3.9b) can now be used to solve for the stress increments in the elastic elements and the plastic strain-hardening elements, $\left\{\Delta\sigma^{(1)}\right\}$ and $\left\{\Delta\sigma^{(2)}\right\}$, respectively. The solution is carried out by using $\left\{\Delta\epsilon^{(3)}\right\}$, determined from Eq. (3.21), and again using values for the plastic strain increment, $\left\{\Delta\epsilon^{(2)}\right\}$, determined in the preceding step.

Substitution of $\left\{\Delta\sigma^{(2)}\right\}^{(k)}$ into Eq. (3.11) yields a solution for $\left\{\Delta\epsilon^{(2)}\right\}^{(k)}$, which can be used as an estimate of $\left\{\Delta\epsilon^{(2)}\right\}$ in the next loading step.

When the material has unlimited strain-hardening properties, Eq. (3.9c) is not present, and the intermediate steps involved in the solution for $\{\Delta\omega\}^{(k)}$ can be omitted.

The predictor procedure has been used, in various forms, in Refs. 4, 6, 9, and 12 and has been referred to in Ref. 6 as a "constant stress" procedure. It has been shown in Refs. 9 and 12 that this procedure leads to a characteristic numerical instability when the material is assumed to have unlimited strain-hardening properties. This instability has been eliminated in the present investigation by the introduction of limited strain-hardening. This is possible because the instability occurs only when the slope of the stress-strain curve falls below a critical level. In the present procedure, the flatter portion of the stress-strain curve is replaced by perfectly plastic behavior, which is treated differently in the analysis.

Stepwise linearization procedure. -

This alternative procedure, which does not require the use of estimated values of plastic strain increments in the strain-hardening elements, but does involve the solution of a linearized problem within each loading step, will now be outlined.

Substitution of Eqs. (3.11) and (3.21') into Eq. (3.9b) results in,

$$\{\Delta\sigma^{(2)}\} = [\,B_2\,]\{\Delta P\} + [\,H_{22}\,][C]\{\Delta\sigma^{(2)}\} + [\,H_{23}\,][\tilde{E}]\{\Delta\omega\} \quad (3.27)$$

If we define

$$[Z^{(2)}] = [I] - [\,H_{22}\,][C] \quad (3.28)$$

where $[I]$ is the unit matrix, Eq. (3.27) can be written as,

$$\left[Z^{(2)}\right]\left\{\Delta\sigma^{(2)}\right\} = \left[\ B_2\ \right]\left\{\Delta P\right\} + \left[\ H_{23}\ \right]\left[\tilde{E}\right]\left\{\Delta\omega\right\} \tag{3.29}$$

Using Eq. (3.11) to substitute for $\left\{\Delta\epsilon^{(2)}\right\}$ in Eq. (3.24), we obtain the following equation,

$$\left[Z^{(3)}\right]\left\{\Delta\omega\right\} = \left[\ B_3\ \right]\left\{\Delta P\right\} + \left[\ H_{32}\ \right]\left[C\right]\left\{\Delta\sigma^{(2)}\right\} \tag{3.30}$$

The unknowns in Eqs. (3.29) and (3.30) are the vectors $\{\Delta\omega\}$ and $\left\{\Delta\sigma^{(2)}\right\}$, and a simultaneous solution of these equations may be effected. In this process it is convenient to introduce the notation,

$$\left[z^{(2)}\right] \equiv -\left[\ H_{23}\ \right]\left[\tilde{E}\right] \tag{3.31a}$$

and

$$\left[z^{(3)}\right] \equiv -\left[\ H_{32}\ \right]\left[C\right] \tag{3.31b}$$

Equations (3.29) and (3.30) are now combined and written in partitioned form as follows,

$$\left[\begin{array}{c|c} Z^{(2)} & z^{(2)} \\ \hline z^{(3)} & Z^{(3)} \end{array}\right]\left\{\begin{array}{c} \Delta\sigma^{(2)} \\ \hline \Delta\omega \end{array}\right\} = \left[\begin{array}{c} B_2 \\ \hline B_3 \end{array}\right]\left\{\Delta P\right\} \tag{3.32}$$

It should be noted that the order of the coefficient matrix of Eq. (3.32) is equal to the total number of stress component increments in all the plastically deforming elements.

After solution of Eq. (3.32), Eqs. (3.19), (3.21), (3.11) and (3.9a) may be used to determine the stress and plastic strain increments in the entire structure.

If the material possesses unlimited strain-hardening properties, Eq. (3.32) becomes

$$\left[Z^{(2)}\right] \left\{\Delta\sigma^{(2)}\right\} = \left[\ B_2\ \right] \left\{\Delta P\right\} \tag{3.33}$$

If, on the other hand, the material is elastic, perfectly plastic, Eq. (3.32) becomes

$$\left[Z^{(3)}\right] \left\{\Delta\omega\right\} = \left[\ B_3\ \right] \left\{\Delta P\right\} \tag{3.34}$$

The magnitude of the load increment can be varied during the course of loading when either of the procedures discussed above is used. When the predictor procedure is used, the estimated value of the initial strain increment must be multiplied by the ratio of load increment used in the current step to that used in the preceding step. No modifications are needed when the stepwise linearization procedure is implemented.

Consideration will now be given to the solution of the matrix equation for the increments of total strain, Eq. (3.10).

Strain Method

The total strain increment, $\{\Delta e\}$, can be decomposed into elastic and plastic parts, as shown in Eq. (3.12),

$$\left\{\Delta e\right\} = \left\{\Delta e'\right\} + \left\{\Delta\epsilon\right\} \tag{3.12}$$

Substitution of Eq. (3.12) into Eq. (3.10c) results in the following equation,

$$\left\{\Delta e^{(3)\,\prime}\right\} + \left\{\Delta\epsilon^{(3)}\right\} = \left[\ A_3\ \right]\left\{\Delta P\right\} + \left[\ J_{32}\ \right]\left\{\Delta\epsilon^{(2)}\right\} + \left[\ J_{33}\ \right]\left\{\Delta\epsilon^{(3)}\right\} \tag{3.35}$$

The elastic components of strain increment, $\Delta e'_{ij}$, are related to the stress increment through Hooke's law,

$$\left\{\Delta e'\right\} = \left[\overset{\vee}{E}\right]\left\{\Delta\sigma\right\} \tag{3.13}$$

Substituting Eq. (3.13) into Eq. (3.35), and making use of Eqs. (3.19') and (3.21'), we obtain

$$\left[\overset{\vee}{E}\right]\left[\overset{\vee}{\bar{E}}\right]\left\{\Delta\omega\right\} + \left[\overset{\vee}{\tilde{E}}\right]\left\{\Delta\omega\right\} = \left[\ A_3\ \right]\left\{\Delta P\right\} + \left[\ J_{32}\ \right]\left\{\Delta\epsilon^{(2)}\right\} + \left[\ J_{33}\ \right]\left[\overset{\vee}{\tilde{E}}\right]\left\{\Delta\omega\right\} \tag{3.36}$$

or

$$\left[Y^{(3)}\right]\left\{\Delta\omega\right\} = \left[\ A_3\ \right]\left\{\Delta P\right\} + \left[\ J_{32}\ \right]\left\{\Delta\epsilon^{(2)}\right\} \tag{3.37}$$

where

$$\left[Y^{(3)}\right] = \left[\overset{\vee}{E}\right]\left[\overset{\vee}{\bar{E}}\right] + \left(\left[I\right] - \left[\ J_{33}\ \right]\right)\left[\overset{\vee}{\tilde{E}}\right] \tag{3.38}$$

The solution to the total strain increment equations can be realized by either the predictor procedure or the stepwise linearization procedure. These procedures parallel those presented in connection with the stress method.

Predictor procedure. -

Estimates of plastic strain in the strain-hardening elements are used to obtain a solution for $\{\Delta\omega\}$ in Eq. (3.37). The estimated values of $\left\{\Delta\epsilon^{(2)}\right\}$ will again correspond to those computed in the preceding load step. Thus, we can write Eq. (3.37) as

$$\left[Y^{(3)}\right]\left\{\Delta\omega\right\}^{(k)} = \left[\ A_3\ \right]\left\{\Delta P\right\} + \left[\ J_{32}\ \right]\left\{\Delta\epsilon^{(2)}\right\}^{(k-1)} \qquad (3.37')$$

where the superscripts (k) and (k-1) have the same meaning as in Eq. (3.24').

As a consequence of using estimated values of $\left\{\Delta\epsilon^{(2)}\right\}$ in Eq. (3.37'), the only remaining unknowns in this equation are the elements of the solution vector, $\{\Delta\omega\}$. Thus, we can write

$$\left\{\Delta\omega\right\}^{(k)} = \left[Y^{(3)}\right]^{-1}\left(\left[\ A_3\ \right]\left\{\Delta P\right\} + \left[\ J_{32}\ \right]\left\{\Delta\epsilon^{(2)}\right\}^{(k-1)}\right) \qquad (3.39)$$

The order of the matrix, $\left[Y^{(3)}\right]$, is equal to the number of strain component increments in all the perfectly plastic elements.

Equations (3.10a) and (3.10b) can now be used to solve for the increments of total strain in the elastic elements and the plastic strain-hardening elements, $\left\{\Delta e^{(1)}\right\}$ and $\left\{\Delta e^{(2)}\right\}$, respectively. The solution is carried out by using the values of $\left\{\Delta\epsilon^{(3)}\right\}$ determined from Eqs. (3.39) and (3.21'), and again using values for the plastic strain increments, $\left\{\Delta\epsilon^{(2)}\right\}$, computed in the preceding step.

Substitution of $\left\{\Delta e^{(2)}\right\}^{(k)}$ into Eq. (3.17) yields a solution for $\left\{\Delta\epsilon^{(2)}\right\}^{(k)}$, which can then be used as an estimate of $\left\{\Delta\epsilon^{(2)}\right\}$ in the next loading step.

A form of the predictor procedure associated with the strain method has been used in Ref. 6, and also in Refs. 9 and 12, where it is referred to as a "constant strain" procedure.

Stepwise linearization procedure. -

Using Eq. (3.19'), and substituting the expression for $\{\Delta\epsilon^{(2)}\}$ in Eq. (3.17) into Eq. (3.10b), we obtain the following equation,

$$\{\Delta e^{(2)}\} = [\ A_2\ ]\{\Delta P\} + [\ J_{22}\ ][\overset{\curvearrowright}{C}][\overset{\curvearrowright}{R}]^{-1}\{\Delta e^{(2)}\} + [\ J_{23}\ ][\overset{\curvearrowright}{\tilde{E}}]\{\Delta\omega\} \quad (3.40)$$

If we define,

$$[Y^{(2)}] \equiv [\overset{\curvearrowright}{I}] - [\ J_{22}\ ][\overset{\curvearrowright}{C}][\overset{\curvearrowright}{R}]^{-1} \quad (3.41)$$

Eq. (3.40) can be written as,

$$[Y^{(2)}]\ \{\Delta e^{(2)}\} = [\ A_2\ ]\ \{\Delta P\} + [\ J_{23}\ ][\overset{\curvearrowright}{\tilde{E}}]\ \{\Delta\omega\} \quad (3.42)$$

Using the incremental relation between plastic strain and total strain given in Eq. (3.17), we can write Eq. (3.37) in the form,

$$[Y^{(3)}]\ \{\Delta\omega\} = [\ A_3\ ]\ \{\Delta P\} + [\ J_{32}\ ][\overset{\curvearrowright}{C}][\overset{\curvearrowright}{R}]^{-1}\ \{\Delta e^{(2)}\} \quad (3.43)$$

We can now combine Eqs. (3.42) and (3.43) into the single matrix equation,

$$\left[\begin{array}{c|c} Y^{(2)} & y^{(2)} \\ \hline y^{(3)} & Y^{(3)} \end{array}\right] \left\{\begin{array}{c} \Delta e^{(2)} \\ \hline \Delta\omega \end{array}\right\} = \left[\begin{array}{c} A_2 \\ \hline A_3 \end{array}\right] \{\Delta P\} \quad (3.44)$$

where

$$\left[y^{(2)}\right] \equiv - \left[J_{23} \right] \left[\tilde{E}\right] \tag{3.45}$$

and

$$\left[y^{(3)}\right] \equiv - \left[J_{32} \right] \left[C\right] \left[R\right]^{-1} \tag{3.46}$$

The order of the coefficient matrix of Eq. (3.44) is equal to the total number of strain components in all the plastically deforming elements. Solution of Eq. (3.44) yields the vectors $\{\Delta\omega\}$ and $\left\{\Delta\epsilon^{(2)}\right\}$, which may then be used in conjunction with Eqs. (3.19'), (3.21'), (3.14), (3.17) and (3.10a) to determine the stress and strain increments in the entire structure.

In the case of unlimited strain-hardening, Eq. (3.44) becomes

$$\left[Y^{(2)}\right] \left\{\Delta e^{(2)}\right\} = \left[A_2 \right] \left\{\Delta P\right\} \tag{3.47}$$

In the case of elastic, perfectly plastic behavior, Eq. (3.44) becomes

$$\left[Y^{(3)}\right] \left\{\Delta\omega\right\} = \left[A_3 \right] \left\{\Delta P\right\} \tag{3.48}$$

4. APPLICATION OF PLASTIC ANALYSIS METHODS FOR STABLE STRUCTURES

Computer programs implementing the methods and procedures discussed in Section 3 have been prepared and applied successfully to three sample structures. The first of these structures, shown in Fig. 1, consists of a rectangular panel with a centrally located tapered integral stiffener through which load is applied and transmitted to the panel. This structure was previously chosen for use in a combined experimental and theoretical investigation (Ref. 8), in which experimental data for tensile loading into the plastic range were generated. As indicated in Ref. 8, the stiffened panel possesses additional desirable features recommending its use in an investigation of discrete-element, plastic analysis methods, namely,

1) The elastic structural analysis of the stiffened panel is representative of that associated with aerospace structures.

2) The diffusion of the load into the panel causes high stress gradients in the elastic range, resulting in a significant stress redistribution in the plastic range.

3) The shape of the structure is such that the analysis can be carried out very conveniently by standard matrix methods.

In addition to the combined investigation of Ref. 8, the stiffened panel has been used in a theoretical investigation (Ref. 31) to determine the effects of initial anistropy on plastic and creep response. Both of these references employ discrete-element analyses similar to the predictor procedure associated with the stress and strain methods described in Section 3.

The second sample structure, a uniformly loaded notched bar, as shown in Fig. 2, was studied experimentally in Ref. 32 to determine the plastic behavior in the region of the notch under constant-amplitude cyclic loading involving equal tension and compression. The dimensions of the notched bar are such that the elastic stress-concentration factor is 2 at the root of the notch. Although the experimental data given in Ref. 32 are limited to local plastic conditions at the root of the notch, such data still provide a valuable basis for comparison with the computed results of the present investigation.

The third sample structure, representing a simplified wing structure, is a multicell box beam of rectangular cross section with straight central portion and swept outer portion. Single loads are applied at each tip. The configuration of the structure and the points of application of the external loads are shown in Fig. 3. Experimental data on the elastic behavior of a plexiglass model of this structure are presented in Ref. 33. Despite the lack of experimental data in the plastic range, the swept box beam was chosen for use because it is representative of structures encountered in aircraft design. In addition, there are high stress gradients in the elastic range caused by a concentration of stress in the vicinity of the reentrant corner formed by the trailing edges of the straight and swept portions. The high elastic stress gradient results in a more pronounced redistribution of stress in the plastic range than in the case of a straight multicell box beam.

The analytical results, as determined in the present investigation, are now presented and discussed for each of these sample structures.

Stiffened Panel

The discrete-element idealization of a quadrant of the stiffened panel is shown in Fig. 4. Consistent with the matrix force method, the idealization is comprised of a network of bars and shear panels. The stress in a bar is assumed to vary linearly along its length, and a constant shear-flow is assumed to exist in each shear panel. The stresses and strains in the elements adjacent to individual nodes are averaged and are defined at the nodes. Thus, the linear influence coefficient matrices, given in Eqs. (3.1) and (3.5), relate stresses or strains at the nodes to the loads and to initial strains at the nodes. A further discussion of this idealization and the method of taking into account the effects of Poisson's ratio are presented in Ref. 31. An alternative idealization, associated with the matrix displacement method and involving the same node locations, is also presented in Ref. 34, and it is found that both methods yield very similar results for the elastic properties.

As indicated in Fig. 1, the stiffened panel is constructed of an aluminum alloy, 2024-T4. Stress-strain curves for rolled sheets of this material, obtained from tensile tests in the longitudinal and transverse directions of rolling, have been found to differ, indicating that the material possesses some degree of anisotropy in its plastic behavior. The stress-strain data used in the present investigation were those determined from tests in the transverse direction. This direction coincides with the direction of loading, and is indicated as the y-direction in the figures of this section.

Using the Ramberg-Osgood approximation (Ref. 50), written as

$$e = \frac{\sigma}{E} + \left(\frac{\sigma}{\lambda}\right)^{m} \tag{4.1}$$

the material constants are

$$E = 1.02 \times 10^7 \text{ lb/in.}^2$$

$$\lambda = 0.87 \times 10^5 \text{ lb/in.}^2$$

$$m = 10$$

In the analytic treatment of the stiffened panel, as presented in Refs. 8 and 31, no specific yield stress was chosen to define the elastic limit of the material. Instead, there was assumed to be a nonlinear component of strain, as given by the second term on the right-hand side of Eq. (4.1), throughout the entire history of loading. In the present investigation, initial yielding is treated as a well-defined phenomenon. The yield point in tension, obtained from the transverse stress-strain curve of the material, was found to be equal to 36,000 lb/in.^{2}, and was the value assigned to σ_o in the von Mises yield condition, as given by Eq. (2.1).

Stresses and strains are assumed to increase linearly with load for loadings up to yield. A method of computing the load at which yielding begins in at least one element of the idealized structure, for initial loading and for subsequent reversed loading, is given in Appendix E.

From the elastic analysis of the stiffened panel, it was found that the center of the structure is the most highly stressed point and, consequently, is the point at which yielding begins. Curves of load versus strain at the center in the loading direction, as computed by the various methods of Section 3, are compared with the experimental results of Ref. 8 in Fig. 5.

In Fig. 5a, load versus strain curves, as determined by the stress method using the stepwise linearization procedure,are shown. Each curve was obtained using a different magnitude of load increment. These load increments, written as ΔP, range from 100 lb

to 1000 lb. In the elastic range, the results for all magnitudes of load increment are necessarily identical. However, as the loading progresses further into the plastic range the curves diverge and, at a load level of 20 kips, the maximum difference between the computed results increases to 12 percent. This divergence is attributable to the growing inaccuracies involved in linearizing the problem in each step of the incremental process as the load increment is increased.

In the elastic range ($P \leq 8$ kips), the computed results are seen to agree quite well with the experimental results. However, a continuous divergence of these results is seen to occur as the load increases into the plastic range. At the highest level of load for which there are experimental data ($P = 16.76$ kips) the difference between the experimental and the computed results is 22 percent for $\Delta P = 100$ lb.

The strain method, using the stepwise linearization procedure, was used to obtain the load versus strain curves of Fig. 5b. Once again, five magnitudes of load increment, ranging from $\Delta P = 100$ lb to $\Delta P = 1000$ lb were used in the computations. These curves are quite similar to those previously obtained by the stress method for corresponding magnitudes of load increment. At $P = 20$ kips, the maximum difference between the various computed results is 9 percent. At $P = 16.76$ kips the difference between the computed result for $\Delta P = 100$ lb and the experimental result is 24 percent.

The load versus strain curves shown in Fig. 5c were computed by the strain method using the predictor procedure, and were obtained for six different magnitudes of load increment, ranging from $\Delta P = 50$ lb to $\Delta P = 1000$ lb. As seen from these curves, there is a much greater divergence among computed results in this

case than in the case of the stepwise linearization procedures shown in Figs. 5a and 5b. This large divergence is to be expected, since the predictor procedure uses estimated values of initial strain at each load level, based on values of plastic strain computed at the preceding level. As the load level increases, and as the loading progresses further into the plastic range, these estimated values of initial strain become less accurate. At a load level of 20 kips the maximum difference in computed results is 34 percent. At $P = 16.76$ kips, the computed result for $\Delta P = 50$ lb differs from the experimental result by 24 percent.

Curves similar to those of Figs. 5a-5c could not be obtained by the stress method using the predictor procedure. When this technique is used in the case of unlimited strain-hardening material behavior, a catastrophic numerical instability occurs (Ref. 12). This numerical instability is illustrated by the curve of load versus strain at the center, shown in Fig. 6 for 10 lb load increments. The use of larger load increments will result in the instability occurring at a lower load level. However, the introduction of limited strain-hardening into the analysis makes it possible to obtain numerically stable solutions if the load increments are sufficiently small. In the present problem results have been obtained for load increments of 10 lbs and 25 lbs. These results are similar to those computed by using 50 lb and 100 lb load increments in the previously discussed solution techniques.

Using the smaller load increments, the divergence of the computed results compared with the experimental results, as indicated in Figs. 5a-5c can, in part, be attributed to the effects of the initial anisotropy of the material. An attempt to take these effects into consideration was not made in this investigation, but they were treated in Ref. 31. It was found that the anisotropic analysis of Ref. 31 yielded results which were in slightly better

agreement with the test data than did the isotropic analysis. Thus, it is felt that a consistent treatment of the effects of initial anisotropy within the framework of the kinematic hardening theory will give computed results which are more consistent with the experimental data.

An additional potential source of error is in the determination of the hardening coefficient. The procedure used in this determination, as described in Appendix A, may, in some instances, yield an excessive stiffness for the elements.

While the solution techniques, other than the stress method using the predictor procedure, are not subject to numerical instability, and consequently do not require the introduction of limited strain-hardening behavior for that reason, the capability of treating such behavior was nevertheless provided. This broadens the options available in the characterization of the material behavior, and, as will be discussed in the following section, also makes possible the consideration of the phenomenon of plastic collapse.

Results were obtained using these techniques for the case of limited strain-hardening and are compared with corresponding results for the cases of unlimited strain-hardening in Fig. 7. These results are for the components of normal strain at the center of the structure and were all obtained using 50 lb load increments. It is seen that the limited strain-hardening results are closer to the test data and diverge from the unlimited strain-hardening results as the load increases. This indicates that the limited strain-hardening behavior assumed for this material provides a better approximation to the actual behavior than does the unlimited strain-hardening behavior. It will be noted also that the analytical results obtained by the various techniques are in close agreement.

Computed curves of constant-amplitude cyclic load versus strain at the center of the structure are presented in Fig. 8. The amplitude of load is 15 kips in alternating tension and compression. Since there are no available experimental data for this structure for unloading and reversed loading, the computed results could not be verified. However, these results clearly indicate the Bauschinger effect. The initial yield load in tension is approximately 8 kips, reversed yielding begins at -.9 kips, and subsequent yielding in tension occurs at a load of .4 kips. Because of the Bauschinger effect, the magnitude of the strain at the end of the first three-quarters of a cycle (P = -15 kips) is greater than that at the end of the first quarter-cycle (P = +15 kips).

A cyclic load versus strain curve, such as that given in Fig. 8, is of considerable significance in establishing estimates of fatigue life based on residual strains or residual stresses. The intersection of each of the load versus strain curves of Fig. 8 with the strain axis represents the residual strain associated with an unloading in a particular cycle. The residual strain obtained at the end of the first half-cycle is approximately one-third of that obtained at the end of the first full cycle. This is directly attributable to the Bauschinger effect, since it causes more plastic deformation to occur in reversed loading than in initial loading.

Two sets of curves of load versus stress in the loading direction at the center are presented in Fig. 9. The first set of curves compares the stresses for limited and those for unlimited strain hardening for tensile loading up to a maximum of 20 kips. The results are necessarily identical up to the load at which the

perfect plasticity criterion is satisfied at the center of the structure ($P \approx 14$ kips). At this load, the results diverge, and, as expected, unlimited strain-hardening behavior produces stresses greater than those determined on the basis of limited strain-hardening behavior. It should be noted that the stress versus load curve for limited strain hardening does not become perfectly flat subsequent to the introduction of perfect plasticity, as would occur in the case of uniaxial stress. Instead the curve indicates a moderate slope in the perfectly plastic range. The variation in the component of stress in the loading direction is attributed to the tangency condition imposed on the stress increment vector during plastic deformation.

The second set of curves in Fig. 9 shows constant-amplitude (15 kips) cyclic load versus stress compared for limited and unlimited strain hardening. Only a small difference in results is indicated at the end of the first quarter-cycle. From the intersection of the unloading curves with the stress axis, it is seen that the residual stress component in the loading direction is slightly smaller for unlimited strain-hardening behavior.

Curves of tensile load versus normal stress in the two coordinate directions at several points along the horizontal line of symmetry of the structure (indicated as the x-axis in the figures) are shown in Figs. 10a and 10b. As indicated in these figures, the points under consideration are taken at the center of the structure ($x = 0$), at the edge of the stiffener ($x = 0.5$), and on the panel ($x = 1.0$).

The results shown in Fig. 10a were determined for an unlimited strain-hardening material. It is seen that the rate of change with load of the stress component in the loading direction (σ_y) at $x = 0$ and $x = 0.5$, decreases, with respect to the linear elastic behavior, as the load increases beyond initial yielding.

However, at $x = 1.0$ the rate of change of σ_y initially increases and then decreases with continued loading. The initial increase can be attributed to the stress redistribution which occurs between elastic and neighboring plastic regions. The increase first occurs at a load at which the region at $x = 1.0$ is still elastic, while its neighboring region is plastic. Therefore, the stresses in the structure are redistributed such that the elastic region becomes more severely stressed. This condition persists until plastic flow develops at $x = 1.0$. Beyond the load at which this occurs ($P \approx 16$ kips), a decrease in the rate of change of σ_y is indicated.

The redistribution of stresses acting in the transverse direction (σ_x) results in a reversal of the sense of these stresses, from compressive to tensile, at each of the points considered.

The load versus stress curves of Fig. 10b were determined for a material exhibiting limited strain-hardening behavior. The results are necessarily identical with those presented in Fig. 10a up to the load at which perfect plasticity is introduced into the structure. This initially occurs at the center of the panel, at a load of approximately 14 kips. The rate of change of σ_y with load decreases much more rapidly at the perfectly plastic point ($x = 0$) than at a strain-hardening point ($x = 0.5$). Consequently, the load-stress curves at these points intersect, resulting in a reversal of the relative magnitudes of the stress levels. The stress behavior in the panel at $x = 1.0$ is seen to be very similar to that which occurs in the case of unlimited strain-hardening behavior.

The stresses σ_x at each of these points change from compressive to tensile. Although this behavior is similarly exhibited in Fig. 10a, the curves for $x = 0.5$ and $x = 1.0$ differ in

Fig. 10b in that they intersect at a load of approximately 19 kips, resulting in a reversal in the relative magnitudes of the stresses.

The total strain distribution along the horizontal axis of symmetry is shown, for limited and unlimited strain-hardening behavior, in Fig. 11. The computed results were obtained for a load of 16.60 kips, and are compared with test data taken at 16.76 kips. At this level of loading, perfectly plastic behavior has barely been initiated in the structure. Thus, there is a negligible difference in the computed results. A comparison with test data indicates that, in the vicinity of the center of the structure, the computed results predict lower strains in the loading direction relative to the test data than in the transverse direction. For $x > 1.0$, the correlation with the test data, in both the transverse and loading directions, is quite favorable.

The stress distribution along the horizontal axis of symmetry is shown in Fig. 12 for two load levels. The first level, $P = 8$ kips, corresponds to the maximum load at which the entire structure is in the elastic range, and the higher load level corresponds to that used to obtain the strain distribution curves shown in Fig. 11. Results for limited and unlimited strain-hardening behavior are also given in Fig. 12. A comparison of the curves for σ_y shows the effect of plasticity in decreasing the gradient of this stress. This decrease is more pronounced for limited strain-hardening behavior than for unlimited strain-hardening behavior. The curves for the σ_x stress component show that the compressive elastic stresses become tensile stresses, along almost the entire length of the horizontal symmetry axis of the structure, when the loading is in the plastic range. Figures 13 and 14 relate to the problem of plastic collapse and are discussed in Section 5.

Notched Bar

The discrete-element idealization of a quadrant of the notched bar is shown in Fig. 15. A fine network of triangles is concentrated in the vicinity of the notch, with a coarser network in the remainder of the specimen. A constant stress field is assumed to exist within each element. The linear elastic characteristics of the structure were determined by application of the matrix displacement method.

As indicated in Fig. 2, the material used in the notched bar is an aluminum alloy, 2024-T3. Stress-strain curves of this material for initial tensile loading differ greatly from those obtained for initial compressive loading. This peculiar material behavior poses some difficulties in the present analysis, since the von Mises yield condition assumes an initially isotropic material in which the yield stresses in the normal directions are not only equal to each other, but are also initially equal in tension and compression. A procedure to take this particular behavior into account within the framework of the kinematic hardening theory is presented in Appendix F.

With the Ramberg-Osgood approximation written as in Eq. (A-11), the material constants associated with this material for initial tensile loading are;

$$E = 10.0 \times 10^7 \text{ lb/in.}^2$$

$$\sigma_{0.7} = 0.53 \times 10^5 \text{ lb/in.}^2$$

$$n = 37$$

and for initial compressive loading;

$$E = 10.0 \times 10^7 \text{ lb/in.}^2$$

$$\sigma_{0.7} = 0.47 \times 10^5 \text{ lb/in.}^2$$

$$n = 8.1$$

These material properties were obtained from Ref. 35.

All of the computed results for the notched bar were obtained by the stress method using the predictor procedure. This choice was made on the basis of available storage in the computer program. The program implementing this technique allows a larger number of plastic elements to be considered than any of the programs associated with the other solution techniques. Because of the numerical instability problem encountered with this technique, limited strain-hardening was assumed and 10 lb load increments were used throughout.

Local stress versus strain histories at the root of the notch, computed for a single cycle of loading for each of several load ranges, are presented in Fig. 16. The amplitude of load is denoted in all the figures pertaining to the notched bar by S_{max}, where S is the nominal net-section stress. Test data from Refs. 32 and 36 are shown in Fig. 16, and can be compared with the computed results for each of the four load ranges considered. The comparison indicates that while the agreement is rather good for the strains in both initial and reversed loading, there is a definite tendency for the analysis to predict lower stresses in the reversed loading part of the cycle. This can be attributed to the introduction of perfect plasticity into the analysis on the basis of achieving numerical stability in the computations, rather than, and prior to, its introduction on the basis of the actual physical behavior of the material. The loci of the computed half-cycle and full-cycle residual stresses, as influenced by the nominal stress amplitude, are shown as dashed lines in the figure. A comparison with the residual stresses obtained experimentally in Ref. 36 is favorable.

Curves of cyclic load versus strain at the notch root are presented in Fig. 17. Test data were available (Ref. 36) for three cycles of loading for each of two load ranges, S = 45 ksi,

and S = 50 ksi. The correlation between the analytical and test results for the maximum and minimum strains is quite good, the largest difference being of the order of 6 percent. Although the residual strains predicted by the analysis for the first half and full cycle of loading are quite accurate for both load ranges, the correlation with test data becomes poorer in the second and third cycles of loading. The largest discrepancy in the 45 ksi loading case is 33 percent, and occurs after two and one-half cycles of loading; in the 50 ksi loading case the largest difference is 20 percent, and occurs after two full cycles.

It is felt that the discrepancies in the residual strains can be reduced by a more accurate representation of the cyclic stress-strain behavior of the material in the 2nd and 3rd cycles. As indicated in Ref. 32, a considerable variation of the local stress range occurs during the first 15 to 20 cycles, after which the stress range remains stable. Therefore, for purposes of fatigue estimates, a stabilized cyclic stress-strain relation should be employed in determining the hardening behavior of the material. However, for purposes of comparison with test data, the stress-strain behavior for the second and third cycles was required for use in the present analysis. The material constants associated with the Ramberg-Osgood approximation given in Eq. (2.19) were determined from faired curves through some limited second and third cycle test points of Ref. 36. The stress-strain data were determined by means of tests on unnotched specimens. The values of the constants for tensile loading are;

$$E = 10.0 \times 10^7 \text{ lb/in.}^2$$

$$\sigma_{0.7} = 0.53 \times 10^5 \text{ lb/in.}^2$$

$$n = 7.5$$

and for compressive loading;

$$E = 10.0 \times 10^7 \text{ lb/in.}^2$$

$$\sigma_{0.7} = .49 \times 10^5 \text{ lb/in.}^2$$

$$n = 8.1$$

Figure 18 shows the first-cycle stresses at the notch root for reversed loading. Four characteristic values of stress are significant: the maximum, residual after unloading (half-cycle), minimum, and residual after completing the cycle (full-cycle). As was the case with the residual strains occurring in the first cycle of loading, and as indicated in Fig. 16, there is good correlation between the computed results and the test data for both the half-cycle and full-cycle residual stresses. A procedure that can be used to compute the residual stresses and strains, on the basis of either the stress method or the strain method, is presented in Appendix G.

With the exception of the higher nominal stress ranges, a comparison of analytical and experimental results for the maximum and minimum stresses shows good correlation. Discrepancies at the higher stress ranges can be attributed to the necessarily premature introduction of perfect plasticity into the analysis in order to avoid numerical instability.

The variation of the plastic stress-concentration factor with the nominal stress range is shown in Fig. 19. A comparison between the experimental results of Ref. 32 and the results of the present analysis are presented for monotonically increasing tensile loads, where the factor is denoted by K_p, and for reversed loading from tension in the first cycle, where the factor is denoted by K_p'. The value of K_p is given by

$$K_p = \frac{\sigma}{S} \tag{4.2}$$

where σ is the local stress at the notch root in the loading direction, and the value of K_p' can be computed from

$$K_p' = \frac{S_{max} K_p - \sigma}{(S_{max} - S)}$$

where S_{max} is the maximum nominal stress in tension, and S and σ are the nominal and local stresses, respectively, for which K_p' is sought.

As indicated in Fig. 19, the elastic stress concentration factor determined in the present analysis is slightly smaller than that given in Ref. 32. As the loading progresses, plastic deformation diminishes the stress concentration. A comparison of the two sets of results, as shown in Fig. 19, is quite favorable, except near the upper end of the nominal stress range for both the K_p and K_p' curves. This discrepancy must, once again, be attributed to the premature introduction of perfect plasticity.

The development of the regions of plasticity in the case of initial loading and in the case of unloading and reversed loading is illustrated in Figs. 20a and 20b, respectively. In Fig. 20a, a peculiar pattern of plastic elements occurs at loadings of $S = 48$ ksi and $S = 50$ ksi. At $S = 48$ ksi, there is an isolated plastic element surrounded by elastic elements. Two possible explanations for this behavior are as follows:

1) The procedure used to take into account the effects of the differing tensile and compressive stress-strain behavior, presented in Appendix F, may introduce inaccuracies into the analysis.

2) The discrete-element idealization may not adequately represent the true stress pattern of the actual structure.

Additional computations have been carried out using the stress method in conjunction with the predictor procedure for monotonic tensile loading up to $S = 50$ ksi. The procedure outlined in Appendix F was not used, and elastic, perfectly plastic behavior was assumed. The results did not indicate the peculiarity previously obtained and shown in Fig. 20 for $S = 50$ ksi. Therefore, it would appear that the first explanation above has considerable validity. It should be noted also that the isolated elastic element was found to be on the verge of yielding, while the isolated plastic element had just barely yielded, so that the irregularities indicated are not very pronounced.

Swept Multicell Box Beam

The discrete-element idealization of the swept multicell box beam is shown in Fig. 21. The idealization consists of a network of bars and triangular elements. The idealization of the webs is accomplished by distributing their stiffness properties with respect to bending of the structure into the bars, and using rectangular elements in pure shear to account for their shearing behavior. A linear stress variation is assumed to exist in the bars, the stresses in the triangles are assumed to be constant, and a constant shear flow is assumed in the shear panels. The bars are indicated in Fig. 21 as double lines. The applied loads and their points of application are shown in Figs. 3 and 21. The analysis assumes that the concentrated loads are applied equally at the upper and lower surfaces.

As previously indicated, no experimental data for this structure loaded in the plastic range are available, so that verification of the analytical results was not possible. The material properties chosen for use in the present analysis are the same as those of the stiffened panel.

Results for cyclic load versus strain and cyclic load versus stress are shown in Figs. 22 and 23, respectively. The strains and stresses are measured on the upper or lower surface at the root of the trailing edge of the swept portion, and are normal components in the direction of the trailing edge. By chance, the curves indicate a closed hysteresis loop for a constant-amplitude loading of $P = 5$ kips.

The region of plasticity developed at a load of 5.5 kips is illustrated in Fig. 24. As indicated by the shaded region, plasticity is more widespread in the swept portion than in the unswept portion.

5. FAILURE CRITERIA — PLASTIC COLLAPSE

In the preceding sections, we have been concerned with the establishment of methods for determining the response of a stable structure to given loads, including intermittently applied loads of varying intensity and distribution. We now consider the problem of interpreting such responses in terms of structural integrity. In doing so, we limit attention to those phenomena in which plastic behavior plays a significant role. Thus, fatigue associated with cyclic stressing in the elastic range is not considered. The problem of buckling is taken up in a later section.

The phenomena of concern here are alternating plasticity, or low-cycle fatigue, incremental collapse, shakedown, and plastic collapse. The first of these involves rupture of the material due to plastic deformations occurring alternately in one sense and then in the other. The analysis procedures discussed in the preceding sections can be used to determine the stress and strain history associated with a given sequence of loadings. In order to determine whether rupture will occur as a consequence of these loadings, it would be necessary to have available appropriate test data. Such data could be obtained in a test of a simple specimen of the same material as the structure, and in which the stress and strain history at some critical point in the structure are approximately reproduced. The use of data of a more generalized nature does not appear to be feasible at the present time, except in cases where the critical stresses and strains are essentially uniaxial and the cyclic loading is constant in amplitude. In such cases, data from constant amplitude tests on a tension-compression specimen could be used. A simple example of the application of such a procedure is given in Ref. 32, and relates to the notched bar discussed in the preceding section.

Incremental collapse is a phenomenon associated with intermittent loading causing plastic strains that are in the same sense in successive loadings. These loadings are such that, if applied individually to the virgin material, they will not cause excessive yielding, but, applied successively, the progressive straining produced increases without limit. In practice, either rupture will occur at some point, or the deformations will reach a level beyond which the vehicle cannot function properly. Thus, in an analytical determination of failure it would be necessary either to apply test data on strain levels at which rupture occurs, or to establish criteria on practical deformation limits. It should be noted that thermal effects can also play an important role in incremental collapse (Ref. 6).

Shakedown is related to incremental collapse in that it is also associated with intermittent loading which may cause progressively increasing plastic strains. However, in this case the plastic strains do not increase without limit, but tend to stabilize after a sufficient number of cycles of loading (Ref. 37). The stabilization is due to development of residual stresses that reduce the stresses associated with the most severe loadings to the point where they remain within the elastic range of the material. In the case of strain-hardening materials, the shifting of the yield points or yield surface in accordance with the Bauschinger effect also plays an important role in shakedown (Ref. 38).

In order that shakedown occurs, the loads must be appropriately bounded. Theorems have been established that serve to determine whether, in the case of a particular structure, the given loads are so bounded (Refs. 37 and 38). Their form depends upon whether the material is perfectly plastic or exhibits limited or unlimited strain hardening. Essentially, these theorems provide a test for the existence of a residual stress distribution such that prescribed

loadings cause stresses only within the elastic range. Such a residual stress distribution need not be the actual residual stress distribution attained in an actual shakedown process, but must satisfy the conditions of equilibrium under no external load. Shakedown theorems have been established thus far only for uniaxial stress. In view of this limitation, the shakedown phenomenon was not pursued further in the present investigation.

Plastic collapse represents a state in which a structure can, at some point in the course of a single loading, experience continued and unlimited straining without a further increase in the loading. It is necessarily associated either with perfectly plastic behavior or with limited strain-hardening behavior of the material of the structure. That is, the stress-strain characteristic must be such that, beyond a certain level of strain, the yield surface remains stationary. In truss and framed structures the onset of plastic collapse is associated with the formation of a collapse mechanism. Because of the inability of certain members to resist further increases in load in the case of truss structures, or the formation of yield hinges in the case of framed structures, the structure becomes in effect a mechanism.

The concept of a plastic collapse mechanism is not as straightforward in the case of a continuum subjected to multiaxial stress. It must then be thought of in terms of the formation of a region of perfect plasticity which completely impedes the transmission of increased load through the structure.

The treatment of plastic collapse up to the present has been based on the assumption that the structure retains its initial geometry during the loading process. It is also usually based on the application of one or the other of two alternative theorems developed originally for perfectly plastic materials (Refs. 39 and 40). One states that, given a distribution of loading, the

collapse loading is the maximum loading with that distribution for which a stress distribution, satisfying all equilibrium conditions and nowhere exceeding the limits imposed by the stress-strain characteristic, can be found. The other states that, given a distribution of loading, the collapse loading is the minimum loading with that distribution which is in equilibrium with the stresses in the perfectly plastic portions of the structure in a collapse mechanism. The minimum is taken with respect to all possible collapse mechanisms. The first of these theorems has been shown by Neal (Ref. 38) to apply to materials with limited strain hardening for the case of uniaxial stress.

These theorems may be applied in a direct determination of the collapse loading, without recourse to an analysis of the response of the structure prior to collapse. The procedures involve essentially a search for the appropriate collapse mechanism. In a complex, highly redundant structure there will be a large number of possible collapse mechanisms, so that sophisticated mathematical techniques, such as linear programming, must be used in carrying out this search (Ref. 10).

The philosophy adopted in the present study is that plastic collapse will seldom be treated in practice as an isolated problem. In most cases of structural analysis, particularly in the case of flight vehicles, the behavior of the structure during the loading process is clearly of interest. It would thus appear advantageous to make use, if possible, of information on this behavior in a determination of the plastic collapse loading.

By making the assumption of limited strain hardening in applying the plastic analysis procedures presented in preceding sections, we can use these procedures to determine the growth of regions of perfect plasticity as the loading proceeds. The

problem of plastic collapse may then be treated by determining at what point in the loading process the perfectly plastic regions have grown sufficiently to make the structure a mechanism with respect to the applied loading. It will be noted that the assumption is made here also that the structure retains its initial geometry during the loading process.

Proceeding in this fashion, we rewrite Eqs. (3.9) here for convenience,

$$\left\{\Delta\sigma^{(1)}\right\} = \left[\ B_1\ \right]\left\{\Delta P\right\} + \left[\ H_{12}\ \right]\left\{\Delta\epsilon^{(2)}\right\} + \left[\ H_{13}\ \right]\left\{\Delta\epsilon^{(3)}\right\} \qquad (3.9a)$$

$$\left\{\Delta\sigma^{(2)}\right\} = \left[\ B_2\ \right]\left\{\Delta P\right\} + \left[\ H_{22}\ \right]\left\{\Delta\epsilon^{(2)}\right\} + \left[\ H_{23}\ \right]\left\{\Delta\epsilon^{(3)}\right\} \qquad (3.9b)$$

$$\left\{\Delta\sigma^{(3)}\right\} = \left[\ B_3\ \right]\left\{\Delta P\right\} + \left[\ H_{32}\ \right]\left\{\Delta\epsilon^{(2)}\right\} + \left[\ H_{33}\ \right]\left\{\Delta\epsilon^{(3)}\right\} \qquad (3.9c)$$

The various quantities in these equations are defined in Section 3. It will be recalled that superscript (1) refers to elastic elements, superscript (2) to strain-hardening elements, and superscript (3) to perfectly plastic elements.

In the case of structures, such as truss and framed structures, in which the stresses are essentially uniaxial, it is clear that when the collapse load is reached the stresses experience no further change as collapse proceeds. The stresses in the perfectly plastic regions must remain constant, and the same is true of stresses elsewhere in the structure, since the loads do not change. In the case of structures in which the stresses are multiaxial, the corresponding situation is not as obvious, since stresses in a perfectly plastic region can change as plastic flow proceeds, provided that the stress point remains on the yield surface.

In spite of this, it has been shown by Drucker, Prager and Greenberg (Ref. 41) for an elastic, perfectly plastic continuum that, when the plastic collapse load is reached, there is no further change in stress anywhere in the continuum. It is shown in Appendix H that this conclusion applies also to a continuum with limited strain-hardening properties such that the limiting stress is reached at finite values of strain.

Under these circumstances, it can be concluded that, in Eq. (3.9c), $\{\Delta\sigma^{(3)}\}$ and $\{\Delta\epsilon^{(2)}\}$ will both be zero when the plastic collapse loading is reached. In addition, in accordance with the definition of plastic collapse, Eq. (3.9c) should have a nontrivial solution when $\{\Delta P\}$ is zero. Consequently, Eq. (3.9c) reduces to

$$\left[H_{33} \right] \{\Delta\epsilon^{(3)}\} = 0 \tag{5.1}$$

The condition for the existence of a nontrivial solution to Eq. (5.1) is the singularity of $\left[H_{33} \right]$. A further condition for plastic collapse is that the plastic strain increment vector for each perfectly plastic element be normal to the corresponding loading surface. The relative magnitude of the elements in the solution vector, $\{\Delta\epsilon^{(3)}\}$, of Eq. (5.1) must, therefore, be such as to satisfy this condition, expressed in the following equation reproduced from Section 3 and developed in Appendix C,

$$\{\Delta\epsilon^{(3)}\} = \left[\tilde{E} \right] \{\Delta\epsilon^{(3)}\} \tag{3.21}$$

It is, in fact, conceivable that $\left[H_{33} \right]$ may, at some point in the loading process, become singular without a plastic collapse state being indicated. This may occur if the loading is not appropriate to the particular collapse mechanism associated with the singularity of $\left[H_{33} \right]$.

It may be stated, in general, that singularity of $\left[H_{33} \right]$ is associated with linear dependence of stress components in the perfectly plastic elements. This linear dependence is easy to see in the case of simple redundant structures such as redundant trusses. In such a structure, redundant members may be imagined to be removed and replaced by pairs of equal and opposite external forces of the same magnitude as the internal forces in these members. If the members removed are such that the remaining structure becomes a mechanism, the forces replacing them must be related in order to satisfy equilibrium.

In the case of a two or three dimensional continuum replaced by a discrete-element idealization, there are various situations which can give rise to a plastic collapse mechanism. For example, if all elements adjacent to a node are perfectly plastic, the stresses in those elements must be related in order to satisfy equilibrium at the node. Consequently, the matrix $\left[H_{33} \right]$ will be singular and a collapse mechanism will be indicated, even though the perfectly plastic region may be a contained region. In this case plastic collapse will occur only if an external force is actually applied at the node in question. Similarly, if a region of perfect plasticity completely separates the structure into two parts, the equilibrium of each part will require that the stresses in the perfectly plastic elements be related. The matrix $\left[H_{33} \right]$ will again be singular and a plastic collapse mechanism indicated. In this case, plastic collapse will occur only if the external loading is such that there is necessarily a transmission of load across the region of perfect plasticity. It can be presumed, in such cases, that the region of perfect plasticity associated with a specific loading will develop during the loading process in such a way as to satisfy the condition of normality of the strain increment vectors to the loading surface.

The two conditions necessary for collapse may be combined. Recalling that $\left[\tilde{E}\right]$ in Eq. (3.21) is a matrix in which only every third column is nonzero, we rewrite Eq. (3.21) in the equivalent form,

$$\left\{\Delta\epsilon^{(3)}\right\} = \left[\tilde{E}_r\right]\left\{\Delta\epsilon_r^{(3)}\right\} \tag{5.2}$$

where $\left[\tilde{E}_r\right]$ is obtained from $\left[\tilde{E}\right]$ by deleting the zero columns, and $\left\{\Delta\epsilon_r^{(3)}\right\}$ is obtained from $\left\{\Delta\epsilon^{(3)}\right\}$ by deleting those elements which multiply the zero columns of $\left[E\right]$.

Substituting Eq. (5.2) into Eq. (5.1), we obtain,

$$\left[H_{33}\right]\left[\tilde{E}_r\right]\left\{\Delta\epsilon_r^{(3)}\right\} = 0 \tag{5.3}$$

or

$$\left[\tilde{H}_{33}\right]\left\{\Delta\epsilon_r^{(3)}\right\} = 0 \tag{5.4}$$

in which $\left[\tilde{H}_{33}\right]$ is formed from $\left[H_{33}\right]$ by linearly combining the three columns in each set corresponding to a structural element in accordance with Eq. (5.3). Since $\left[\tilde{H}_{33}\right]$ is not a square matrix, satisfaction of Eq. (5.4) cannot be established solely by a single determinant evaluation. It can, however, be established by extracting from $\left[\tilde{H}_{33}\right]$ any square matrix of order equal to the number of columns in $\left[\tilde{H}_{33}\right]$ and testing it for singularity. If it is singular, the solution vector may be substituted into the remaining linear equations associated with the remaining rows of $\left[\tilde{H}_{33}\right]$ to check whether they are also satisfied.

The form of Eq. (5.4) suggests that there is linear dependence among columns of $\left[\tilde{H}_{33}\right]$. We know from matrix theory (e.g. Ref. 42, p. 56) that if there is linear dependence among rows of $\left[H_{33}\right]$, there must also be linear dependence among columns of that matrix, and Eq. (5.4) suggests that this linear dependence is preserved in the contraction to $\left[\tilde{H}_{33}\right]$.

An alternative approach to the plastic collapse problem involves a more direct application of the governing relations as they are set up for analysis prior to collapse. As shown in Section 3, application of the condition of normality of the strain increment vector and tangency of the stress increment vector to the yield surface for each perfectly plastic element permits the rewriting of Eq. (3.9c) in the form,

$$\left[Z^{(3)}\right]\left\{\Delta\omega\right\} = \left[B_3\right]\left\{\Delta P\right\} + \left[H_{32}\right]\left\{\Delta\epsilon^{(2)}\right\} \tag{3.24}$$

where

$$\left[Z^{(3)}\right] = \left[\bar{E}\right] - \left[H_{33}\right]\left[\tilde{E}\right] \tag{3.25}$$

and $\{\Delta\omega\}$ is defined in Eq. (3.22).

Applying also the fact that there will be no further change in strain in the strain-hardening elements and the fact that plastic collapse implies straining in the perfectly plastic elements without increase in load, we can reduce Eq. (3.24) to the form,

$$\left[Z^{(3)}\right]\left\{\Delta\omega\right\} = 0 \tag{5.5}$$

While it is known from the extended theorem of Drucker, Prager and Greenberg, presented in Appendix H, that the stress increments in $\{\Delta\omega\}$ are necessarily zero, and that, consequently, the columns in $\left[Z^{(3)}\right]$ that are multiplied by these elements can be arbitrary, satisfaction of Eq. (5.5) for nonzero strain increments still requires that $\left[Z^{(3)}\right]$ be singular. This suggests strongly that there is linear dependence among the remaining columns of $\left[Z^{(3)}\right]$. These columns are precisely the columns appearing in $\left[\tilde{H}_{33}\right]$ in Eq. (5.4). Thus, singularity of the matrix $\left[Z^{(3)}\right]$ is an alternative form of the collapse criterion. It has the advantage that it combines both of the conditions for collapse and involves the evaluation of the determinant of a matrix which is set up routinely in the course of analysis.

It will be realized, of course, that a test for singularity of a matrix given in terms of digitally computed numbers cannot be an exact process because of round-off. The test must, therefore, be based on the determinant of the matrix attaining values that, while not actually zero, are small compared with other values obtained in earlier steps.

Both criteria were applied to the stiffened panel specimen. Application could not be made to the other two sample structures because of computer storage limitations. In the application to the stiffened panel specimen of the criterion that the matrix $\left[Z^{(3)}\right]$ become singular, it was found that the determinant of this matrix grew very rapidly in value as the matrix enlarged with the spread of perfect plasticity. This is attributable to the large size of the numbers entering this matrix. It was necessary, consequently, to apply a scaling process. It was then found that the determinant values increased moderately with enlargement of the matrix until the region of perfect plasticity had grown to the

point where plastic collapse could be expected to occur. There was subsequently a decrease in the value of the determinant, but at a moderate rate, rather than the abrupt decrease to a value near zero that one would expect on the basis of singularity of $\left[Z^{(3)}\right]$. This was attributed to the manner in which the matrix [H] had been set up in the linear analysis of the structure. As discussed in Section 4, the stresses and initial strains which this matrix serves to relate were defined at nodes rather than within elements of the structural idealization. It is believed that, in transforming the matrix from an element to a nodal basis, the satisfaction of equilibrium implicit in its initial formation tended to be made less precise. This might well have had the effect of preventing the matrix $\left[Z^{(3)}\right]$ from closely approaching a condition of singularity.

The other criterion was not applied fully. The matrix $\left[\ H_{33}\ \right]$ was tested for singularity, but the normality condition for strain increment vectors was not checked. Applying a scaling process to $\left[\ H_{33}\ \right]$, the determinant of this matrix was found to decrease with enlargement of the matrix, this decrease being much more pronounced at the nominal point of collapse than previously.

The pattern of perfectly plastic nodes at the nominal point of collapse, that is, the point at which a plastic collapse mechanism can be considered to exist, is shown in Fig. 14. It is seen that the region of perfect plasticity fully separates the two stiffeners from one another. A plot of normal plastic strain in the direction of loading at the center of the panel versus applied load is shown in Fig. 13 for loads increasing to values exceeding the nominal collapse load. It is seen that the rate of straining increases rapidly, but not abruptly, in the neighborhood of the nominal collapse load. This again is attributed to the manner in which the matrix [H] had been set up.

It should be noted, finally, that a plastic collapse criterion can similarly be established for use in conjunction with the strain method. Just as singularity of the matrix $\left[Z^{(3)}\right]$ in Eq. (3.24) constitutes a criterion for collapse in the stress method, it is reasonable to expect that singularity of the matrix $\left[Y^{(3)}\right]$ in Eq. (3.37) will constitute a criterion for collapse in the strain method. It can, in fact, be shown that these two matrices are closely related, as follows,

$$\left[Y^{(3)}\right] = \left[E\right]\left[Z^{(3)}\right] \tag{5.6}$$

Since multiplication by $\left[E\right]$ transforms stresses into elastic strains, and since linear dependence among stresses will necessitate linear dependence among corresponding elastic strains, the argument presented previously in connection with the singularity of $\left[Z^{(3)}\right]$ should carry over to the singularity of $\left[Y^{(3)}\right]$. An alternative criterion would be the singularity of the matrix $\left(\left[I\right] - \left[J_{33}\right]\right)$, which is equal to $\left[E\right]\left[H_{33}\right]$, to be applied along with the normality of the plastic strain increment vector to the yield surface in the perfectly plastic elements.

6. PLASTIC BUCKLING

In order to describe buckling phenomena in plate and shell structures, it is necessary to include the effect that membrane stresses in the prebuckling configuration have on subsequent deformation. In classical plate and shell theory this effect is accounted for by the inclusion of higher order terms containing the membrane stresses in the strain energy functional. This leads to nonlinear terms in the governing equations.

Similarly, an analysis of the buckling problem using discrete-element techniques also must include the effect of initial membrane stresses on subsequent deformation. This may be accomplished, within the framework of the displacement or stiffness method of discrete-element analysis, by the introduction of an additional component part to the usual stiffness matrix for bending of the structure. This component part, derivable from the higher order terms of the strain energy functional, has the effect of reducing the stiffness of the idealized structure when the membrane stresses are compressive. A clear explanation of the meaning, and a consistent development, of this additional matrix can be found in Ref. 22. Consistent with the terminology of Ref. 22, the additional matrix is referred to here as the initial stress stiffness matrix.

This matrix was first used for an elastic buckling analysis of flat rectangular plates in Ref. 23. A more recent publication, Ref. 24, uses the stiffness method approach to solve for the elastic buckling of rectangular plates with various edge loadings and boundary conditions. Extensive numerical results are presented in Ref. 24, all of which indicate excellent agreement with corresponding results based on other analytical techniques.

A similar technique may be used in the plastic buckling analysis of structures. It requires a further modification of the stiffness matrix to take into account the altered stiffness properties of the material associated with plastic deformation. This modification is effected by altering the usual elastic bending stiffness matrix so that it contains coefficients which depend on the state of plasticity in the structure and, therefore, the state of stress.

The extent to which the elastic bending stiffness matrix is modified depends on the plastic buckling theory used. Plastic buckling analyses based both on flow theory and on deformation theory have been used, the former, for instance in Refs. 43 and 48 and the latter in Refs. 45-47. A comparison of results from some of these references with experimental data (Ref. 44) shows the deformation theory results to be in better agreement with experiment than the flow theory results. This is paradoxical, since, in the case of some simple stable structures, flow theory provides results which are in better agreement with experiment than corresponding results using deformation theory. Furthermore, deformation theory contains fundamental inconsistencies not present in flow theory.

Two different explanations have been offered for the inaccuracy of flow theory in this problem. One of these is that the Lévy-Mises flow theory, based on the second invariant of stress, is inadequate to provide a proper description of material behavior in this situation, so that more sophisticated flow theories are required. This point is made strongly by Sewell (Ref. 18), who shows that bifurcation buckling is quite sensitive to the direction of the normal to the loading surface and that, consequently, the shape of this surface in a local region near the stress point is very important.[1]

[1] Sewell discusses the various plastic buckling theories in Section 2.6 of Ref. 18.

In another reference (Ref. 17), Batdorf discusses this point and shows, on a qualitative basis, that the slip theory of Batdorf and Budiansky can provide an explanation of plastic buckling behavior. He also states that the qualitative argument presented "justifies the use of deformation theory in the analysis of the plastic buckling of plates."

The other explanation is that the plastic buckling of plates and shells is sensitive to small imperfections, so that the treatment of the problem as a bifurcation phenomenon may lead to errors. This has been shown by Onat and Drucker (Ref. 19) in an analysis of the torsional buckling of a compressively loaded member of hollow cruciform cross section. Besseling (Ref. 20) has extended this work to the case of a member of solid cruciform cross section, and reached similar conclusions.

Although these theoretical objections to bifurcation buckling analysis based on deformation theory do exist, agreement with experiment suggests the use of such analysis in engineering computations (Ref. 49). Consequently, a plastic buckling theory based on a deformation theory of plasticity was used in the present analysis. The manner of introducing deformation theory is based on the work of Stowell (Ref. 46).

It should be noted that the basic procedure developed in the present work can readily accommodate other plasticity theories. In fact, all that is necessary to incorporate another theory is to redefine certain coefficients which enter into the modified bending stiffness matrix.

Discrete-Element Buckling Formulation

A discussion of the formulation of the elastic buckling problem on the basis of the discrete-element displacement method can

be found in Refs. 22-24. The technique of analysis is reviewed below and extended to the plastic buckling problem.

The equation relating the nodal generalized forces to nodal generalized displacements can be written as

$$\{f\} = [K]\{\delta\} \tag{6.1}$$

where

$\{f\}$ is the vector of nodal generalized forces

$[K]$ is the stiffness matrix of the structure

$\{\delta\}$ is the vector of nodal generalized displacements

The stiffness matrix, $[K]$, can be separated into two parts, a matrix, $\left[K_B \right]$, representing the bending stiffness of the structure, and $\left[K_M \right]$, the initial-stress stiffness matrix, representing the modification of stiffness due to membrane stresses in the prebuckling state. The bending stiffness matrix, $\left[K_B \right]$, is either the usual matrix for elastic deformation or, as discussed above, it may be appropriately modified to take into account the effects of plasticity.

The buckling problem is formulated on the basis of the homogeneous problem associated with zero lateral external loads, that is $\{f\} = 0$. Thus Eq. (6.1) assumes the form

$$[K]\{\delta\} = \left(\left[K_B \right] + \left[K_M \right] \right) \{\delta\} = 0 \tag{6.2}$$

In this form, the vanishing of the determinant of the stiffness matrix, $\det \left(\left[K_B \right] + \left[K_M \right] \right) = 0$, is the buckling criterion. The state of stress necessary to cause the determinant to be zero is the critical state of stress.

The problem can be recast in another form. For the elastic case, the initial-stress stiffness matrix may be written as

$$\left[K_M \right] = \lambda \left[\tilde{K}_M \right] \tag{6.3}$$

where $\left[\tilde{K}_M \right]$ represents the initial-stress stiffness matrix computed for a nominal stress state having the desired distribution. The parameter, λ, is a multiplying factor determining the actual buckling stress state, and is initially unknown.

Substituting Eq. (6.3) into Eq. (6.2), we obtain the equation

$$\left(\left[K_B \right] + \lambda \left[\tilde{K}_M \right] \right) \{\delta\} = 0 \tag{6.4a}$$

or

$$\left[K_B \right] \{\delta\} = - \lambda \left[\tilde{K}_M \right] \{\delta\} \tag{6.4b}$$

or, alternatively,

$$- \left[\tilde{K}_M \right] \{\delta\} = \frac{1}{\lambda} \left[K_B \right] \{\delta\} \tag{6.4c}$$

Equation (6.4c) is in the form of a generalized eigenvalue problem. After solution of this problem, the critical stress state is determined by multiplying the nominal stress state assumed initially by the eigenvalue, λ.

When the prebuckling stresses are in the plastic range, the elastic bending stiffness matrix, $\left[K_B \right]$, in Eq. (6.4), must be replaced by the modified bending stiffness matrix, $\left[K_B^P \right]$. This matrix depends upon the state of plasticity and is therefore a function of stress. Consequently, the eigenvalues are now also functions of stress. This substantially complicates the nature of

the eigenvalue problem. We can no longer solve the problem directly as in the elastic case, but must employ a trial-and-error procedure.

In this procedure, we replace Eq. (6.4) by,

$$\left(\left[K_B^P \right] + \bar{\lambda} \left[K_M \right] \right) \{\delta\} = 0 \tag{6.5a}$$

or

$$\left[K_B^P \right] \{\delta\} = - \bar{\lambda} \left[K_M \right] \{\delta\} \tag{6.5b}$$

$$- \left[K_M \right] \{\delta\} = \frac{1}{\bar{\lambda}} \left[K_B^P \right] \{\delta\} \tag{6.5c}$$

where $\bar{\lambda}$ is introduced as a tracer and differs in meaning from λ in Eq. (6.4c). The initial-stress stiffness matrix, $\left[K_M \right]$, and the modified bending stiffness matrix, $\left[K_B^P \right]$, in this case are determined for an actual state of stress corresponding to a trial loading level. At this load level, the eigenvalue problem, Eq. (6.5b) or (6.5c), associated with these stresses, is solved and the lowest eigenvalue $\bar{\lambda}$ examined. If this eigenvalue is equal to one, the state of stress introduced is the critical one. That is, this state of stress causes the determinant of the stiffness matrix to be zero, $\det \left(\left[K_B^P \right] + \left[K_M \right] \right) = 0$. Thus, the eigenvalue problem reduces to the determinant criterion discussed previously. If $\bar{\lambda} < 1$, the initial or prebuckling stresses exceed the critical stresses, and if $\bar{\lambda} > 1$, the initial stresses have not yet become critical. Thus, a succession of eigenvalue problems is solved for various stress levels, in order to establish the critical buckling stress.

An alternative procedure, valid for both elastic and plastic buckling calculations, makes use of the determinant criterion directly. With $\bar{\lambda}$ set equal to one, we seek a stress level in

the prebuckling configuration which will satisfy Eq. (6.5a). The procedure is similar to that discussed previously for the eigenvalue problem. A succession of stress states at various load levels is substituted into Eq. (6.5a). The determinant of $\left([K_B^P] + [K_M]\right)$ is evaluated at each load level. The critical state of stress is then identified by a change in the sign of the determinant. In this procedure, care must be exercised to ensure that the detected crossover point corresponds to the fundamental buckling mode. This requires a sufficiently close spacing of the load levels.

The details of the computational procedures associated with the eigenvalue formulation are discussed in NASA CR-66364.

Discussion of the Stowell-Ilyushin Theory of Plastic Buckling

In Ref. 45, Ilyushin presents a plastic buckling theory based on a deformation theory of plasticity. This formulation includes the possibility of elastic unloading, during buckling, in a portion of a cross section that is completely plastic in the prebuckling state.

Stowell, in Ref. 46, simplifies the analysis of Ref. 45 on the basis of results for plastic column buckling. He assumes that, during buckling,

a) there is no further change in the membrane stresses,

b) a completely plastic cross section remains completely plastic; that is, there is no elastic unloading.

These assumptions, along with the further restriction to a constant stress field in the prebuckling configuration, significantly reduce the complexities of the analysis, since the possibility of an

elastic-plastic boundary in the cross section of the buckled configuration is excluded.

Consistent with deformation theory, the analysis assumes that a unique relation exists between the effective stress and effective strain. That is,

$$e_i = \phi(\sigma_i) = \frac{\sigma_i}{E_s} \tag{6.6}$$

where the effective stress and effective strain are defined as follows for plane stress,

$$\sigma_i = \sqrt{\sigma_x^2 + \sigma_y^2 - \sigma_x\sigma_y + 3\tau_{xy}^2}$$

$$e_i = \frac{2}{\sqrt{3}} \sqrt{e_x^2 + e_y^2 + e_x e_y + \frac{e_{xy}^2}{4}}$$

and E_s is the secant modulus.

In the development of Eq. (6.6), the assumption is made that the material is incompressible, so that Poisson's ratio, ν, is taken as one-half. The stress-strain relations which are consistent with Eq. (6.6) are

$$\epsilon_x = \frac{1}{E_s}\left[\sigma_x - \frac{1}{2}\sigma_y\right]$$

$$\epsilon_y = \frac{1}{E_s}\left[\sigma_y - \frac{1}{2}\sigma_x\right] \tag{6.7}$$

$$\gamma_{xy} = \frac{3\tau_{xy}}{E_s}$$

Figure 25 shows a typical curve of effective stress versus effective strain. Such curves are based on the uniaxial stress-strain characteristics determined experimentally. Also shown are the secant modulus, $E_s = \frac{\sigma_i}{e_i}$, and the tangent modulus, $E_t = \frac{d\sigma_i}{de_i}$.

Throughout the analysis, the functional relation between effective strain and effective stress is approximated by the Ramberg-Osgood stress-strain relation (Ref. 50).

The relations of Eqs. (6.6) and (6.7) can be used along with the usual assumptions of classical plate theory (Ref. 51) to develop the pertinent moment-curvature relations for a slightly out-of-plane deformed configuration. The resulting relations explicitly contain the effect of plastic yielding in the prebuckling configuration.

The moment-curvature relations from Ref. 46 are,

$$\begin{Bmatrix} M_x \\ M_y \\ 2M_{xy} \end{Bmatrix} = -D' \begin{bmatrix} C_1 & \bar{C}_3 & -\frac{C_2}{2} \\ \bar{C}_3 & C_5 & -\frac{C_4}{2} \\ -\frac{C_2}{2} & -\frac{C_4}{2} & 2\tilde{C}_3 \end{bmatrix} \begin{Bmatrix} \chi_1 \\ \chi_2 \\ \chi_3 \end{Bmatrix} \tag{6.8}$$

where

$$\chi_1 = \frac{\partial^2 w}{\partial x^2}, \quad \chi_2 = \frac{\partial^2 w}{\partial y^2}, \quad \chi_3 = \frac{\partial^2 w}{\partial x \partial y}$$

are the curvature and twist in terms of the transverse deflection ,

$$\begin{Bmatrix} M_x \\ M_y \\ M_{xy} \end{Bmatrix} = \int_{-\frac{h}{2}}^{\frac{h}{2}} z \begin{Bmatrix} \sigma_x \\ \sigma_y \\ \tau_{xy} \end{Bmatrix} dz$$

defines the bending and twisting moments, h is the plate thickness, and

$$D' = \frac{E_s h^3}{9}$$

$$C_1 = 1 - \frac{3}{4} \frac{\sigma_x^2}{\sigma_i^2} \left(1 - \frac{E_t}{E_s}\right)$$

$$C_2 = \frac{3\sigma_x \tau_{xy}}{\sigma_i^2} \left(1 - \frac{E_t}{E_s}\right)$$

$$\bar{C}_3 = \frac{1}{2}\left[1 - \frac{3}{2} \frac{\sigma_x \sigma_y}{\sigma_i^2} \left(1 - \frac{E_t}{E_s}\right)\right]$$

$$\tilde{C}_3 = \frac{1}{2}\left[1 - 3 \frac{\tau_{xy}^2}{\sigma_i^2} \left(1 - \frac{E_t}{E_s}\right)\right] \qquad (6.10)$$

$$C_3 = \tilde{C}_3 + \bar{C}_3$$

$$C_4 = 3 \frac{\sigma_y \tau_{xy}}{\sigma_i^2} \left(1 - \frac{E_t}{E_s}\right)$$

$$C_5 = 1 - \frac{3}{4} \frac{\sigma_y^2}{\sigma_i^2} \left(1 - \frac{E_t}{E_s}\right)$$

Equation (6.8) can be substituted into the following moment equilibrium equation for a plate with an inplane stress field (Ref. 51),

$$\frac{\partial^2 M_x}{\partial x^2} + 2\frac{\partial^2 M_{xy}}{\partial x \partial y} + \frac{\partial^2 M_y}{\partial y^2} = -h\left[\sigma_x \frac{\partial^2 w}{\partial x^2} + \sigma_y \frac{\partial^2 w}{\partial y^2} + 2\tau_{xy}\frac{\partial^2 w}{\partial x \partial y}\right] \tag{6.11}$$

to yield the following equation, specialized further to the case of a constant stress field in the prebuckling state,

$$C_1\frac{\partial^4 w}{\partial x^4} - C_2\frac{\partial^4 w}{\partial x^3 \partial y} + 2C_3\frac{\partial^4 w}{\partial x^2 \partial y^2} - C_4\frac{\partial^4 w}{\partial x \partial y^3} + C_5\frac{\partial^4 w}{\partial y^4} = \frac{h}{D'}\left[\sigma_x \frac{\partial^2 w}{\partial x^2} + \sigma_y \frac{\partial^2 w}{\partial y^2} + 2\tau_{xy}\frac{\partial^2 w}{\partial x \partial y}\right] \tag{6.12}$$

This equation is identical in form with the governing equation for elastic buckling of an anisotropic plate[2] (Ref. 52). The plate, therefore, deforms as if it were anisotropic, the anisotropy being due to plastic deformation and, consequently, a function of the state of stress in the prebuckling configuration.

---

[2] Equation (6.12) is in the form of the governing equation for an anisotropic elastic plate when the following substitutions are made,

$$C_1 = D_{11};\ C_2 = -4D_{16};\ C_3 = (D_{12} + D_{66});\ C_4 = -4D_{26};\ C_5 = D_{22}$$

where the D_{ij} describe the material properties of the plate as defined in Ref. 52.

In the elastic case, $C_1 = C_3 = C_5 = 1$ and $C_2 = C_4 = 0$, so that Eq. (6.12) reduces to[3]

$$\nabla^4 w = \frac{h}{D}\left[\sigma_x \frac{\partial^2 w}{\partial x^2} + \sigma_y \frac{\partial^2 w}{\partial y^2} + 2\tau_{xy} \frac{\partial^2 w}{\partial x \partial y}\right] \tag{6.13}$$

In order to formulate the plastic buckling problem for a discrete-element analysis, it is necessary to find the functional from which Eq. (6.12) is derivable. Toward this end, the following expression for the strain energy of bending in terms of the moments and curvature is used,

$$U_B = -\frac{1}{2}\int_A \left[M_x \chi_1 + M_y \chi_2 + 2M_{xy}\chi_3\right] dxdy \tag{6.14}$$

Substituting the moment-curvature relation, Eq. (6.8), into Eq. (6.14), we obtain the functional,

$$U_B = \frac{D'}{2}\int_A \left(C_1\chi_1^2 - C_2\chi_1\chi_3 + 2\left[\bar{C}_3\chi_1\chi_2 + \tilde{C}_3\chi_3^2\right] - C_4\chi_2\chi_3 + C_5\chi_2^2\right) dxdy \tag{6.15}$$

When the contribution from the membrane stress field (Ref. 51, p. 387) is added to Eq. (6.15), we obtain the functional,

$$\begin{aligned}\tilde{U} = \int_A \Bigg[\frac{D'}{2}\Big[C_1\chi_1^2 - C_2\chi_1\chi_3 + 2\left[\bar{C}_3\chi_1\chi_2 + \tilde{C}_3\chi_3^2\right] - C_4\chi_2\chi_3 \\ + C_5\chi_2^2\Big] + \frac{h}{2}\left[\sigma_x\left(\frac{\partial w}{\partial x}\right)^2 + \sigma_y\left(\frac{\partial w}{\partial y}\right)^2 + 2\tau_{xy}\frac{\partial w}{\partial x}\frac{\partial w}{\partial y}\right]\Bigg] dxdy\end{aligned} \tag{6.16}$$

[3] D in this case can be taken as the usual flexural rigidity.

It can be shown that the stationary problem associated with Eq. (6.16) yields the plate boundary value problem associated with Eq. (6.12).[4]

Equation (6.16) is used in the subsequent analysis to develop the stiffness matrices for the discrete elements. Since all of the plate plastic buckling formulations based on deformation and flow theory, Refs. 18, 43, 45-48, lead to a governing equation similar to Eq. (6.12), associated functionals similar to Eq. (6.16) can be found for these equations, differing from Eq. (6.16) only in the definition of the quantities C_1 through C_5.

Development of the Element Stiffness Matrices

The techniques used in the development of the element stiffness matrices and the application of these matrices in a discrete-element elastic analysis have been discussed previously by a number of authors. The derivation of the initial-stress stiffness matrix in the present work follows specifically from the analysis presented in Ref. 22. That is, the energy functional associated with the deformation of a discrete element is written in terms of the nodal generalized displacements. The element stiffness matrices are then derived from Castigliano's first theorem,

---

[4] This functional differs slightly from that given in Ref. 46. The term $2\left[\bar{C}_3\chi_1\chi_2 + \tilde{C}\chi_3^2\right]$ in Eq. (6.16) replaces the term $C_3\left[\chi_1\chi_2 + \chi_3^2\right]$ in Eq. (18) of Ref. 46. The stationary problem associated with the latter functional is found to yield the correct differential equation, but does not yield the correct boundary condition.

$$k_{ij} = \frac{\partial^2 U}{\partial \delta_i \partial \delta_j} \tag{6.17}$$

where

k_{ij} is an element in the stiffness matrix

δ_i, δ_j are generalized nodal displacements

U is the energy functional associated with the element deformation

Once developed, the element stiffness matrices can be formed into the over-all stiffness matrix of the complete idealized structure by applying compatibility and equilibrium conditions at each node.

In the buckling analysis of a planar elastic structure, the following energy functional, including the effect of membrane stresses (Ref. 51, p. 387), is used in Eq. (6.17),

$$U = \frac{D}{2} \int_A \left[(\chi_1 + \chi_2)^2 - 2(1 - \nu)\left[\chi_1\chi_2 - \chi_3^2\right] \right] dxdy$$

$$+ \frac{h}{2} \int_A \left[\sigma_x \left(\frac{\partial w}{\partial x}\right)^2 + \sigma_y \left(\frac{\partial w}{\partial y}\right)^2 + 2\tau_{xy} \frac{\partial w}{\partial x} \frac{\partial w}{\partial y} \right] dxdy \tag{6.18}$$

The first integral of Eq. (6.18), which represents the bending strain energy, and is a function of the material properties of the plate, leads to the usual bending stiffness matrix. The second integral, developable from geometric considerations, gives rise to the initial-stress stiffness matrix. As discussed previously, the effect of plasticity can be included in the analysis by modifying the bending strain energy. The complete functional

containing the effect of plasticity is presented in Eq. (6.16). It may be introduced into Eq. (6.17) to yield the appropriate element stiffness matrix containing the effect of plasticity.

Since attention is restricted in the present treatment of plastic buckling to flat rectangular panels, the idealizations considered consist of initially flat rectangular discrete elements. Various types of displacement functions used to derive the stiffness matrices for a rectangular bending element are presented in the current literature. In Ref. 53, results obtained using three of these types of displacement functions are compared with exact results for various cases of laterally loaded rectangular plates. One of these, due to Papenfuss (Ref. 54), leads to compatible rotations and deflections along the element interfaces. However, due to the exclusion of a term representing uniform twist in the displacement function, calculations with this element lead to results which do not converge to correct values. Another derivation of the stiffness matrix for this element, using interpolation formulas to arrive at the displacement function, as well as one involving a correction of the aforementioned deficiency, can be found in Ref. 55. The correction was effected by the inclusion of additional terms in the displacement function. The order of the resulting stiffness matrix is increased from 12 x 12 to 16 x 16. Results shown in Ref. 55, using this modified element, indicate rapid convergence to the correct solution. Consequently, this element was chosen for use in most of the buckling calculations in the present investigation.

The initial-stress stiffness matrix based on the Papenfuss displacement function was derived in Ref. 23. This matrix is a subset of the corresponding initial-stress stiffness matrix derivable from the displacement function of Ref. 55. Therefore, all that was necessary to develop the initial-stress stiffness

matrix for the present analysis was to add the contributions of the additional terms of the displacement function of Ref. 55 to the matrix presented in Ref. 23. The resulting initial-stress stiffness matrix, as well as the modified bending stiffness matrix based on the displacement function of Ref. 55, are presented in Appendix I for a rectangular element.

7. DISCUSSION OF RESULTS FROM THE DISCRETE-ELEMENT BUCKLING ANALYSIS

To verify the accuracy of the method of analysis presented in Section 6, a number of calculations were performed on the buckling of flat rectangular plates with various boundary and loading conditions. Results of these calculations are first presented for the elastic buckling of uniformly loaded plates. Then, results of a series of plastic buckling calculations for simply-supported plates with various uniform edge loadings are presented and compared with exact results. Results are finally shown for plastic buckling in cases for which exact solutions are lacking. These are: a) a clamped square plate with a uniform load on two opposite edges, b) a simply-supported square plate with a triangular load distribution on two opposite edges, and c) a simply-supported plate with a uniform edge shear load. All results shown were determined using the eigenvalue formulation in the preceding section entitled Plastic Buckling.

The elastic buckling calculations were performed for the case of a square plate with a uniform compressive load on two opposite edges, for both clamped and simply-supported edge conditions. In each case, the effect of a progressive refinement of the discrete-element idealization was investigated. Results for the elastic buckling coefficient, k, are shown in Tables 1a and 1b for different idealizations using the displacement functions of Papenfuss (Ref. 54), denoted by P, Melosh (Ref. 56), denoted by M, and Bogner, Fox, Schmit (Ref. 55), denoted by BFS. These results are compared with corresponding exact results for k. In Tables 1a and 1b the size of the mesh in the idealization is indicated by $n \times n$, where n denotes the number of element subdivisions along each edge of the plate. Except in the case of the 3×3 idealization, it was

possible to take advantage of the double symmetry of the buckling configuration and treat only one-quarter of the plate.

Referring to the different displacement function representations for the elements simply as "elements," we see that the results corresponding to each element converge monotonically as the idealization is refined. In the case of the P and BFS elements the results are seen to converge from above, and in the case of the M element they converge from below. The BFS and M element results converge to the exact value. The P element results, however, appear to be converging to a value that is higher than the exact value in both the case of the clamped and that of the simply-supported edge condition. For example, in the case of the simply-supported plate, the error appears to be converging toward a value of about +5 percent. Similar observations have been made in connection with the analysis of transversely loaded rectangular plates using this element (Ref. 53).

As indicated in the tables, the results using the M element converge rapidly from below. The error for the finest mesh size (12 x 12) for the simply-supported plate is -.76 percent and for the clamped plate it is -1.45 percent. The results of extensive elastic buckling calculations, using this element, for a wide range of edge support and loading conditions, can be found in Ref. 24. Excellent accuracy is indicated.

The results based on the BFS element exhibit the most rapid convergence and best accuracy. In the case of the simply-supported plate, even the relatively coarse 3 x 3 and 4 x 4 idealizations produce errors that are only +.084 percent and +.026 percent, respectively. Within the limitations of computer accuracy, the results can be said to be exact for the 8 x 8 and the 12 x 12 idealizations. The results for the clamped plate also show

excellent convergence, solutions for the 8 x 8 and 12 x 12 idealizations showing errors of +.124 percent and +.058 percent, respectively, when compared with a series solution presented in Ref. 57.

The fact that solutions provided by the M element converge from below and those provided by the BFS element converge from above, suggests the interesting possibility of establishing upper and lower bounds for the buckling loads of more complex panels. On the basis of the accuracy demonstrated in the elastic buckling problem, the BFS element was chosen for use in the subsequent plastic buckling calculations.

In all of the plastic buckling calculations, the secant and tangent moduli are found using the Ramberg-Osgood stress-strain relation Eq. (A-11) , which is written in terms of two characteristic material constants, $\sigma_{0.7}$ and n. The resulting expressions, formed as ratios to the elastic modulus, are

$$\frac{E_t}{E} = \frac{1}{1 + \frac{3n}{7}\left(\frac{\sigma_i}{\sigma_{0.7}}\right)^{n-1}} \tag{7.1}$$

$$\frac{E_s}{E} = \frac{1}{1 + \frac{3}{7}\left(\frac{\sigma_i}{\sigma_{0.7}}\right)^{n-1}} \tag{7.2}$$

Values of $\sigma_{0.7} = 10^5$ psi and $n = 10$ were used in all the calculations. A curve of effective stress versus effective strain, using these parametric values, is shown in Fig. 26. Since the Ramberg-Osgood relation does not identify a distinct yield point,

all the calculations contain some effect of plasticity. The first noticeable departure from linearity of the curve of Fig. 26 occurs at about $\sigma_i = 70{,}000$ psi.

In order to determine the accuracy of the discrete-element analysis when applied to the plastic buckling problem, a series of computations were performed and the results compared with corresponding exact solutions to the governing equations as presented by Stowell. The cases selected for comparison have simply-supported edge conditions and uniformly distributed loads normal to the boundary.

The solution to the governing equation, Eq. (6.12), for the above boundary conditions and loading situations has the form,

$$w(x,y) = w_{mn} \sin \frac{n\pi x}{a} \sin \frac{m\pi y}{b} \tag{7.3}$$

where a and b are the plate length and width respectively. Substituting Eq. (7.3) into Eq. (6.12) and canceling common trigonometric factors yields,

$$C_1\left(\frac{m\pi}{a}\right)^4 + 2C_3\left(\frac{m\pi}{a}\right)^2\left(\frac{n\pi}{b}\right)^2 + C_5\left(\frac{n\pi}{b}\right)^4 = -\frac{h}{D'}\left[\sigma_x\left(\frac{m\pi}{a}\right)^2 + \sigma_y\left(\frac{n\pi}{b}\right)^2\right] \tag{7.4}$$

Equation (7.4) can be recast in the form,

$$h = \frac{a}{\pi}\left[\frac{9\sigma_*\left(\alpha m^2 + \beta n^2\left(\frac{a}{b}\right)^2\right)}{E_s\left[C_1 m^4 + 2C_3 m^2 n^2\left(\frac{a}{b}\right)^2 + C_5 n^4\left(\frac{a}{b}\right)^4\right]}\right]^{\frac{1}{2}} \tag{7.5}$$

where σ_* is a nominal stress intensity, $\alpha = -\frac{\sigma_x}{\sigma_*}$, $\beta = -\frac{\sigma_y}{\sigma_*}$, and C_1, C_3, C_5, E_s are as defined in the section entitled Plastic Buckling.

Equation (7.5) is used to generate input to the discrete-element program in the following way. For a given aspect ratio, a/b, a critical stress state and a buckling mode shape, m, n, are chosen and substituted into Eq. (7.5). This yields the thickness associated with the chosen buckled configuration and critical stress. The thickness calculated in this manner is used as input to the discrete-element buckling analysis. The resulting buckling stresses are then compared with the stresses used in the determination of the plate thickness from Eq. (7.5).

Using this procedure, critical stresses were found for simply-supported plates with $a/b = 1$ and $a/b = 1.5$, for three different loading situations;

a) $\sigma_x = -\sigma_* \quad , \quad \sigma_y = 0$

b) $\sigma_x = \sigma_y = -\sigma_*$

c) $\sigma_x = 2\sigma_y = -\sigma_*$

The idealization used in these calculations consisted of square elements in a 4×4 grid when $a/b = 1$, and a 6×4 grid when $a/b = 1.5$, as shown in Fig. 27. Symmetry was taken into account, so that it was necessary to consider only one-quarter of the plate.

Calculations were carried out for all three loading situations, with the nominal stress, σ_*, given values in the range 65,000 psi to 125,000 psi. The results are shown in Tables 2 and 3. These results encompass a widely varying degree of plastic

deformation at the critical stress. The tables show the thickness, the corresponding exact value of the nominal stress and the stress computed from the discrete-element analysis. The various loading situations are identified by the parameters, $\alpha = -\frac{\sigma_x}{\sigma_*}$, $\beta = -\frac{\sigma_y}{\sigma_*}$ and $\gamma = -\frac{\tau_{xy}}{\sigma_*}$.

The results for the square plate, shown in Table 2, are based on a buckling mode shape consisting of a half-sine wave in each direction, and indicate agreement which is virtually exact. The maximum error is found to be +.031 percent.

The results for the rectangular plate, shown in Table 3, are based on a buckling mode shape consisting of a full sine wave in the direction of the longer side and a half-sine wave in the direction of the shorter side. Agreement is again seen to be excellent, the maximum error in this case being +.039 percent.

We now consider the case of a clamped square plate loaded uniformly on two opposite edges. Taking into account once more the double symmetry of the buckling configuration, it is necessary to consider only one-quarter of the plate. The idealization that was used is shown in Fig. 28, and corresponds to the 12 x 12 grid discussed in connection with the elastic buckling results presented in Table 1. The error in the elastic case, using this idealization and the BFS element, was +.058 percent. The plate considered has the dimensions, a = b = 20 in.

Calculations were made for various thicknesses, ranging from h = .5 in. to h = .8 in. This thickness range corresponds to a range of buckling stress from a value close to the elastic limit up to a value well into the plastic range. Table 4 shows both plastic and elastic buckling stresses corresponding to the various thicknesses. As the state of stress penetrates further into the

plastic range, the material stiffness decreases, so that the plastic buckling stress decreases relative to the corresponding elastic buckling stress. For $h = .8$ in., the maximum thickness considered, this decrease amounts to 44.8 percent. This can be seen graphically in Fig. 29, which shows the plasticity reduction factor, η, defined as the ratio of the plastic buckling stress to the elastic buckling stress, $\frac{\sigma_p}{\sigma_e}$, plotted versus the plastic buckling stress.

The next case considered is that of a simply-supported square plate with a triangular distribution of load on two opposite edges. It was selected to demonstrate the applicability of the method to nonconstant stress field situations. As mentioned previously, the Stowell formulation of the plastic buckling problem involves the assumption of a uniform stress state throughout the plate. This does not preclude the use of this formulation in a discrete-element analysis of a plate which is not uniformly stressed. The stress can still be considered to be uniform within each element, but can vary from element to element. The stress distribution is thus approximated in the form of finite jumps over the planform of the plate. The state of plasticity, consistent with the Stowell formulation, is therefore constant within each discrete-element. By taking advantage of the single symmetry of the buckling mode, only one-half of the plate need be considered. The idealization of the half-plate consists of thirty-two square elements, as shown in Fig. 30. The idealized stress distribution is also shown in Fig. 30.

To check the accuracy obtainable with such an idealization, an elastic case for a simply-supported square plate, $a = b = 20$ in., was analyzed. Based on a nominal stress of $\sigma_x = 1$ at $y = 0$, for the actual triangular load, the idealized nominal stress intensities vary from .9375 in elements located at $0 \leq y/b \leq .125$

to .0625 in elements located at $.875 \leq y/b \leq 1$, as shown in Fig. 30. The exact solution, taken from Ref. 58, can be written in the form, $\sigma_* = k \frac{E\pi^2 t^2}{12(1 - \nu^2)b^2}$, where σ_* is the stress intensity at $y = 0$, and k is the elastic buckling coefficient. For the case considered, Ref. 58 gives a value of 7.8 for k. The discrete-element analysis yielded the value, $k = 7.8068$, which represents an error of only +.087 percent.

Plastic buckling calculations were carried out using the same idealization, for thicknesses ranging from $h = .5$ in. to $h = 1$ in. The results, in the form of the idealized critical stress distribution in the y direction, are presented in Table 5a. Each case represents a different degree of plastic deformation. The case, $h = .5$ in., can be considered to be fully elastic. As a consequence of not defining a definite yield point, however, there is still a small reduction of the buckling stress due to the inclusion of a small plasticity effect. As seen in Fig. 26, a noticeable departure from linearity in the stress-strain relation occurs at about 70,000 psi. Therefore, based on this value as the yield stress, we can trace an elastic plastic boundary in the idealized structure. This boundary is indicated by a dashed line in Table 5a. As the thickness increases, the number of elements stressed beyond the yield point at the critical load also increases. When $h = 1$ in., half the plate is in the plastic range when the critical stress is reached.

In Table 5b, the normalized buckling stress (the maximum value in the triangular distribution) is shown for the various thicknesses, compared with the corresponding elastic results. The plasticity reduction factor, η, is shown in Fig. 31, plotted versus the plastic buckling stress.

The effectiveness of the BFS element when applied to the buckling analysis of a plate loaded in pure shear is considered next. The case of a simply-supported square plate, with an idealization consisting of a 6 x 6 grid of square elements, as shown in Fig. 32, was studied. Calculations to determine the elastic buckling coefficient, using this idealization, yielded the value, $k = 9.3458$, as compared to a value of 9.34 given by a series solution (Ref. 58).

The results of plastic buckling calculations are shown in Table 6. As before, the plastic buckling stress is compared with corresponding elastic buckling results for a range of thicknesses. The plasticity reduction factor, η, is shown plotted versus the plastic buckling stress in Fig. 33.

8. THERMAL EFFECTS ON PLASTIC DEFORMATION

No specific consideration has been given to thermal effects in the presentation and discussion of methods of structural analysis in the preceding sections. We now give brief consideration to this problem.

In the case of elastic analysis, the treatment of thermal effects is routine. The elastic constants can be introduced as known functions of temperature, and thermal strains can be introduced as initial strains into Eqs. (3.1) and (3.5). The variation of the elastic constants with temperature requires that the influence coefficient matrices be recomputed with each change in temperature, unless the temperature distribution can be presumed to remain uniform, the structure is constructed of a single isotropic material, and Poisson's ratio does not change. The problem is essentially one of programming detail.

In the case of plastic analysis, thermal strains can still be introduced as initial strains and simply added to the initial strains associated with plastic deformation. However, we now have, in addition, the vexing problem of temperature effects on the plastic behavior of the material. In treating this problem, it is advantageous to distinguish between two rather different situations as follows: 1) The temperature can be assumed to remain constant during any individual cycle of load application, but vary from one cycle to another. 2) Simultaneous changes in temperature and load can occur within a given cycle of loading and must be taken into account.

Experimental data applicable to either of these situations are largely lacking. The available experimental data on temperature effects in plasticity appear to be limited to uniaxial tests

involving monotonic loading of virgin materials at various temperatures (Refs. 59-61). Such data do not really provide information applicable even to the first situation mentioned above. Even data on cyclic loading into the plastic range at constant temperature, from tests performed at a variety of temperature levels, are lacking, as pointed out in Ref. 62.

In view of the dearth of information on thermal effects on plastic behavior, consideration of the problem is limited here to a necessarily tentative and heuristic approach, making use of data obtained from elevated temperature tests on virgin materials. In the simpler case of constant temperature within individual loading cycles, we modify the parameters associated with plastic behavior in each loading cycle to correspond to the temperature in that cycle.

When the stresses are uniaxial and we can assume linear strain-hardening, we simply introduce values of yield stress, σ_o, and hardening coefficient, c, appropriate to the temperature level in each cycle, disregarding the effect of prior yielding in previous cycles. In the case of nonlinear strain-hardening, the Ramberg-Osgood approximation can be used to represent the stress-strain relation, and the parameters in this relation can be treated as functions of temperature. That is, we can write the inverse of the hardening coefficient as,

$$\frac{1}{c^{(k)}_{(T)}} = \frac{3\, n_{(T)}}{7E_{(T)}} \left[\frac{\sigma^{(k)}}{\sigma_{0.7(T)}}\right]^{n_{(T)}-1} \tag{8.1}$$

An experimental investigation (Ref. 35) has been performed to determine the variation of the Ramberg-Osgood parameters with temperature for virgin materials at elevated temperatures. Stress-strain curves for tensile loading at various temperatures are presented in Refs. 59 and 61. In addition, data on the variation of secant and tangent moduli with stress for various materials in compression at elevated temperatures are presented in Ref. 60.

The variation of the yield stress, σ_o, with temperature, has been the subject of several experimental investigations (Refs. 59-61). The results indicate a decrease in the yield stress with increasing temperature. One relation between the yield stress and temperature is that suggested in Ref. 59, and written as follows,

$$\sigma_0 = A - \left(\frac{T + B}{\log h + C}\right) \tag{8.2}$$

where A, B, and C are constants characterizing the material, T is the temperature at which the yield stress is to be determined, and h is the temperature rate.

The decrease of the yield stress with increasing temperature in the uniaxial case implies a decrease in the volume (or area) contained by the yield surface (or yield curve) in the multiaxial case. Thus, in the present case of constant temperature during any individual cycle of load application, with variation of temperature from one cycle to the next, the following modifications may be made to the solution techniques for each successive load cycle:

1) Compute the thermal strains and add them to the inelastic strains.

2) Determine the hardening coefficient on the same basis as in Appendix A, Eq. (A-13) or on such

other improved basis as may subsequently be developed to replace that of Appendix A. The parameters involved are given values appropriate to the current temperature.

3) Adjust the size of the yield surface on the basis of the value of the yield stress corresponding to the temperature in the current cycle.

Consideration of simultaneous changes in load and temperature will clearly require a more complex modification of the existing solution procedures. We have seen that, in the case of isothermal plasticity, the yield function, f, is a function of σ_{ij} and α_{ij}, as indicated in Eq. (2.2). In treating nonisothermal plasticity, it will be assumed that there exists a function of the state variables, $g(\sigma_{ij}, \alpha_{ij}, T)$, such that $g < 0$ for elastic states, and $g = 0$ for plastic states. This assumption was initially employed by Prager (Ref. 63) to determine the nonisothermal constitutive plasticity relations.

When a solid is in the plastic state $(g = 0)$, infinitesimal changes in temperature and stress will lead to neighboring states, which can be elastic or plastic. Since

$$g = g(\sigma_{ij}, \alpha_{ij}, T) \tag{8.3a}$$

we can write

$$dg = \frac{\partial g}{\partial \sigma_{ij}} d\sigma_{ij} + \frac{\partial g}{\partial \alpha_{ij}} d\alpha_{ij} + \frac{\partial g}{\partial T} dT \tag{8.3b}$$

If $dg < 0$, the changes of temperature and stress constitute unloading from the plastic state; consequently $d\alpha_{ij} = 0$, and

$$\frac{\partial g}{\partial \sigma_{ij}} d\sigma_{ij} + \frac{\partial g}{\partial T} dT < 0 \tag{8.4a}$$

If

$$\frac{\partial g}{\partial \sigma_{ij}} d\sigma_{ij} + \frac{\partial g}{\partial T} dT = 0 \tag{8.4b}$$

and the material is strain-hardening, there is no further plastic deformation, and the condition expressed by Eq. (8.4b) is neutral loading. The corresponding condition for the existence of neutral loading in the isothermal case is given in Eq. (2.6b). Equation (8.4b) also applies to perfectly plastic behavior.

When

$$\frac{\partial g}{\partial \sigma_{ij}} d\sigma_{ij} + \frac{\partial g}{\partial T} dT > 0 \tag{8.4c}$$

there will necessarily be plastic deformation, and Eq. (8.4c) indicates loading from one plastic state to another. Since $g = 0$ and is not defined for values greater than zero, dg cannot be positive. It therefore follows that $d\alpha_{ij}$ is nonzero in this case.

If we assume that the effect of temperature is to change the size of the yield surface, without changing its shape or orientation, the von Mises yield condition may be written as,

$$g(\sigma_{ij}, \alpha_{ij}, T) = (\sigma_x - \alpha_x)^2 - (\sigma_x - \alpha_x)(\sigma_y - \alpha_y) + (\sigma_y - \alpha_y)^2 + 3(\tau_{xy} - \alpha_{xy})^2 - \sigma_o^2(T) = 0 \tag{8.5}$$

We thus find that,

$$\frac{\partial g}{\partial \alpha_{ij}} = - \frac{\partial g}{\partial \sigma_{ij}} \tag{8.6}$$

Equation (8.3b) becomes

$$dg = (d\sigma_{ij} - d\alpha_{ij}) \frac{\partial g}{\partial \sigma_{ij}} + \frac{\partial g}{\partial T} dT = 0 \tag{8.7}$$

If, as before, we recognize that the vector $cd\epsilon_{ij}$, shown in Fig. 39, approximates the projection of $d\alpha_{ij}$ on the exterior normal to the loading surface at the instantaneous stress state, Eq. (8.7) becomes

$$(d\sigma_{ij} - cd\epsilon_{ij}) \frac{\partial g}{\partial \sigma_{ij}} + \frac{\partial g}{\partial T} dT = 0 \tag{8.8}$$

The flow law can be written in terms of g, as follows,

$$d\epsilon_{ij} = d\lambda \frac{\partial g}{\partial \sigma_{ij}} \tag{8.9}$$

and substitution of Eq. (8.9) into Eq. (8.8) results in the following expression for $d\lambda$,

$$d\lambda = \frac{1}{c_{(T)}} \frac{\frac{\partial g}{\partial \sigma_{ij}} d\sigma_{ij} + \frac{\partial g}{\partial T} dT}{\left(\frac{\partial g}{\partial \sigma_{k\ell}}\right) \left(\frac{\partial g}{\partial \sigma_{k\ell}}\right)} \tag{8.10}$$

where the hardening coefficient, c, is a function of the instantaneous temperature level, as well as the previous history of temperature and stress.

If we now consider Ziegler's modification to Prager's rule, Eq. (2.10), and substitute this expression for $d\alpha_{ij}$ into Eq. (8.7), we find that the expression for the proportionality factor, $d\mu$, becomes

$$d\mu = \frac{\frac{\partial g}{\partial \sigma_{ij}} d\sigma_{ij} + \frac{\partial g}{\partial T} dT}{(\sigma_{k\ell} - \alpha_{k\ell}) \frac{\partial g}{\partial \sigma_{k\ell}}} \tag{8.11}$$

Application of the above relations to plastic analysis requires a knowledge of the effect of temperature on the initial yield stress, σ_o, and the hardening coefficient, c. As discussed previously, while some data on initial yield exist, data on the hardening coefficient are lacking. Much further effort in this area is required.

All of these procedures have been programmed for digital computation. Application has been made to three different sample structures, namely, a stiffened panel, a notched bar, and a simplified swept wing structure. Results for cyclic loading in the case of the notched bar have been compared with available experimental data and found to show good agreement.

The methods discussed above determine the stress and strain response of the structure to applied loading. Criteria for plastic collapse, to be used in conjunction with these methods, have been established, and partially tested in computations on the stiffened panel.

The method developed for plastic buckling analysis applies a deformation theory of plasticity in conjunction with a discrete-element treatment based on the matrix displacement method. It has been developed in detail for application to rectangular plates with a wide variety of edge loadings and boundary conditions and has been programmed for digital computation. Computed results indicate good accuracy with a relatively coarse network of elements. The method can be readily applied to cases that would be difficult to analyze on a continuum basis. Where necessary, the methods previously discussed can be used to determine the stresses in the unbuckled configuration, and the buckling analysis can then be used in testing for stability at various load levels.

The digital computer programs implementing the methods developed in the present study are presented in a separate report, NASA CR- 66364.

Certain limitations in the methods as developed suggest directions for future effort. In the case of the methods for the plastic analysis of unbuckled structures, these are itemized and discussed as follows:

1. The methods, for the most part, involve the assumption of a uniform stress and strain field within the individual discrete elements in the idealization. It would be desirable to provide for a linear distribution of stress and strain in the elements. This would permit the use of a coarser idealization.

2. There is, at present, a limitation to membrane stress in the discrete-elements. It would be desirable to provide also for bending in the elements. This would permit the analysis of plate bending and of shells in which bending of the wall, as well as membrane action, is important.

3. The treatment of plasticity is straightforward when perfectly plastic behavior or linear strain-hardening can be assumed. In the case of nonlinear strain-hardening, however, the determination of the hardening coefficient in the incremental stress-strain relations requires further study. Much more experimental information will have to be generated before a satisfactory disposition of this problem can be made. In fact, a satisfactory experimental basis for the prediction of the general hardening behavior of structural metals is still largely lacking, particularly with respect to cyclic loading and intermittent loading of an arbitrary nature.

4. The assumption of geometric linearity is unduly restrictive in some applications. The development of methods capable of taking simultaneous account of finite deflections and plastic deformation is desirable.

5. In work performed elsewhere, it has been indicated that the use of flat elements in the analysis of curved shells can introduce substantial errors. Work is currently under way to develop appropriate curved elements for elastic analysis. This work should be extended to include plastic effects.

6. While work has already been done on discrete-element methods for plastic analysis with initial anisotropy, it does not treat the case of stress reversal into the plastic range. An extension of the methods of this report to include initial anisotropy would be particularly important in the treatment of composite materials.

7. The criteria for plastic collapse presented here require further testing to establish their practicability.

8. Experimental data on the plastic behavior of materials under varying temperature conditions are very limited. A substantial effort in this area is needed.

In the case of plastic buckling, further work is needed to develop the basic procedure of this report for application to a wider class of structures, particularly stiffened and unstiffened shells. A capability of treating buckling of the "top-of-the-knee" variety is desirable, particularly in view of indications that plastic buckling is especially sensitive to initial imperfections. Such a treatment could stem from methods discussed above for the combined finite-deflection and plastic analysis of structures.

APPENDIX A

A Discussion of Some Pertinent Plasticity Theories

In the following, some of the currently available plasticity theories, including the theory chosen for use in the present investigation, are reviewed and examined for their applicability to the problem of cyclic loading into the plastic range. A better understanding of the various theories may be facilitated by reviewing first some of the terminology and concepts employed in the theory of plasticity.

In simple tension or compression, the elastic limit of a material is represented by a single value of stress or strain. However, in the case of multiaxial stress, a single value or a finite number of values of stress or strain cannot be used to define the boundary of the elastic range. A functional representation, constituting a generalization of the yield point associated with uniaxial stress, is required. In this representation, some appropriate function of the stress components is equated to zero. In the case of initial yielding, the function is termed the yield function and the equation constitutes the yield condition. In the case of subsequent yielding from a plastic state, the function is referred to either as the subsequent yield function or the loading function (Ref. 64), and the equation represents the subsequent yield condition or loading condition.

The yield and loading conditions can be given a geometrical interpretation. When plotted in stress space, that is, a space in which the coordinates are components of stress at a point, they determine surfaces in that space. These surfaces are referred to as yield surfaces and loading surfaces, respectively. In the most general case the stress space has nine dimensions, but may have

fewer dimensions if symmetry of the stress tensor is taken into account or if certain of the stress components are always zero. When the material is elastic, perfectly plastic, the loading surfaces are coincident with the yield surface. In the case of strain-hardening, the loading surface changes continuously as yielding proceeds, the variation depending upon the strain-hardening characteristics of the material. Analytically, it is evidenced by a dependence of the loading function on both the current state of stress and the history of stress.

The yield condition (or yield surface) can be represented as

$$f(\sigma_{ij}) = 0 \tag{A-1}$$

where σ_{ij} is the stress tensor, and $f(\sigma_{ij})$ is the yield function, and the loading function (or loading surface) can be represented as

$$f(\sigma_{ij}, \alpha_{ij}) = 0 \tag{2.2}$$

where α_{ij} is a measure of the degree of work hardening.

The simplest form of the yield condition is the Tresca yield condition. This condition is based on the assumption that the material yields whenever the maximum shear stress reaches a critical value. Mathematically, it can be represented as

$$(\sigma_{max} - \sigma_{min}) = K \tag{A-2}$$

where σ_{max} and σ_{min} are the maximum and minimum principal stresses, and K is the uniaxial yield stress in tension. Geometrically, the Tresca yield condition is represented as a piecewise linear surface.

Another simple and easily applied yield condition is the von Mises yield condition. Mathematically, this condition implies that yielding occurs whenever the second invariant of the deviatoric stress tensor, J_2', equals some critical value. Equivalent interpretations of this yield condition are:

1) Yielding begins whenever the internal energy of distortion exceeds a certain value.

2) Yielding begins whenever the shear stress on an octahedral plane exceeds a certain limit, the octahedral plane being referred to the principal stress directions.

Geometrically, the von Mises yield function is represented as a smooth surface in stress space.

In the present analysis, the von Mises function was chosen for use as the yield function. Although the functional representation of a piecewise linear yield surface is simpler than the von Mises function, the choice of the smooth surface eliminates the necessity of considering singular regimes (corners), as in the case of the piecewise linear Tresca yield surface.

Since we shall be concerned with cases of plane stress only, for which $\sigma_z = \tau_{xz} = \tau_{yz} \equiv 0$, the von Mises yield condition can be represented by Eq. (2.1), which defines the yield surface as an ellipsoid in σ_x, σ_y, and τ_{xy} stress space,

$$f(\sigma_{ij}) = \sigma_x^2 - \sigma_x\sigma_y + \sigma_y^2 + 3\tau_{xy}^2 - \sigma_o^2 = 0 \qquad (2.1)$$

where σ_o is the yield stress in tension.

The form of the loading function will be considered shortly.

On the basis of Drucker's postulate (Ref. 65), which states that the work done by an external agency during a complete cycle of loading and unloading must be nonnegative, the following two requirements must be satisfied:

1) The yield and loading surfaces must be convex with respect to the origin in stress space.

2) The plastic strain increment vector must lie on the outward normal to the loading surface at the instantaneous stress state.

The ellipsoid given by Eq. (2.1) satisfies the convexity condition imposed upon the yield surface. The second requirement provides a means of obtaining a constitutive relation among the plastic strain increment and stresses and stress increment. This constitutive relation, termed the flow rule, is given in Eq. (2.7), and for completeness is rewritten here as follows,

$$d\epsilon_{ij} = d\lambda \frac{\partial f(\sigma_{ij}, \alpha_{ij})}{\partial \sigma_{ij}} \tag{2.7}$$

where $d\lambda$ is a positive scalar quantity.

The flow rule leads to an incremental or flow theory of plasticity, in which there is path dependence of a final state of stress and strain as reached from some previous state. Flow theory is, in general, distinct from the deformation theory of plasticity, in which the total plastic strains are related to the final stress state. According to this latter theory, a relationship between final states of stress and strain exists for any given loading process, unloading being specified by a separate law. In the case of proportional loading, in which the stress vector remains fixed in direction, flow and deformation theories coincide.

Assuming Drucker's postulate to constitute a criterion for physical soundness, Budiansky (Ref. 66) has shown deformation theories to be consistent with this postulate only for loading paths in the vicinity of proportional loading. Since the problem under consideration is concerned with general loading paths, including reversed loading, the use of deformation theory was not considered to be appropriate. Thus, the flow theory of plasticity was chosen for use on the basis of its more general validity.

Having selected a yield condition and a flow law, we must now consider the choice of a loading function to be used. The loading function will represent a convenient mathematical idealization of some macroscopically observed behavior. It should have the ability to describe quantitatively hardening behavior as determined from experimental results for a particular material.

There have been several hardening rules proposed for use in the plastic analysis of structures. The choice of a specific hardening rule will depend upon the ease with which it can be applied in the method of analysis to be used, in addition to its capability of representing the actual hardening behavior of structural metals. These requirements, together with the necessity of maintaining mathematical consistency with the yield function, constitute the criteria for the final choice of the hardening rule. An appraisal of the various hardening rules currently available is now presented. These are:

Isotropic Hardening - This theory assumes that during plastic flow the loading surface expands uniformly about the origin in stress space, maintaining the same shape, center and orientation as the yield surface. Figure 34 illustrates, on the basis of a simplification to a two-dimensional plot, the yield and loading surfaces when the stress state shifts from point 1 to 2. Unloading and subsequent reloading in the reverse direction will result

in yielding at the stress state represented by point 3. The path 2-3 will be elastic and 0-2 is equal to 0-3.

It is seen that the isotropic type of representation of work hardening does not account for the Bauschinger effect exhibited by most structural materials. In fact, this theory provides that, due to work hardening, the material will exhibit an increase in the compressive yield stress equal to the increase in the tensile yield stress. Furthermore, since plastic deformation is an anisotropic process, it cannot be expected that a theory which predicts isotropy in the plastic range will lead to realistic results when complex loading paths, involving changes in direction of the stress vector in stress space (not necessarily completely reversed), are considered. This conclusion has been indicated experimentally in Refs. 67-70.

Thus, despite its mathematical simplicity, isotropic hardening was rejected for use in this analysis because of its inability to describe a realistic hardening behavior.

Slip Theory - Utilizing the physical concept of slip surfaces in crystals, Batdorf and Budiansky (Ref. 71) have developed a theory which describes a loading surface that is distorted relative to the yield surface and previous loading surfaces. This theory predicts the formation of corners at the instantaneous stress state on the loading surface during plastic deformation. A representation of the growth of the yield function in going from a stress state at the origin, 0, to the final state represented by point 3, is given in Fig. 35. In this figure, the unshaded region is that enclosed by the yield surface, and the various shaded regions indicate the stages in the formation of the loading surfaces in going from 0 to 3.

Since the stress state is almost always in a corner, the resulting constitutive relation between stresses and strains becomes quite complex. For this reason this theory was rejected for application in the present investigation. Although there are some experimental results indicating the formation of corners and the distortion of the loading surface (Refs. 27, 68 and 69), these results and those of Ref. 72 do not fully substantiate the behavior represented by slip theory. Furthermore, the Bauschinger effect is not taken into account.

Piecewise Linear Plasticity - In this representation, the yield surface consists of a finite number of plane surfaces, whose intersections constitute corners. The oldest and most widely used piecewise linear yield surface is that associated with the Tresca yield condition, represented in Eq. (A-2). The loading surface is assumed also to consist of plane surfaces, and the subsequent hardening behavior can be classified as

(1) The hardening rule of independent plane loading surfaces: One of the earliest discussions of this representation of the hardening behavior is given in Ref. 73 and is illustrated in Fig. 36a. As seen from this figure, in which σ_1 and σ_2 are the only nonzero stress components, a loading path, 0-2, in any quadrant of the stress plane does not affect the loading surface in the remaining quadrants. Thus, this hardening rule does not take the Bauschinger effect into account.

(2) The hardening rule of interdependent loading surfaces: This type of hardening rule, originally proposed by Hodge (Ref. 74), is a generalization of the hardening rule described in (1). By specifying a dependence between the planes that comprise the loading surface, a loading path intersecting any one plane of this surface may effect changes in each of the remaining planes. As illustrated in Fig. 36b, this hardening rule can be used to specify any

piecewise linear loading surface, and is capable of taking the Bauschinger effect into account.

A special case of the interdependent loading surfaces is considered in Ref. 75. It is assumed that plastic strain is due to slipping along three independent slip planes, along any one of which the shear is a maximum. Piecewise linear stress-strain relations are written in terms of coefficients representing the hardening behavior of the material. These coefficients are functions of stress and are dependent upon a linear strain-hardening rule employed in the analysis. By specifying the correspondence between various segments of the yield surface and the slip planes, total plastic strains for any loading are computed as the sum of the contributions from the three independent sets of slip planes. It is further assumed that the corresponding segments of the yield surface must maintain a constant elastic range from positive to negative yielding. An illustration of the subsequent loading surfaces determined in this way is shown in Fig. 36c. It is seen from this figure that the Bauschinger effect can be taken into account.

Of the hardening rules discussed thus far, the hardening rule of interdependent loading surfaces is the most general. However, its generality is limited to piecewise linear yield surfaces. Thus, the use of interdependent loading surfaces would not be mathematically consistent with the von Mises yield function, previously discussed and chosen for use in the analysis.

Kinematic Hardening - The hardening behavior postulated in this theory assumes that, during plastic deformation, the loading surface translates as a rigid body in stress space, maintaining the size, shape and orientation of the yield surface. The primary aim of this theory, due to Prager (Refs. 29 and 30), is to provide

a means of accounting for the Bauschinger effect. For piecewise linear yield surfaces, kinematic hardening may be considered to be a special case of the hardening rule of interdependent loading surfaces. However, it is not limited to piecewise linear yield surfaces.

An illustration of kinematic hardening, as applied in conjunction with the von Mises yield curve in the σ_1, σ_2 plane, is provided in Fig. 37. The yield surface and loading surface are shown in this figure for a shift of the stress state from point 1 to point 2. Denoting the translation of the center of the yield surface by α_{ij}, the loading function, f, may be represented in the form $f(\sigma_{ij} - \alpha_{ij})$ and the subsequent yield condition is given by Eq. (2.8) and rewritten here as follows,

$$f(\sigma_{ij} - \alpha_{ij}) = 0 \tag{2.8}$$

As a consequence of assuming a rigid translation of the loading surface, kinematic hardening predicts an ideal Bauschinger effect for completely reversed loading conditions. That is, the magnitude of the increase of yield stress in one direction will result in a decrease of yield stress of the same magnitude, in the reversed direction. Kadashevitch and Novozhilov (Ref. 76) have concurrently developed a hardening rule identical to Prager's kinematic hardening rule. In their theory, the total translation of the yield surface is regarded as being associated with "internal microstresses" which remain in the body upon unloading. It is these internal microstresses which are considered to be responsible for the Bauschinger effect.

Since the kinematic hardening theory does take into account the essential features of plastic deformation and, specifically, reversed plastic deformation, and since it is conceptually simple

and easily applied in an analytical procedure, it was chosen for use in the present investigation. Furthermore, experiments concerned with the determination of subsequent yield surfaces (Ref. 77) indicate approximate agreement with the translational behavior of the yield surface predicted by kinematic hardening.

This hardening theory, as set forth by Prager, predicts that the increments of translation of the loading surface in 9-dimensional stress space occur in the direction of the exterior normal to the surface at the instantaneous stress state. However, as indicated in Refs. 78-80, inconsistencies arise when the theory is applied in various subspaces of stress, that is, when the symmetry of the stress tensor is taken into account or when there are zero stress components.

Denoting zero stress components by σ''_{ij} and nonzero components by σ'_{ij}, the yield function, $f(\sigma_{ij})$, can be written as

$$f(\sigma_{ij}) = \left[f(\sigma'_{ij}, \sigma''_{ij}) \right]_{\sigma''_{ij}=0} = g(\sigma'_{ij}) \tag{A-3}$$

where $g(\sigma'_{ij})$ is the yield function written in terms of the nonzero stress components. However, as indicated in Ref. 64, after some plastic deformation the loading function, Eq. (2.8), cannot be represented only in terms of the nonzero stress components when Prager's hardening rule is used; that is,

$$f(\sigma_{ij} - \alpha_{ij}) = f(\sigma'_{ij} - \alpha'_{ij}, \alpha''_{ij}) \neq g(\sigma'_{ij} - \alpha'_{ij}) \tag{A-4}$$

since $\sigma''_{ij} = 0$ does not imply $\alpha''_{ij} = 0$. Thus, Prager's rule is not invariant with respect to subspaces of stress.

A means of circumventing this difficulty is provided by the introduction of direct kinematic hardening. Zero stress components are deleted initially in the formation of the yield function and, therefore, do not appear in the loading function. Thus, the inconsistency indicated in Eq. (A-4) does not occur since the behavior in 9-dimensional stress space is never considered. However, it has been indicated in Ref. 80 that, in consequence, direct kinematic hardening can only serve as an approximation to complete kinematic hardening, where all components of translation of the yield surface are considered.

In both direct and complete kinematic hardening, the increment of translation of the loading surface, denoted by $d\alpha_{ij}^{(P)}$ in Fig. 38, is in the direction of the exterior normal to the loading surface. This geometrical relation can be expressed analytically by

$$d\alpha_{ij} = c\,d\epsilon_{ij} \tag{A-5}$$

where $d\epsilon_{ij}$ is the increment of plastic strain, which, according to the flow rule, Eq. (2.7), is in the direction of the exterior normal to the loading surface, and c is a parameter characterizing the hardening behavior of the material.

The inconsistencies mentioned in connection with Prager's rule produce the result that the loading surface will not, in general, translate in the direction of the exterior normal in a subspace of stress when it is made to do so in the full 9-dimensional stress space. Reference 79 specifies stress conditions under which a linear transformation of variables enables the loading surface, in the transformed subspace, to translate in the direction of the exterior normal. It is also indicated in Ref. 79 that the application of Prager's rule to the Tresca yield condition, in the case in which more than one normal stress is zero, results in a deformed yield locus.

In order to avoid the difficulties associated with the implementation of complete kinematic hardening, Ziegler (Ref. 25) has proposed a modification of Prager's rule. This modification replaces Eq. (A-5) with the expression for the increment of translation given in Eq. (2.10) and rewritten here as follows,

$$d\alpha_{ij} = d\mu(\sigma_{ij} - \alpha_{ij}) \qquad d\mu > 0 \tag{2.10}$$

The geometrical significance of this modification is shown in Fig. 38. In this figure, the increment of translation, $d\alpha_{ij}^{(P)}$, computed on the basis of Prager's rule is compared with the increment of translation, $d\alpha_{ij}^{(Z)}$, computed on the basis of Ziegler's modified rule. Note that in the latter case the increment of translation, $d\alpha_{ij}^{(Z)}$, is in the direction of the vector from the center of the yield or loading surface to the stress state.

The scalar, $d\mu$, appearing in Eq. (2.10), is determined from the condition that the stress state must remain on the translated loading surface during plastic deformation. From Fig. 39 it is seen that this condition may be represented as

$$(d\sigma_{ij} - d\alpha_{ij}) \frac{\partial f}{\partial \sigma_{ij}} = 0 \tag{A-6}$$

Substituting Eq. (2.10) into Eq. (A-6),

$$d\mu = \frac{\frac{\partial f}{\partial \sigma_{ij}} d\sigma_{ij}}{(\sigma_{ij} - \alpha_{ij}) \frac{\partial f}{\partial \sigma_{ij}}} \tag{A-7}$$

An expression for the scalar factor, $d\lambda$, associated with the flow rule, Eq. (2.7), can be determined by recognizing that the vector $cd\epsilon_{ij}$, shown in Fig. 39, is approximately the projection of $d\sigma_{ij}$ on the exterior normal to the loading surface at

the instantaneous stress state. Thus, for small increments of stress and strain, we can write

$$(d\sigma_{ij} - c d\epsilon_{ij}) \frac{\partial f}{\partial \sigma_{ij}} = 0 \tag{A-8}$$

Using the flow rule, Eq. (2.7), to substitute for $d\epsilon_{ij}$ in Eq. (A-8), results in the following expression for $d\lambda$,

$$d\lambda = \frac{1}{c} \frac{\frac{\partial f}{\partial \sigma_{ij}} d\sigma_{ij}}{\left(\frac{\partial f}{\partial \sigma_{k\ell}}\right)\left(\frac{\partial f}{\partial \sigma_{k\ell}}\right)} \tag{A-9}$$

The flow rule now becomes,

$$d\epsilon_{ij} = \frac{1}{c} \frac{\partial f}{\partial \sigma_{ij}} \frac{\frac{\partial f}{\partial \sigma_{mn}} d\sigma_{mn}}{\left(\frac{\partial f}{\partial \sigma_{k\ell}}\right)\left(\frac{\partial f}{\partial \sigma_{k\ell}}\right)} \tag{2.11}$$

The results in Eqs. (2.16) and (2.17) are equally applicable when Prager's rule or Ziegler's modification is used.

The application of Ziegler's modification, Eq. (2.12), results in the following equality,

$$f(\sigma_{ij} - \alpha_{ij}) = f(\sigma'_{ij} - \alpha'_{ij}, \sigma''_{ij} - \alpha''_{ij}) = g(\sigma'_{ij} - \alpha'_{ij}) \tag{A-10}$$

where $\sigma'_{ij} \neq 0$ and $\sigma''_{ij} = 0$ implies $\alpha''_{ij} = 0$.

Thus, there is no inconsistency between the behavior in any subspace and in the full 9-dimensional stress space, and the loading surface will translate without distortion in the former when it is presumed to do so in the latter.

The loading function for plane stress can now be written in terms of the nonzero stress components, and for the von Mises yield condition is given in Eq. (2.9), rewritten here as follows,

$$f(\sigma_{ij},\alpha_{ij}) = (\sigma_x - \alpha_x)^2 - (\sigma_x - \alpha_x)(\sigma_y - \alpha_y) + (\sigma_y - \alpha_y)^2 + 3(\tau_{xy} - \alpha_{xy})^2 - \sigma_o^2 = 0 \tag{2.9}$$

Comparisons between Prager's rule and the modification of Ziegler, Ref. 25, indicate that, in general, the two rules do not coincide. However, as shown by Nagdhi (Ref. 64), the application of Prager's rule results in a translation of the loading surface, coincident with that predicted by Ziegler's modification, in the case of plane stress, with the following additional conditions:

(1) The von Mises yield condition is used,

(2) The hardening coefficient is constant.

A multiaxial hardening coefficient -

The implementation of any hardening rule requires a knowledge of the inelastic behavior of the material. In the case of kinematic hardening, the parameter characterizing the inelastic behavior of a given material is the quantity c in Eq. (A-9). In the general case of nonlinear strain hardening, c is a variable quantity. It can, in fact, be expected that, even for a given position of the loading surface, c will vary with the location of the stress state on the loading surface.

The material properties generally used in inelastic analysis are obtained from simple tensile or compressive tests of samples of the material. If the structure to be analyzed is in a state

of uniaxial stress, the stress-strain relation is identical to that obtained from the tension or compression tests. The hardening coefficient c can then be taken simply as the slope of the stress versus plastic strain curve at the current stress level. This is illustrated in Fig. 40, where $c^{(k)}$ is the value of c corresponding to the stress $\sigma^{(k)}$ at the k^{th} step in the incremental procedures described in Section 3.

If the state of stress is multiaxial, there exists no established procedure for the specification of c on the basis of uniaxial test data. This differs from isotropic hardening theory, in which the states of stress and strain are characterized by single scalar quantities referred to as effective stress and effective strain, respectively. The relationship between these two quantities can be based on the uniaxial stress-strain relation for the material. In the present application of the kinematic hardening theory, a heuristic approach to this problem is proposed, based on an averaging procedure using data from simple tests. In this procedure we treat each stress component as though it alone were present, and determine a corresponding value for c, denoted c_{ij}, on the basis of a uniaxial stress-strain curve, or a stress-strain curve for pure shear. These curves are based on the Ramberg-Osgood representation of the stress-strain relation (Ref. 50),

$$e = \frac{\sigma}{E} + \frac{3\sigma}{7E}\left[\frac{\sigma}{\sigma_{0.7}}\right]^{(n-1)} \qquad \text{(A-11)}$$

where n is a shape parameter given by

$$n = 1 + \frac{\log(17/7)}{\log(\sigma_{0.7}/\sigma_{0.85})}$$

e is the total strain, E is the slope of the linear portion of the stress-strain curve, and $\sigma_{0.7}$ and $\sigma_{0.85}$ are the stresses at which the curve has secant moduli of 0.7E and 0.85E, respectively.

We recognize the nonlinear term in Eq. (A-11) as the plastic strain and use it in determining the inverse of the hardening coefficient evaluated at the k^{th} load level,

$$\frac{1}{c^{(k)}} = \left(\frac{d\epsilon^{(p)}}{d\sigma}\right)^{(k)} = \frac{3n}{7E}\left[\frac{\sigma^{(k)}}{\sigma_{0.7}}\right]^{(n-1)} \tag{A-12}$$

where $\epsilon^{(p)}$, the inelastic strain, is equal to $\frac{3\sigma}{7E}\left[\frac{\sigma}{\sigma_{0.7}}\right]^{(n-1)}$

The single value of c to be introduced into Eq. (A-9) for multiaxial stress is finally computed as a weighted average of the values of c_{ij} determined for the various stress components. The expression for this quantity at the k^{th} load level is

$$\frac{1}{c^{(k)}} = \left(\frac{1}{c_x^{(k)}}\right)\ell_{xx}^2 + \left(\frac{1}{c_y^{(k)}}\right)\ell_{yy}^2 + \left(\frac{1}{c_{xy}^{(k)}}\right)\ell_{xy}^2 \tag{A-13}$$

where $$\frac{1}{c_{ij}} = \frac{3n}{7E_{ij}}\left[\frac{\sigma_{ij}^{(k)}}{\left(\sigma_{0.7}^{(k)}\right)_{ij}}\right]^{(n-1)}$$

$$\ell_{ij} = \frac{\sigma_{ij}}{\bar{\sigma}}$$

and

$$\bar{\sigma} = \left(\sigma_{xx}^2 + \sigma_{yy}^2 + \tau_{xy}^2\right)^{\frac{1}{2}}$$

It is seen that this empirical approach takes into account the fact that the hardening coefficient varies with the location of the stress point on the loading surface, and reduces to the correct value in the special case of a single nonzero stress component. In another special case, that of linear strain hardening, the value of the hardening coefficient is still determined by Eq. (A-13), except that the values of c_{ij} are then constant.

In the general case, the approach may, under some circumstances, lead to an inaccurate representation of the hardening behavior. At present there is a lack of experimental data to describe the general multiaxial hardening behavior of structural metals, particularly with respect to intermittent loading. Further study of this problem, including the generation of additional experimental data, is required to place the determination of the hardening coefficient on a sounder basis.

A further generalization of Eq. (A-13) is necessary to accommodate reversed loading. This generalization can be carried out by first considering the uniaxial case. The displacement of the yield surface in multiaxial stress reduces to the displacement of the yield point in uniaxial stress, and is denoted as α in Fig. 41. If, as shown in Fig. 41, the assumption is made that the shape of the inelastic portion of the stress-strain curve upon reversed yielding is the same as that upon initial yielding, the value of the hardening coefficient becomes

$$\frac{1}{c^{(k)}} = \frac{3n}{7E}\left[\frac{\sigma^{(k)} - \bar{\alpha}}{\sigma_{0.7}}\right]^{(n-1)} \qquad \text{(A-14)}$$

where $\bar{\alpha}$ is the last computed value of α prior to unloading and reversed loading in the plastic range.

For multiaxial stress the procedure follows that previously outlined and indicated in Eq. (A-13), with $\sigma_{ij}^{(k)}$ replaced by $\left(\sigma_{ij}^{(k)} - \bar{\alpha}_{ij}\right)$.

APPENDIX B

Multiaxial Perfect Plasticity Criteria

The uniaxial stress-strain characteristics of some materials can be represented in the plastic range by a strain-hardening portion, applicable below some finite value of strain, followed by a perfectly plastic portion in which the strain increases indefinitely without further increase in stress. This type of plastic behavior is termed limited strain hardening, and is illustrated in Fig. 41. In the case of uniaxial stress, the onset of limited strain hardening can be specified by a limiting stress corresponding to a minimum value of the hardening coefficient, c. Correspondingly, in the case of multiaxial stress, the boundary of the strain-hardening region can be defined by specifying a minimum value of the hardening coefficient, c_{min}, as determined from Eq. (A-13).

As an alternative approach, a bound on the displacement of the center of the loading surface can be specified to indicate the onset of perfect plasticity. For the case of uniaxial stress this displacement can be specified by some maximum displacement of the yield point, α_o, chosen to coincide with the point at which the hardening coefficient is c_{min}, as shown in Fig. 40. For multiaxial stress, a scalar function of the same form as the yield function, written in terms of α_{ij} and α_o, instead of σ_{ij} and σ_o, can be used to represent the perfect plasticity criterion. This criterion, which we term the flow criterion, is written as

$$h(\alpha_{ij}) = \alpha_x^2 - \alpha_x\alpha_y + \alpha_y^2 + 3\alpha_{xy}^2 - \alpha_o^2 = 0 \qquad \text{(B-1)}$$

The surface represented by Eq. (B-1) is concentric with the yield surface given by Eq. (2.1), and will be referred to as the flow surface. Thus, the onset of perfect plasticity will be assumed to occur whenever the center of the loading surface translates to a position which lies on the flow surface. The initial yield and flow surfaces are illustrated in Fig. 42. It should be noted that this criterion will not, in general, be equivalent to the specification of c_{min}, except in the special case of uniaxial stress.

For reversed plastic yielding, it is assumed that the flow surface is translated to a concentric position with respect to the loading surface, determined just prior to unloading. The loading surface and subsequent flow surface are shown in Fig. 42. Equation (B-1) can now be generalized to accommodate reversed plastic flow by modifying it as follows:

$$h(\alpha_{ij}, \bar{\alpha}_{ij}) = (\alpha_x - \bar{\alpha}_x)^2 - (\alpha_x - \bar{\alpha}_x)(\alpha_y - \bar{\alpha}_y) + (\alpha_y - \bar{\alpha}_y)^2 + 3(\alpha_{xy} - \bar{\alpha}_{xy})^2 - \alpha_o^2 = 0 \tag{B-2}$$

where $\bar{\alpha}$ has the same significance as in Eq. (A-14).

The shifting of the flow surface, for reversed plastic behavior, is tantamount to assuming that the amount of hardening prior to perfectly plastic behavior is the same in the reversed direction as in the original direction. An illustration of this assumption for uniaxial stress is given in Fig. 41.

APPENDIX C

Development of Some Matrix Relations Used in Section 3

The submatrices of the diagonally partitioned matrix $\left[{}^{\gamma}E_{\swarrow}\right]$, initially appearing in Eq. (3.13), are comprised of the coefficients associated with Hooke's law. For a typical element subjected to a state of plane stress, Eq. (3.13) can be written as

$$\begin{Bmatrix} \Delta e_x' \\ \Delta e_y' \\ \Delta \gamma_{xy}' \end{Bmatrix} = \frac{1}{E} \begin{bmatrix} 1 & -\nu & 0 \\ -\nu & 1 & 0 \\ 0 & 0 & 2(1+\nu) \end{bmatrix} \begin{Bmatrix} \Delta\sigma_x \\ \Delta\sigma_y \\ \Delta\tau_{xy} \end{Bmatrix} \qquad \text{(C-1a)}$$

This equation defines the matrix, $\left[{}^{\gamma}E_{\swarrow}\right]$, in Eq. (3.13). The inverse of the coefficient matrix, $\left[{}^{\gamma}E_{\swarrow}\right]$, appears in Eq. (3.3), and a typical submatrix of $\left[{}^{\gamma}E_{\swarrow}\right]^{-1}$ can be written as

$$\left[\ E\ \right]^{-1} = \frac{E}{(1-\nu^2)} \begin{bmatrix} 1 & \nu & 0 \\ \nu & 1 & 0 \\ 0 & 0 & \dfrac{1-\nu}{2} \end{bmatrix} \qquad \text{(C-1b)}$$

The flow law, written in tensor notation in Eq. (2.7), can be expanded and expressed as follows for each component of plastic strain in a typical element:

$$d\epsilon_x = \frac{(\bar{\sigma}_x - \frac{1}{2}\bar{\sigma}_y)^2 d\sigma_x + (\bar{\sigma}_x - \frac{1}{2}\bar{\sigma}_y)(\bar{\sigma}_y - \frac{1}{2}\bar{\sigma}_x) d\sigma_y + (\bar{\sigma}_x - \frac{1}{2}\bar{\sigma}_y)(3\bar{\tau}_{xy}) d\tau_{xy}}{D} \qquad \text{(C-2a)}$$

$$d\epsilon_y = \frac{(\bar{\sigma}_y - \tfrac{1}{2}\bar{\sigma}_x)(\bar{\sigma}_x - \tfrac{1}{2}\bar{\sigma}_y)\,d\sigma_x + (\bar{\sigma}_y - \tfrac{1}{2}\bar{\sigma}_x)^2 d\sigma_y + (\bar{\sigma}_y - \tfrac{1}{2}\bar{\sigma}_x)(3\bar{\tau}_{xy})\,d\tau_{xy}}{D} \qquad \text{(C-2b)}$$

$$d\gamma_{xy} = \frac{(3\bar{\tau}_{xy})(\bar{\sigma}_x - \tfrac{1}{2}\bar{\sigma}_y)\,d\sigma_x + (3\bar{\tau}_{xy})(\bar{\sigma}_y - \tfrac{1}{2}\bar{\sigma}_x)\,d\sigma_y + (3\bar{\tau}_{xy})^2 d\tau_{xy}}{D} \qquad \text{(C-2c)}$$

where

$$\bar{\sigma}_{ij} = (\sigma_{ij} - \alpha_{ij})$$

and

$$D = \frac{c}{4}\left(5\bar{\sigma}_x^2 - 8\bar{\sigma}_x\bar{\sigma}_y + 5\bar{\sigma}_y^2 + 36\bar{\tau}_{xy}^2\right) .$$

If we put $d\sigma_{ij} = \Delta\sigma_{ij}$ and $d\epsilon_{ij} = \Delta\epsilon_{ij}$, Eqs. (C-2) can be written in a matrix form that defines a submatrix of the diagonally partitioned matrix, $\lceil C \rfloor$, appearing in Eq. (3.11).

$$\begin{Bmatrix} \Delta\epsilon_x^{(2)} \\ \Delta\epsilon_y^{(2)} \\ \Delta\gamma_{xy}^{(2)} \end{Bmatrix} =$$

$$\frac{1}{D}\begin{bmatrix} (\bar{\sigma}_x - \tfrac{1}{2}\bar{\sigma}_y)^2 & (\bar{\sigma}_x - \tfrac{1}{2}\bar{\sigma}_y)(\bar{\sigma}_y - \tfrac{1}{2}\bar{\sigma}_x) & (\bar{\sigma}_x - \tfrac{1}{2}\bar{\sigma}_y)(3\bar{\tau}_{xy}) \\ (\bar{\sigma}_y - \tfrac{1}{2}\bar{\sigma}_x)(\bar{\sigma}_x - \tfrac{1}{2}\bar{\sigma}_y) & (\bar{\sigma}_y - \tfrac{1}{2}\bar{\sigma}_x)^2 & (\bar{\sigma}_y - \tfrac{1}{2}\bar{\sigma}_x)(3\bar{\tau}_{xy}) \\ (3\bar{\tau}_{xy})(\bar{\sigma}_x - \tfrac{1}{2}\bar{\sigma}_y) & (3\bar{\tau}_{xy})(\bar{\sigma}_y - \tfrac{1}{2}\bar{\sigma}_x) & (3\bar{\tau}_{xy})^2 \end{bmatrix} \begin{Bmatrix} \Delta\sigma_x^{(2)} \\ \Delta\sigma_y^{(2)} \\ \Delta\tau_{xy}^{(2)} \end{Bmatrix} \qquad \text{(C-3)}$$

The incremental total strain-stress relation that appears in Eq. (3.14) contains the diagonally partitioned coefficient matrix, $\left[{}^{Y}R_{\lambda}\right]$. Equation (3.15) indicates that a submatrix of $\left[{}^{Y}R_{\lambda}\right]$ can be obtained by summing the coefficient matrices of Eqs. (C-1) and (C-3) to yield the following:

$$[R] = \begin{bmatrix} \frac{(\bar{\sigma}_x - \frac{1}{2}\bar{\sigma}_y)^2}{D} + \frac{1}{E} & \frac{(\bar{\sigma}_x - \frac{1}{2}\bar{\sigma}_y)(\bar{\sigma}_y - \frac{1}{2}\bar{\sigma}_x)}{D} - \frac{\nu}{E} & \frac{3(\bar{\sigma}_x - \frac{1}{2}\bar{\sigma}_y)(\bar{\tau}_{xy})}{D} \\ \frac{(\bar{\sigma}_y - \frac{1}{2}\bar{\sigma}_x)(\bar{\sigma}_x - \frac{1}{2}\sigma_y)}{D} & -\frac{\nu}{E}\frac{(\bar{\sigma}_y - \frac{1}{2}\bar{\sigma}_x)^2}{D} + \frac{1}{E} & \frac{3(\bar{\sigma}_y - \frac{1}{2}\bar{\sigma}_x)(\bar{\tau}_{xy})}{D} \\ \frac{3(\bar{\sigma}_x - \frac{1}{2}\bar{\sigma}_y)(\bar{\tau}_{xy})}{D} & \frac{3(\bar{\sigma}_y - \frac{1}{2}\bar{\sigma}_x)(\bar{\tau}_{xy})}{D} & \frac{(3\bar{\tau}_{xy})^2}{D} + \frac{2(1+\nu)}{E} \end{bmatrix} \qquad \text{(C-4)}$$

The tangency condition associated with perfect plasticity appears in Eq. (2.6b) in tensor notation. This condition can be expressed as follows:

$$\frac{\partial f}{\partial \sigma_{ij}} d\sigma_{ij} = (\bar{\sigma}_x - \tfrac{1}{2}\bar{\sigma}_y)d\sigma_x + (\bar{\sigma}_y - \tfrac{1}{2}\bar{\sigma}_x)d\sigma_y + 3(\bar{\tau}_{xy})d\tau_{xy} = 0 \qquad \text{(C-5)}$$

where $\bar{\sigma}_{ij}$ is given in Eq. (C-2d). If we put $d\sigma_{ij} = \Delta\sigma_{ij}$, and choose to express $\Delta\sigma_x$ in terms of $\Delta\sigma_y$ and $\Delta\tau_{xy}$, then Eq. (C-5) can be represented in matrix form as follows

$$\begin{Bmatrix} \Delta\sigma_x^{(3)} \\ \Delta\sigma_y^{(3)} \\ \Delta\tau_{xy}^{(3)} \end{Bmatrix} = \begin{bmatrix} 0 & -\frac{(\bar{\sigma}_y - \frac{1}{2}\sigma_x)}{(\bar{\sigma}_x - \frac{1}{2}\bar{\sigma}_y)} & -\frac{3\bar{\tau}_{xy}}{(\bar{\sigma}_x - \frac{1}{2}\bar{\sigma}_y)} \\ 0 & 1 & 0 \\ 0 & 0 & 1 \end{bmatrix} \begin{Bmatrix} \Delta\sigma_x^{(3)} \\ \Delta\sigma_y^{(3)} \\ \Delta\tau_{xy}^{(3)} \end{Bmatrix} \qquad \text{(C-6)}$$

The coefficient matrix of Eq. (C-6) is a submatrix, $\left[\ \bar{E}\ \right]$, of the diagonally partitioned matrix, $\left[\bar{E}\right]$, which first appears in Eq. (3.19).

The normality condition associated with perfect plasticity is the flow law given in Eq. (2.7) and rewritten in Eq. (3.20). This condition can be expressed as follows:

$$d\lambda = \frac{d\epsilon_x}{(\bar{\sigma}_x - \frac{1}{2}\bar{\sigma}_y)} = \frac{d\epsilon_y}{(\bar{\sigma}_y - \frac{1}{2}\bar{\sigma}_x)} = \frac{d\gamma_{xy}}{(3\bar{\tau}_{xy})} \tag{C-7}$$

Setting $d\epsilon_{ij} = \Delta\epsilon_{ij}$ in Eq. (C-7) leads to the incremental matrix relation that exists among the components of plastic strain increment in a perfectly plastic element. This matrix relation is given by,

$$\begin{Bmatrix} \Delta\epsilon_x^{(3)} \\ \Delta\epsilon_y^{(3)} \\ \Delta\gamma_{xy}^{(3)} \end{Bmatrix} = \begin{bmatrix} 1 & 0 & 0 \\ \dfrac{(\bar{\sigma}_y - \frac{1}{2}\bar{\sigma}_x)}{(\bar{\sigma}_x - \frac{1}{2}\bar{\sigma}_y)} & 0 & 0 \\ \dfrac{(3\bar{\tau}_{xy})}{(\bar{\sigma}_x - \frac{1}{2}\bar{\sigma}_y)} & 0 & 0 \end{bmatrix} \begin{Bmatrix} \Delta\epsilon_x^{(3)} \\ \Delta\epsilon_y^{(3)} \\ \Delta\gamma_{xy}^{(3)} \end{Bmatrix} \tag{C-8}$$

The coefficient matrix of Eq. (C-8) is a submatrix, $\left[\ \tilde{E}\ \right]$, of the diagonally partitioned matrix, $\left[\tilde{E}\right]$, which first appears in Eq. (3.21).

APPENDIX D

Relations Between the Linear Influence Coefficient Matrices Associated with the Stress and Strain Methods

As indicated in Section 3, the matrix equations associated with the stress method, Eq. (3.1), and the strain method, Eq. (3.5), are related. A relationship exists between the linear influence coefficient matrices, [B] and [A], and between [H] and [J]. In proceeding to establish these relationships, we rewrite Eqs. (3.1) and (3.5),

$$\{\sigma\} = [B]\{P\} + [H]\{\epsilon\} \tag{3.1}$$

$$\{e\} = [A]\{P\} + [J]\{\epsilon\} \tag{3.5}$$

In the absence of any initial strains, Eqs. (3.1) and (3.5) become

$$\{\sigma\} = [B]\{P\} \tag{D-1}$$

$$\{e\} = [A]\{P\} \tag{D-2}$$

The stresses are related to the strains through the generalized Hooke's law,

$$\{\sigma\} = \left[\!\left[E \right]\!\right]^{-1}\{e\} \ , \tag{D-3}$$

where a submatrix of $\left[\!\left[E \right]\!\right]^{-1}$ is given in Eq. (C-1b).

Premultiplication of both sides of Eq. (D-2) by $\left[\!\left[E \right]\!\right]^{-1}$ yields

$$\left[\!\left[E \right]\!\right]^{-1}\{e\} = \left[\!\left[E \right]\!\right]^{-1}[A]\{P\} \tag{D-4a}$$

or

$$\{\sigma\} = \left[\begin{matrix}\diagdown\\ \diagup\end{matrix} E \right]^{-1} [A]\{P\} \quad . \tag{D-4b}$$

Thus, from Eqs. (D-2) and (D-4b), we find

$$[B] = \left[\begin{matrix}\diagdown\\ \diagup\end{matrix} E \right]^{-1} [A] \tag{D-5a}$$

or

$$[A] = \left[\begin{matrix}\diagdown\\ \diagup\end{matrix} E \right] [B] \quad . \tag{D-5b}$$

In the absence of any external load, Eqs. (3.1) and (3.5) become

$$\{\sigma\} = [H]\{\epsilon\} \tag{D-6}$$

$$\{e\} = [J]\{\epsilon\} \quad . \tag{D-7}$$

The total strain $\{e\}$ can be decomposed into elastic strain and initial strain:

$$\{e\} = \{e'\} + \{\epsilon\} \tag{D-8}$$

where $\{e'\}$ is the elastic component of strain. Equation (D-8) can be used to substitute for $\{e\}$ in Eq. (D-7), resulting in the following equation,

$$\left[\begin{matrix}\diagdown\\ \diagup\end{matrix} E \right]\{\sigma\} + \{\epsilon\} = [J]\{\epsilon\} \quad . \tag{D-9}$$

Substituting Eq. (D-6) into Eq. (D-9), we obtain

$$\left(\left[\begin{matrix}\diagdown\\ \diagup\end{matrix} E \right][H] + \left[\begin{matrix}\diagup\\ \diagdown\end{matrix} I \right]\right)\{\epsilon\} = [J]\{\epsilon\} \tag{D-10}$$

where $\left[\begin{matrix}\diagup\\ \diagdown\end{matrix} I \right]$ is the unit matrix. This provides the following relationship between the linear influence coefficient matrices, $[H]$ and $[J]$,

$$[J] = \left(\left[\begin{matrix} Y \\ E \end{matrix} \right] [H] + \left[\begin{matrix} \\ I \end{matrix} \right] \right) \qquad \text{(D-11a)}$$

or

$$[H] = \left[\begin{matrix} Y \\ E \end{matrix} \right]^{-1} \left([J] - \left[\begin{matrix} \\ I \end{matrix} \right] \right) \qquad \text{(D-11b)}$$

APPENDIX E

A Procedure to Compute the Load Level Necessary to Cause Yielding from an Elastic State

In the present investigation, because of the assumption of small deflections and the assumption that unloading from a plastic state can be treated as a purely elastic process (hysteretic effects are neglected), the elastic response during initial loading and unloading from a plastic state is a linear function of the applied loads. Therefore, it is necessary to implement the incremental procedures only when yielding has occurred in at least one element of the idealized structure. The procedure outlined below was used to determine the loads at which this occurs.

Considering proportional loading only, we can denote one of the loads by P^* and let each of the other loads be some given multiple of P^*. Thus,

$$\{P\} = P^*\{\bar{P}\} \tag{E-1}$$

where $\{\bar{P}\}$ is the vector of loads, normalized with respect to P^*. In addition, we can define

$$\{\bar{B}\} = [B]\{\bar{P}\} \tag{E-2}$$

where $[B]$ is defined in Eq. (3.1).

For the general case of unloading and reversed loading from some plastic state, the residual stresses, as given in Appendix G, can be written as

$$\{\sigma_R\} = [H]\{\epsilon\} \quad \text{from the stress method ;} \tag{G-1}$$

or

$$\{\sigma_R\} = \left[E\right]^{-1}\left([J] - [I]\right)\{\epsilon\} \quad \text{from the strain method .} \tag{G-7}$$

The stresses at any level of loading can be computed from the following equation,

$$\{\sigma\} = P^*\{\bar{B}\} + \{\sigma_R\} \quad . \tag{E-3}$$

In the j^{th} element of the idealized structure, the three components of stress can be written as follows using an indicial notation,

$$\begin{aligned} \sigma_x &= \sigma_{(3j-2)} = P^*\bar{B}_{(3j-2)} + \sigma_{R_{(3j-2)}} \\ \sigma_y &= \sigma_{(3j-1)} = P^*\bar{B}_{(3j-1)} + \sigma_{R_{(3j-1)}} \\ \tau_{xy} &= \sigma_{(3j)} = P^*\bar{B}_{(3j)} + \sigma_{R_{(3j)}} \quad . \end{aligned} \tag{E-4}$$

Substituting these values of stress into the von Mises yield function results in the following expression,

$$\begin{aligned} &\left[\left(P^*\bar{B}_{(3j-2)} + \sigma_{R_{(3j-2)}}\right) - \bar{\alpha}_{(3j-2)}\right]^2 \\ &- \left[\left(P^*B_{(3j-2)} + \sigma_{R_{(3j-2)}}\right) - \bar{\alpha}_{(3j-2)}\right]\left[\left(P^*B_{(3j-1)} + \sigma_{R_{(3j-1)}}\right) - \bar{\alpha}_{(3j-1)}\right] \\ &+ \left[\left(P^*B_{(3j-1)} + \sigma_{R_{(3j-1)}}\right) - \bar{\alpha}_{(3j-1)}\right]^2 + 3\left[\left(P^*B_{(3j)} + \sigma_{R_{(3j)}}\right) - \bar{\alpha}_{(3j)}\right]^2 - \sigma_o^2 \quad . \end{aligned} \tag{E-5}$$

For an arbitrary value of P^*, we can determine the element at which the value of the function given in Eq. (E-5) has the largest magnitude. Designating this element as the k^{th} element, we can write the von Mises yield condition as a quadratic equation in P^*.

$$(P^*)^2 + C_1(P^*) + C_2 = 0 \qquad \text{(E-6)}$$

where

$$C_1 = -\frac{1}{C_3}\Big[\left(\bar{\alpha}_{(3k-2)} - \sigma_{R_{(3k-2)}}\right)\left(2\bar{B}_{(3k-2)} - \bar{B}_{(3k-1)}\right) + \left(\bar{\alpha}_{(3k-1)} - \sigma_{R_{(3k-1)}}\right)\left(2\bar{B}_{(3k-1)} - \bar{B}_{(3k-2)}\right)\Big]$$

$$C_2 = \frac{1}{C_3}\Big[\left(\bar{\alpha}_{(3k-2)} - \sigma_{R_{(3k-2)}}\right)^2 - \left(\bar{\alpha}_{(3k-2)} - \sigma_{R_{(3k-2)}}\right)\left(\bar{\alpha}_{(3k-1)} - \sigma_{R_{(3k-1)}}\right) + \left(\bar{\alpha}_{(3k-1)} - \sigma_{R_{(3k-1)}}\right)^2 + 3\left(\bar{\alpha}_{(3k)} - \sigma_{R_{(3k)}}\right)^2 - \sigma_o^2\Big] \qquad \text{(E-7)}$$

and

$$C_3 = \left[\bar{B}^2_{(3k-2)} - \bar{B}_{(3k-2)}\bar{B}_{(3k-1)} + \bar{B}^2_{(3k-1)} + 3\bar{B}^2_{(3k)}\right]$$

For initial loading in the absence of any initial strains, Eq. (E-6) reduces to the form,

$$P^* = \frac{\bar{\sigma}}{\sigma_o}$$

where

$$\bar{\sigma} = \left(\bar{B}^2_{(3k-2)} - \bar{B}_{(3k-2)}\bar{B}_{(3k-1)} + \bar{B}^2_{(3k-1)} + 3\bar{B}^2_{(3k)}\right)^{\frac{1}{2}} . \qquad \text{(E-8)}$$

In all other situations, Eq. (E-6) must be solved. Since two solutions are obtained, it is necessary to establish which of them is applicable. In the case of initial loading with initial strains

present, the two solutions will be opposite in sign, and the positive solution is the correct one, unless the initial strains are sufficient in themselves to cause yielding. In the case of unloading from a plastic state and subsequent reversed loading, one solution will correspond to the load at which unloading starts, so that the other solution is the applicable one.

APPENDIX F

A Yield Condition for the Notched Bar

As indicated in Section 4, the material of the notched bar is an aluminum alloy that exhibits anisotropic plastic behavior. The anisotropy is evidenced by differing yield points and a differing hardening behavior in tension and compression. The differing yield points present some difficulties in connection with the use of the von Mises yield condition, which assumes initial isotropy. Thus, it is desirable to establish a yield condition that will provide for the initial anisotropy, and will reduce to the von Mises yield condition in the limiting case of initial isotropy.

It is conjectured that the initial anisotropic plastic behavior results from some plastic deformation that has occurred in the manufacturing process. Within the framework of the kinematic hardening theory, this would imply that the initial yield surface experiences a translation. We will assume that this translation occurs only in the plane of the normal stress components (the x-y plane) in stress space. If we represent the initial translation as β_{ij}, the von Mises yield condition becomes

$$(\sigma_x - \beta_x)^2 - (\sigma_x - \beta_x)(\sigma_y - \beta_y) + (\sigma_y - \beta_y)^2 - \sigma_o^2 = 0 \qquad (F\text{-}1)$$

where σ_o^2 is to be defined.

It is further assumed that there is initial plastic isotropy with respect to tension only or compression only. That is, the yield stresses in tension, $(\sigma_{ij})^T$, are the same in the x and y directions, $\sigma_x^T = \sigma_y^T = \sigma^T$, and the yield stresses in compression are the same in the x and y directions, $\sigma_x^C = \sigma_y^C = \sigma^C$. As a consequence of this assumption, the initial translations, β_x and β_y, will be equal, or $\beta_x = \beta_y = \beta$.

Since the yield condition must pass through the points, $(\sigma_x^T, 0)$ and $(\sigma_x^C, 0)$ $\left(\text{or } (0, \sigma_y^T) \text{ and } (0, \sigma_y^C)\right)$, we can write from Eq. (G-1),

$$(\sigma_x^T - \beta)^2 - (\sigma_x^T - \beta)(0 - \beta) + (0 - \beta)^2 - \sigma_o^2 = 0 \qquad (F\text{-}2)$$

and

$$(\sigma_x^C - \beta)^2 - (\sigma_x^C - \beta)(0 - \beta) + (0 - \beta)^2 - \sigma_o^2 = 0 \ . \qquad (F\text{-}3)$$

From Eqs. (F-2) and (F-3), we find the initial translation to be

$$\beta = \sigma^T + \sigma^C \qquad (F\text{-}4)$$

and

$$\sigma_o^2 = \beta^2 - \sigma^T\sigma^C \ . \qquad (F\text{-}5)$$

For complete initial isotropy, $\sigma^T = -\sigma^C$, and, from Eqs. (F-4) and (F-5), we find

$$\beta = 0 \qquad (F\text{-}6)$$

$$\sigma_o = (\sigma^T)^2 \qquad (F\text{-}7)$$

indicating that Eq. (F-1) will reduce to the von Mises yield condition for initially isotropic materials.

APPENDIX G

Residual Stresses and Strains

As previously mentioned in Section 4, reliable predictions of residual stresses or strains resulting from cyclic loading in the plastic range are important in establishing estimates of fatigue life and the ultimate strength of aircraft structures. Either of the two methods presented in Section 3 can be used to determine the residual stresses or strains at any stage of loading.

The stress method:

The matrix equation for stresses is given in Eq. (3.1), and is rewritten here,

$$\{\sigma\} = [B]\{P\} + [H]\{\epsilon\} \ . \tag{3.1}$$

In the absence of any external loads, the residual stresses are given by

$$\{\sigma_R\} = [H]\{\epsilon\} \ . \tag{G-1}$$

The residual strains will be the sum of the permanent plastic strains and the strains due to the residual stresses.

$$\{e_R\} = \left[\begin{matrix} Y \\ E \\ \wedge \end{matrix}\right]\{\sigma_R\} + \{\epsilon\} \tag{G-2}$$

where the matrix $\left[\begin{matrix} Y \\ E \\ \wedge \end{matrix}\right]$ is defined in Eq. (C-1a) of Appendix C.

Substituting for $\{\sigma_R\}$ from Eq. (G-1), we can write the residual strains in terms of the inelastic strains, as follows,

$$\{e_R\} = \left(\left[\begin{matrix} Y \\ E \\ \wedge \end{matrix}\right][H] + \left[\begin{matrix} \\ I \\ \wedge \end{matrix}\right]\right)\{\epsilon\} \tag{G-3}$$

where the matrix of influence coefficients multiplying the initial strains is recognized to be the matrix, [J], defined in Eq. (D-11a) of Appendix D.

The strain method. -

The matrix equation for strains is given in Eq. (3.5), and is rewritten here,

$$\{e\} = [A]\{P\} + [J]\{\epsilon\} \tag{3.5}$$

In the absence of any external loads, the residual strains are given by

$$\{e_R\} = [J]\{\epsilon\} \tag{G-4}$$

The residual stresses can be computed from the elastic component of the residual strain,

$$\{e_R'\} = \{e_R\} - \{\epsilon\} \ . \tag{G-5}$$

Therefore,

$$\{\sigma_R\} = \left[E\right]^{-1}\left(\{e_R\} - \{\epsilon\}\right) \tag{G-6}$$

where the matrix $\left[E\right]^{-1}$ is defined in Eq. (C-1) of Appendix C. The residual stresses can be written in terms of the inelastic strains by substituting for $\{e_R\}$ from Eq. (G-4) into Eq. (G-6),

$$\{\sigma_R\} = \left[E\right]^{-1}\left([J] - [I]\right)\{\epsilon\} \tag{G-7}$$

where the matrix of influence coefficients multiplying the initial strains is recognized to be the matrix, [H], defined in Eq. (D-11b) of Appendix D.

The residual stresses and strains, as computed by means of the above procedures, are valid at the end of any cycle of loading only if the zero load state is reached without the occurrence of reversed yielding. Where this is not the case, incremental plasticity calculations must be performed from the point of initiation of reversed yielding, as determined by the procedure outlined in Appendix E, until the zero load state is reached. At this point the above relations for residual stresses and strains can again be used.

APPENDIX H

Plastic Collapse of Continuous Media With Limited Strain-Hardening Properties

Reference 41 presents theorems applicable to the plastic collapse of continuous media with elastic, perfectly plastic properties. In particular, it establishes that, if all changes in geometry occurring during collapse are neglected, all stresses remain constant during collapse. We now proceed to extend the applicability of this theorem to a medium with limited strain-hardening properties in the plastic range.

Using the notation of Ref. 41, we rewrite some relations that are established in Ref. 41 and are equally applicable to our present case. These relations involve strain rate rather than strain itself.

The total strain rate, $\dot{\epsilon}_{ij}$, can be decomposed into an elastic part, $\dot{\epsilon}^{e}_{ij}$, and a plastic part $\dot{\epsilon}^{p}_{ij}$:

$$\dot{\epsilon}_{ij} = \dot{\epsilon}^{e}_{ij} + \dot{\epsilon}^{p}_{ij} \ . \tag{H-1}$$

On the basis of the generalized form of Hooke's law, it can be shown that,

$$\dot{\epsilon}^{e}_{ij}\dot{\sigma}_{ij} > 0 \qquad \text{except when} \quad \dot{\epsilon}^{e}_{ij} = \dot{\sigma}_{ij} = 0 \ , \tag{H-2}$$

where $\dot{\sigma}_{ij}$ is the stress rate, and the summation convention on repeated indices applies.

In perfectly plastic regions of the medium, the following relation follows from normality of the strain rate vector and tangency of the stress rate vector to the loading surface,

$$\dot{\sigma}_{ij}\dot{\epsilon}^{p}_{ij} = 0 \tag{H-3}$$

From the definition of plastic collapse, the following conditions are found to apply during collapse,

$$\int T_i'^c v_i^c \, dS = 0 \quad \text{and} \quad F_i'^c = 0 \quad \text{for some} \quad v_i^c \neq 0 \qquad \text{(H-4)}$$

where v_i are velocities, T_i are surface tractions, F_i are body forces, primes indicate rates of change, superscript c refers to collapse, and the integration is carried out over the surface of the body.

Application of the principle of virtual work to the velocity field and the rates of change of the surface tractions, body forces, stresses and strains during collapse yields the following,

$$\int T_i'^c v_i^c \, dS + \int F_i'^c v_i^c \, dV = \int \sigma_{ij}'^c \epsilon_{ij}^c \, dV \, , \qquad \text{(H-5)}$$

where the first integration is carried out over the surface of the body and the last two integrations are carried out through the volume of the body.

In the present case, we need an additional relation applicable in regions where the medium is experiencing strain hardening. On the basis that the stress increment vector and the plastic strain increment vector must both be directed outward from the yield surface, we can write for such regions,

$$\sigma_{ij}' \epsilon_{ij}^p > 0 \, , \quad \text{except when} \quad \epsilon_{ij}^p = \sigma_{ij}' = 0 \, . \qquad \text{(H-6)}$$

Returning now to Eq. (H-5), we see that the left-hand side must vanish in consideration of Eq. (H-4). Thus, decomposing the strain rate on the right-hand side of Eq. (H-5) into elastic and plastic parts, we have

$$\int \sigma'^{c}_{ij} \epsilon^{ec}_{ij} \, dV + \int \sigma'^{c}_{ij} \epsilon^{pc}_{ij} \, dV = 0 \ . \qquad \text{(H-7)}$$

According to Eq. (H-3), the second integral in Eq. (H-7) must vanish in the perfectly plastic regions. Since, according to Eqs. (H-2) and (H-6), the first integral, in the entire body, and the second integral, in the strain-hardening regions, cannot be negative, it follows that Eq. (H-5) can be satisfied only if the stress rate, σ'^{c}_{ij}, vanishes throughout the body and the strain rate, ϵ^{pc}_{ij}, vanishes in the strain-hardening portions of the body.

APPENDIX I

Rectangular Finite Element Stiffness Matrices

The element stiffness matrix is derived by using the following displacement function given in Ref. 55,

$$w(x,y) = \sum_{i=1}^{2}\sum_{j=1}^{2}\left[H_{oi}^{(1)}(\xi)H_{oj}^{(1)}(\eta)w_{ij} + H_{1i}^{(1)}(\xi)H_{oj}^{(1)}(\eta)a\ w_{,xij} + H_{oi}^{(1)}(\xi)H_{1j}^{(1)}(\eta)b\ w_{,yij} + H_{1i}^{(1)}(\xi)H_{1j}^{(1)}(\eta)a\ b\ w_{,xyij}\right] \tag{I-1}$$

where

$$\xi = \frac{x}{a} \quad , \quad \eta = \frac{y}{b}$$

$$H_{o1}^{(1)}(v) = 2v^3 - 3v^2 + 1$$

$$H_{o2}^{(1)}(v) = -2v^3 + 3v^2$$

$$H_{11}^{(1)}(v) = v^3 - 2v^2 + v$$

$$H_{12}^{(1)}(v) = v^3 - v^2$$

and the quantities w_{ij}, $aw_{,xij}$, $bw_{,yij}$, $abw_{,xyij}$ are nodal generalized displacements, arranged according to the convention shown in Fig. 43.

The modified bending stiffness matrix can be written in terms of component parts multiplied by the coefficients, C_1, C_2, $\bar{C}_3$, $\tilde{C}_3$, C_4, and C_5. The resulting matrix is in the form,

$$\left[K_B^P\right] = \frac{D'}{ab}\left[\frac{C_1}{35}\left(\frac{b}{a}\right)^2[K_{C1}] + C_2\frac{b}{a}[K_{C2}] + \frac{2}{25}C_3\delta[K_{\overline{C3}}]\right.$$
$$\left. + \frac{2}{25}\tilde{C}_3\lambda[K_{\tilde{C3}}] + C_4\frac{a}{b}[K_{C4}] + \frac{C_5}{35}\left(\frac{a}{b}\right)^2[K_{C5}]\right] . \qquad \text{(I-2)}$$

The quantities, λ and δ, multiplying the matrices, $[K_{\overline{C3}}]$ and $[K_{\tilde{C3}}]$, respectively, are used as tracers. When the modified bending stiffness matrix is desired for a plastic buckling calculation, λ and δ are taken as equal to one. For an elastic buckling calculation, λ and δ are taken as $2(1 - \nu)$ and 2ν, respectively, and the coefficients become $C_1 = C_5 = 1$, $C_2 = C_4 = 0$, and $\bar{C}_3 = \tilde{C}_3 = \frac{1}{2}$.

The initial stress stiffness matrix can be written in terms of component parts due to σ_x, σ_y, and τ_{xy}, as follows,

$$[K_M] = \frac{\sigma_x h}{4200}\frac{b}{a}[K_{Mx}] + \frac{\sigma_y h}{4200}\frac{a}{b}[K_{My}] + \frac{\tau_{xy} h}{300}[K_{Mxy}] . \qquad \text{(I-3)}$$

Only the elements in the first four columns of the component parts of the stiffness matrices need be computed, since values for these elements reappear in the remaining columns according to the pattern shown in Figs. 43 and 44. The matrices multiplied by C_1, $\bar{C}_3$, $\tilde{C}_3$, C_5, and σ_x, σ_y follow the pattern shown in Fig. 43a. The matrices multiplied by C_2, C_4, and τ_{xy} follow the pattern shown in Fig. 43b. Numerical values for the first four columns of these matrix component parts are given in Figs. 44 and 45.

REFERENCES

1. Wilson, E. L., "Matrix Analysis of Nonlinear Structures," Second Conference on Electronic Computation, Pub. by ASCE, 1960, p. 415.
2. Goldberg, J. E., and Richard, R. M., "Analysis of Nonlinear Structures," Proc. of ASCE, Journal of Struct. Div., Vol. 89, No. ST4, August 1963, p. 333.
3. Denke, P. H., "The Matric Solution of Certain Nonlinear Problems in Structural Analysis," Journal of Aero. Sciences, Vol. 23, No. 3, March 1956, p. 231.
4. Argyris, J. H., Kelsey, S., and Kamel, H., Matrix Methods of Structural Analysis, Edited by B. N. Fraeijs de Veubeke, Pergamon Press, 1964.
5. Denke, P. H., "Effect of Compressive Loads on Structural Fatigue at Elevated Temperatures," Air Force Systems Command, Tech. Doc. Report ASD-TDR 66-448, October 1962.
6. Padlog, J., Huff, R. D., and Holloway, F. F., "Unelastic Behavior of Structures Subjected to Cyclic, Thermal and Mechanical Stressing Conditions," WADD Tech. Report 60-271, December 1960.
7. Gallagher, R. H., Padlog, J., and Bijlaard, P. P., "Stress Analysis of Heated Complex Shapes," ARS Journal, Vol. 32, No. 5, May 1962, p. 700.
8. Percy, J. H., Loden, W. A., and Navaratna, D. R., "A Study of Matrix Analysis Methods for Inelastic Structures," Air Force Systems Command, Tech. Doc. Report No. RTD-TDR-63-4032, October 1963.
9. Lansing, W., Jensen, W. R., and Falby, W., "Matrix Analysis Methods for Inelastic Structures," Proc. of Conf. on Matrix Methods in Structural Mechanics," Wright-Patterson AFB, Ohio, October 26-28, 1965, AFFDL-TR-66-80, p. 605.

10. Argyris, J. H., "Continua and Discontinua," Proc. of Conf. on Matrix Methods in Structural Mechanics, Wright-Patterson AFB, Ohio, October 26-28, 1965, AFFDL-TR-66-80, p. 11.
11. Mentel, T. J., "On Evaluation of Matrix Methods for Nonlinear Biaxial Stress Analysis," Grumman Advanced Development Report No. ADR 02-11-64.2, June 1964.
12. Mentel, T. J., "Study and Development of Simple Matrix Methods for Inelastic Structures," Jour. of Spacecraft and Rockets, Vol. 3, No. 4, April 1966, p. 449.
13. Pope, G. G., "The Application of the Matrix Displacement Method in Plane Elasto-Plastic Problems," Proc. of Conf. on Matrix Methods in Structural Mechanics, Wright-Patterson AFB, Ohio, October 26-28, 1965, AFFDL-TR-66-80, p. 635.
14. Besseling, J. F., "Matrix Analysis of Creep and Plasticity Problems," Proc. of Conf. on Matrix Methods in Structural Mechanics, Wright-Patterson AFB, Ohio, October 26-28, 1965, AFFDL-TR-66-80, p. 655.
15. Gallagher, R. H., Padlog, J., and Huff, R. D., "Thermal Stress Determination Techniques for Supersonic Transport Aircraft Structures, Part III - Computer Programs for Beam, Plate, and Cylindrical Shell Analysis," Air Force Systems Command, ASD-TDR-63-783, January 1964.
16. Warren, D. S., "A Matrix Method for the Analysis of the Buckling of Structural Panels Subjected to Creep Environments," Air Force Systems Command, Tech. Doc. Report ASD-TDR 62-740, November 1962.
17. Batdorf, S. B., "Theories of Plastic Buckling," Journal of Aero. Sciences, Vol. 16, No. 7, July 1949, p. 405.
18. Sewell, M. J., "A General Theory of Elastic and Inelastic Plate Failure - II," Jour. of Mechanics and Physics of Solids, Vol. 12, November 1964,p. 279.

19. Onat, E. T., and Drucker, D. C., "Inelastic Instability and Incremental Theories of Plasticity," Jour. of Aero. Sciences, Vol. 20, No. 3, March 1953, p. 181.
20. Besseling, J. F., "Analysis of the Plastic Collapse of a Cruciform Column with Initial Twist, Loaded in Compression," Jour. of Aero. Sciences, Vol. 23, No. 1, January 1956, p. 49.
21. Lansing, W., Jones, I. W., and Ratner, P., "Nonlinear Analysis of Heated, Cambered Wings by the Matrix Force Method," AIAA Journal, Vol. 1, No. 7, July 1963, p. 1619.
22. Martin, H. C., "On the Derivation of Stiffness Matrices for the Analysis of Large Deflection and Stability Problems," Proc. of Conf. on Matrix Methods in Structural Mechanics, Wright-Patterson AFB, Ohio, October 26-28, 1965, AFFDL-TR-66-80, p. 697.
23. Greene, B. C., "Stiffness Matrix for Bending of a Rectangular Plate Element with Initial Membrane Stresses," Structural Analysis Research Memorandum No. 45, The Boeing Company, Seattle, Washington, August 1962.
24. Kapur, K. K., and Hartz, B. J., "Stability of Plates Using the Finite Element Method," Proc. ASCE, Jour. of Eng. Mech. Div., Vol. 92, No. EM 2, April 1966, p. 177.
25. Ziegler, H., "A Modification of Prager's Hardening Rule," Quart. Appl. Math., Vol. 17, No. 1, 1959, p. 55.
26. Naghdi, P. M., Essenburg, F., and Koff, W., "An Experimental Study of Initial and Subsequent Yield Surfaces in Plasticity," J. Appl. Mech., Vol. 25, June 1958, p. 201.
27. Parker, J. and Basset, M. B., "Plastic Stress-Strain Relationships - Some Experiments to Derive a Subsequent Yield Surface," J. Appl. Mech. Vol. 31, December 1964, p. 676.
28. Bertsch, P. K., and Findley, W. N., "An Experimental Study of Subsequent Yield Surfaces Corners, Normality, Bauschinger and Allied Effects," Proceedings, Fourth U.S. National Congress of Applied Mechanics, 1962, p. 893.

29. Prager, W., "The Theory of Plasticity: A Survey of Recent Achievements," (James Clayton Lecture) Proc. Instn. Mech. Engrs., Vol. 169, 1955, p. 41.
30. Prager, W., "A New Method of Analyzing Stress and Strains in Work-Hardening Plastic Solids," J. Appl. Mech., Vol. 23, 1956, p. 493.
31. Jensen, W. R., Falby, W. E., and Prince, N., "Matrix Analysis Methods for Anisotropic Structures," Air Force Systems Command, AFFDL-TR-65-220, April 1966.
32. Crews, J. H., Jr., "Local Plastic Stresses in Sheet Aluminum-Alloy Specimens with Stress-Concentration Factor of 2 Under Constant-Amplitude Loading," NASA TN D-3152, December 1965.
33. Zender, G. W., "Comparison of Theoretical Stresses and Deflections of Multicell Wings with Experimental Results Obtained from Plastic Models," NACA TN 3813, November 1956.
34. Falby, W. E., and Zalesak, J., "Comparison of Matrix Force and Direct Stiffness Methods of Redundant Structure Analysis," Grumman A.D. Report No. ADR 02-11-65-1, January 1965.
35. Rivello, R. M., "Ramberg-Osgood and Hill Parameters of Aircraft Structural Materials at Elevated Temperatures," University of Maryland, Aero. Eng . Dept. Rep. 60-1, March 1960.
36. Private Communication, NASA - Langley Research Center, January 1966.
37. Symonds, P. S., and Prager, W., "Elastic-Plastic Analysis of Structures Subjected to Loads Varying Arbitrarily Between Prescribed Limits," Jour. of App. Mech., Vol. 17, No. 3, September 1950, p. 315.
38. Neal, B. G., "Plastic Collapse and Shakedown Theorems for Structures of Strain-Hardening Material," Jour. of Aero. Sciences, Vol. 17, No. 5, 1950, p. 297.

39. Hodge, P. G., Plastic Analysis of Structures, McGraw Hill, New York, 1959.
40. Prager, W., Introduction to Plasticity, Addison-Wesley, Reading, Mass., 1959.
41. Drucker, D. C., Prager, W., and Greenberg, H. J., "Extended Limit Design Theorems for Continous Media," Quart. App. Math., Vol. 9, No. 4, 1952, p. 381.
42. Perlis, S., Theory of Matrices, Addison-Wesley, Reading, Mass., 1952.
43. Pearson, C. E., "Bifurcation Criterion and Plastic Buckling of Plates and Columns," Journal of Aero. Sci., Vol. 17, No. 7, July 1950.
44. Pride, R. A., and Heimerl, G. J., "Plastic Buckling of Simply Supported Compressed Plates," NACA Technical Note 1817, April 1949.
45. Ilyushin, A. A., "The Elasto-Plastic Stability of Plates," NACA Technical Memorandum No. 1188, December 1947.
46. Stowell, E. Z., "A Unified Theory of Plastic Buckling of Columns and Plates," NACA Technical Report No. 898, 1948.
47. Bijlaard, P. P., "Theory and Tests on the Plastic Stability of Plates and Shells," Journal of Aero. Sci., Vol. 16, No. 9, September 1949.
48. Handelman, G. H., and Prager, W., "Plastic Buckling of a Rectangular Plate Under Edge Thrusts," NACA Report 946, 1949.
49. Gerard, G. and Becker, H., "Handbook of Structural Stability, Part I - Buckling of Flat Plates," NACA Technical Note 3781, July 1957.
50. Ramberg, W.,and Osgood, W. R., "Description of Stress-Strain Curves by Three Parameters," NACA TN 902, 1943.
51. Timoshenko, S.,and Woinowsky-Krieger, S., Theory of Plates and Shells, McGraw-Hill 1959, p. 379.

52. Lekhnitski, S. G., "Anisotropic Plates," (Contributions to the Metallurgy of Steel, No. 50, American Iron and Steel Institute, N.Y.C. 1956).
53. Clough, R. W., and Tocher, J. L., "Finite Element Stiffness Matrices for Analysis of Plate Bending," presented at the Conference on Matrix Methods in Structural Mechanics, October 26-28, 1965, Wright-Patterson Air Force Base, Dayton, Ohio, AFFDL-TR-66-80, p. 515.
54. Papenfuss, S. W., "Lateral Plate Deflection by Stiffness Methods with Application to a Marquee," M.S. Thesis, Department of Civil Engineering, University of Washington, Seattle, December 1959.
55. Bogner, F. K., Fox, R. L., and Schmit, L. A., Jr., "The Generation of Interelement-Compatible Stiffness and Mass Matrices by the Use of Interpolation Formulas," Proc. of Conf. on Matrix Methods in Structural Mechanics, October 26-28, 1965, Wright-Patterson Air Force Base, Dayton, Ohio, AFFDL-TR-66-80, p. 397.
56. Melosh, R. J., "Basis for Derivation of Matrices for the Direct Stiffness Method," AIAA Journal, Vol. 1, No. 7, July 1963, p. 1631.
57. Levy, S., "Buckling of Rectangular Plates with Built-in Edges," Journal of Appl. Mech., Vol. 9, No. 4, December 1942, p. 171.
58. Timoshenko, S. P., and Gere, J. M., Theory of Elastic Stability, McGraw-Hill, 1961.
59. Heimerl, G. H., and Inge, J. E., "Tensile Properties of 7075-T6 and 2024-T3 Aluminum-Alloy Sheet Heated at Uniform Temperature Rates Under Constant Load," NACA TN 3462, July 1955.
60. Huges, P. J., Inge, J. E., and Prosser, S. B., "Tensile and Compressive Stress-Strain Properties of Some High-Strength Sheet Alloys at Elevated Temperatures," NACA TN 3315, November 1954.

61. Manson, S. S.,and Haferd, A. M., "A Linear Time-Temperature Relation for Extrapolation of Creep and Stress-Rupture Data," NACA TN 2890, March 1953.

62. Manson, S. S., Thermal Stress and Low Cycle Fatigue, McGraw-Hill, 1966.

63. Prager, W., "Non-Isothermal Plastic Deformation," K. Mederl. Ak. Wetensch., Proc. Vol. 61, p. 176, 1958.

64. Naghdi, P. M., "Stress-Strain Relations in Plasticity and Thermoplasticity," Proc. 2nd Symp. Naval Structural Mechanics, 1960, p. 121.

65. Drucker, D. C., "A More Fundamental Approach to Plastic Stress-Strain Relations," Proc. 1st U.S. Natl. Congr. Appl. Mech. (Chicago, 1951), New York, 1952, p. 487.

66. Budiansky, B., "A Reassessment of Deformation Theories of Plasticity," J. Appl. Mech., Vol. 26, June 1959, p. 259.

67. Phillips, A., and Kaechele, L., "Combined Stress Tests in Plasticity," J. Appl. Mech., Vol. 23, 1956, p. 43.

68. Marin, J.,and Hu, L. W., "Biaxial Plastic Stress-Strain Relations of a Mild Steel for Variable Stress Ratios," Trans. ASME, April 1956, p. 499.

69. Hu. L. W.,and Bratt, J. F., "Effect of Tensile Plastic Deformation on the Yield Condition," J. Appl. Mech., Vol. 25, September 1958, p. 111.

70. Marin, J.,and Hu, L. W., "On the Validity of Assumptions Made in Theories of Plastic Flow for Metals," Trans. ASME Vol. 75, No. 6, 1953, p. 1181.

71. Batdorf, S. B.,and Budiansky, B., "A Mathematical Theory of Plasticity Based on the Concept of Slip," NACA TN 1871, 1949.

72. Peters, R. W., Dow, N. F., and Batdorf, S. B., "Preliminary Experiments for Testing Basic Assumptions of Plasticity Theories," Proc. Soc. Exp. Stress Anal., Vol. 7, 1950, p. 127.
73. Sanders, J. L., Jr., "Plastic Stress-Strain Relations Based on Linear Loading Functions," Proc. 2nd U.S. Nat. Congr. Appl. Mech., 1954, p. 455.
74. Hodge, P. G., Jr., "Piecewise Linear Plasticity," Proc. 9th Intern. Congr. Appl. Mech., (Brussels, 1956), Vol. 8, p. 65, 1957.
75. Stricklin, J. A. "Large Elastic, Plastic, and Creep Deflections of Curved Beams and Axisymmetric Shells," AIAA Jour. Vol. 2, No. 9, September 1964, p. 1613.
76. Kadashevitch, Yu. I.,and Novozhilov, B. V., "The Theory of Plasticity Taking Residual Micro-Stresses into Consideration," Prikl. Mat. Mekh., Vol. 22, No. 1, 1955, p. 78.
77. Ivey, H. J., "Plastic Stress-Strain Relations and Yield Surfaces for Aluminum Alloys," J. Mech. Eng. Sciences, Vol. 3, No. 1, 1961, p. 15.
78. Budiansky, B., Discussion of Reference 30, J. Appl. Mech., Vol. 24, 1957, p. 481.
79. Shield, R. T. and Ziegler, H., "On Prager's Hardening Rule," ZAMP, Vol. 9a, 1958, p. 260.
80. Perrone, N. and Hodge, P. G., Jr., "Applications of a Consistent Theory for Strain-Hardening Plastic Solids," PIBAL Report 403, September 1957.

Table 1a

Elastic Buckling Coefficient for Simply-Supported Square Plate, Uniformly Loaded on Two Opposite Sides

$\nu = \frac{1}{3}$

	$k = \frac{N_x b^2}{\pi^2 D}$, $k_{exact} = 4.$					
	2 x 2	4 x 4	8 x 8	3 x 3	6 x 6	12 x 12
P (Ref. 71)	6.8630	4.2638	4.2119	4.3147	4.2255	4.2020
M (Ref. 73)	3.2863	3.7577	3.9336	3.6052	3.8849	3.9697
BFS (Ref. 72)	4.01575	4.00104	4.00009	4.00332	4.00022	4.000099

Table 1b

Elastic Buckling Coefficient for Clamped Square Plate, Uniformly Loaded on Two Opposite Sides

$\nu = \frac{1}{3}$

	$k = \frac{N_x b^2}{\pi^2 D}$, $k_{exact} = 10.07$					
	2 x 2	4 x 4	8 x 8	3 x 3	6 x 6	12 x 12
P (Ref. 71)	10.7242	10.6344	10.4053	10.9081	10.4771	10.3500
M (Ref. 73)	9.7445	9.2147	9.7616	9.1259	9.5717	9.9244
BFS (Ref. 72)	10.7242	10.1916	10.0824	10.4912	10.0993	10.0758

Table 2

Plastic Buckling of a Simply-Supported Square Plate with Various Normal Edge Loadings. Idealization of Fig. 35a.

$a = 20$ in. $b = 20$ in. $E = 10^7$ psi $\nu = 1/2$ $\sigma_{0.7} = 10^5$ psi $n = 10$

$\alpha = 1.0 \quad \beta = 0. \quad \gamma = 0.$

a.)

Thickness h (in.)	σ_* Exact	σ_* Discrete-Element Analysis
.77867	- 65000	- 65002
.85800	- 75000	- 75003
.96449	- 85000	- 85003
1.12019	- 95000	- 95002
1.36678	-105000	-105002
1.76752	-115000	-115000
2.39053	-125000	-125002

$\alpha = 1.0 \quad \beta = 1.0 \quad \gamma = 0.$

b.)

Thickness h (in.)	σ_* Exact	σ_* Discrete-Element Analysis
1.12500	- 65000	- 65018
1.29980	- 75000	- 75014
1.60231	- 85000	- 85009
2.08258	- 95000	- 95008
2.77755	-105000	-105007
3.78569	-115000	-115007
5.26002	-125000	-125007

$\alpha = 1.0 \quad \beta = .5 \quad \gamma = 0.$

c.)

Thickness h (in.)	σ_* Exact	σ_* Discrete-Element Analysis
.94979	- 65000	- 65020
1.03884	- 75000	- 75016
1.15727	- 85000	- 85015
1.33364	- 95000	- 95010
1.58816	-105000	-105008
1.93707	-115000	-115007
2.42382	-125000	-125007

Table 3

Plastic Buckling of a Simply-Supported Rectangular Plate with Various Normal Edge Loadings. Idealization of Fig. 35b.

$a = 30$ in. $b = 20$ in. $E = 10^7$ psi $\nu = 1/2$ $\sigma_{0.7} = 10^5$ psi $n = 10$

$\alpha = 1.0 \quad \beta = 0. \quad \gamma = 0.$

a.)

Thickness h (in.)	σ_* Exact	σ_* Discrete-Element Analysis
.75088	- 65000	- 65005
.83518	- 75000	- 75004
.95429	- 85000	- 85004
1.12710	- 95000	- 95002
1.39064	-105000	-105001
1.80884	-115000	-115001
2.45321	-125000	-125001

$\alpha = 1.0 \quad \beta = 1.0 \quad \gamma = 0.$

b.)

Thickness h (in.)	σ_* Exact	σ_* Discrete-Element Analysis
.95460	- 65000	- 65025
1.10292	- 75000	- 75016
1.35960	- 85000	- 85011
1.76713	- 95000	- 95010
2.35683	-105000	-105009
3.21226	-115000	-115009
4.46327	-125000	-125009

$\alpha = 1.0 \quad \beta = .5 \quad \gamma = 0.$

c.)

Thickness h (in.)	σ_* Exact	σ_* Discrete-Element Analysis
.84370	- 65000	- 65022
.92558	- 75000	- 75018
1.03918	- 85000	- 85015
1.21632	- 95000	- 95009
1.48109	-105000	-105008
1.84729	-115000	-115007
2.35015	-125000	-125007

Table 4

Plastic Buckling of a Clamped Square Plate
with a Uniform Load on Two Opposite Edges

$a = 20$ in. $\quad b = 20$ in. $\quad \nu = .5 \quad E = 10^7$ psi

$\sigma_{0.7} = 10^5$ psi $\qquad\qquad n = 10$

Thickness h (in.)	Plastic Buckling Stress (psi)	Elastic Buckling Stress (psi)
.5	-66414.	- 69018.
.6	-81712.	- 99385.
.7	-91234.	-135277.
.8	-97549.	-176687.

Table 5

Plastic Buckling of a Simply-Supported Square Plate with a Triangular Load on Two Opposite Edges

$a = b = 20$ in. $\quad \nu = .5 \quad$ $E = 10^7$ psi

$\sigma_{0.7} = 10^5$ psi $\quad n = 10$

a.) Plastic Buckling Stress Distribution in the y Direction

y/b	Thickness h (in.)				
	.5	.6	.7	.8	1.
0 to .125	-50140.	-71856.	-93895.	-110553.	-130077.
.125 to .25	-43496.	-62275.	-81377.	- 95813.	-112734.
.25 to .375	-36770.	-52695.	-68857.	- 81070.	- 95390.
.375 to .50	-30084.	-43113.	-56338.	- 66331.	- 78046.
.50 to .625	-23398.	-33531.	-43819.	- 51591.	- 60702.
.625 to .75	-16714.	-23952.	-31299.	- 36851.	- 43359.
.75 to .875	-10028.	-14372.	-18778.	- 22110.	- 26015.
.875 to 1.	- 3342.	- 4790.	-62600.	- 7370.	- 8671.

b.) Normalized Plastic Buckling Stress at y = 0

Thickness h (in.)	Plastic Buckling Stress (psi)	Elastic Buckling Stress (psi)
.5	- 53483.	- 54166.
.6	- 76646.	- 78000.
.7	-100155.	-106166.
.8	-117923.	-138667.
1.0	-138749.	-216667.

Table 6

Plastic Buckling of a Simply-Supported Square Plate
Due to a Uniform Shear Load

$a = 20$ in. $\quad b = 20$ in. $\quad \nu = .5 \quad E = 10^7$ psi

$\sigma_{0.7} = 10^5$ psi $\qquad\qquad n = 10$

Thickness h (in.)	Plastic Buckling Stress (psi)	Elastic Buckling Stress (psi)
.4	-39414.	- 40969.
.5	-50313.	- 64015.
.6	-56604.	- 92182.
.7	-60792.	-125470.

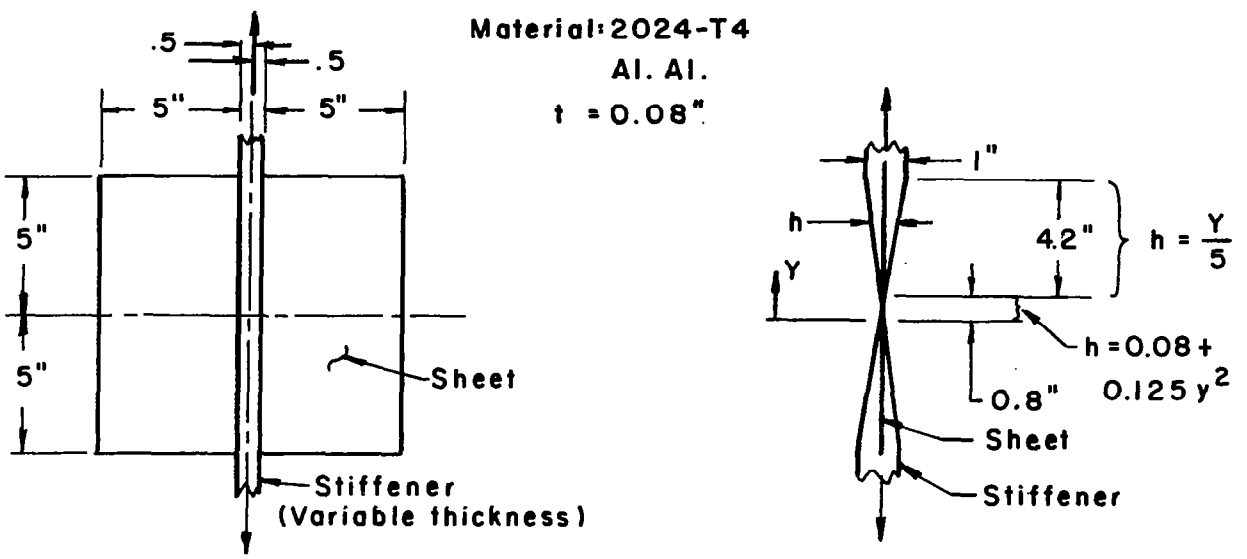

Fig. 1 RECTANGULAR PANEL WITH TAPERED STIFFENERS

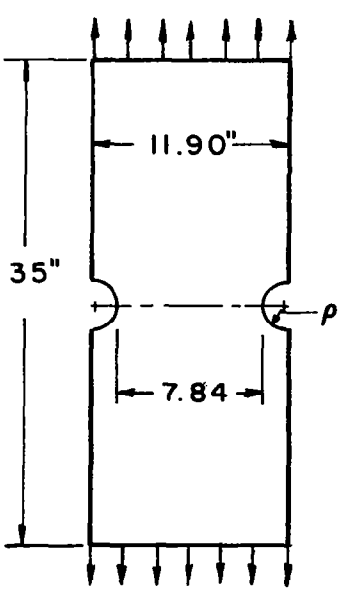

Material: 2024-T3 Al. Al.
t = 0.162"
ρ = 1.672"
K_T = 2.0

Fig. 2 NOTCHED BAR

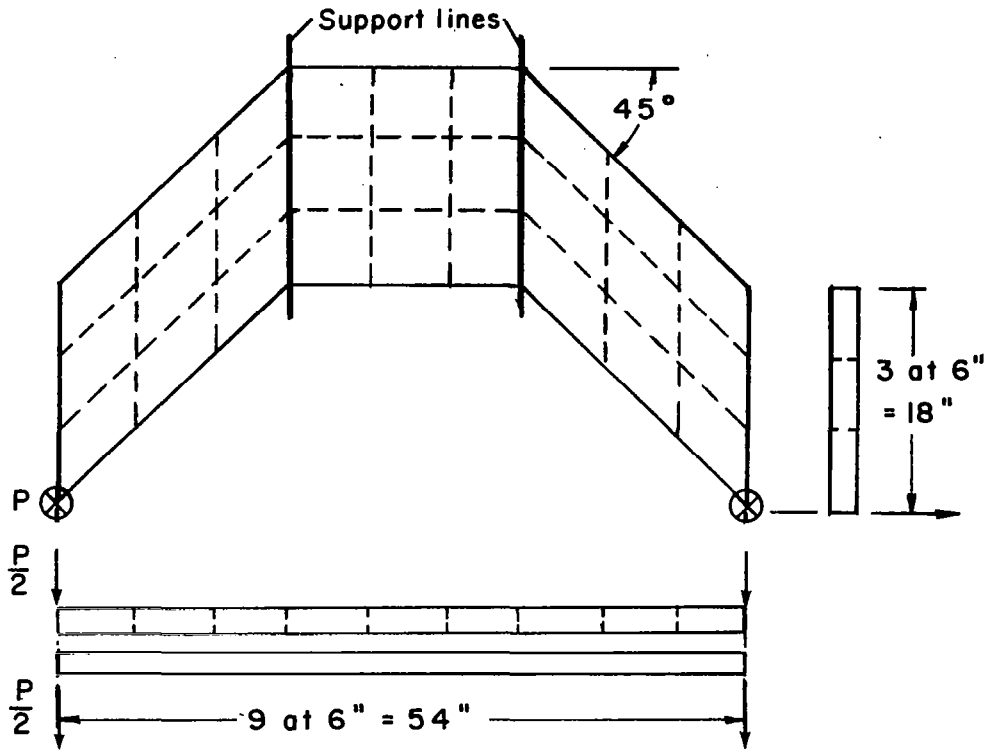

Material: 2024 - T4 Al. Al.

Cover = 0.06"

Ribs Intern = 0.026"

End = 0.013"

Spars Intern = 0.075"

Side = 0.038"

Fig. 3. SWEPT MULTICELL BOX BEAM

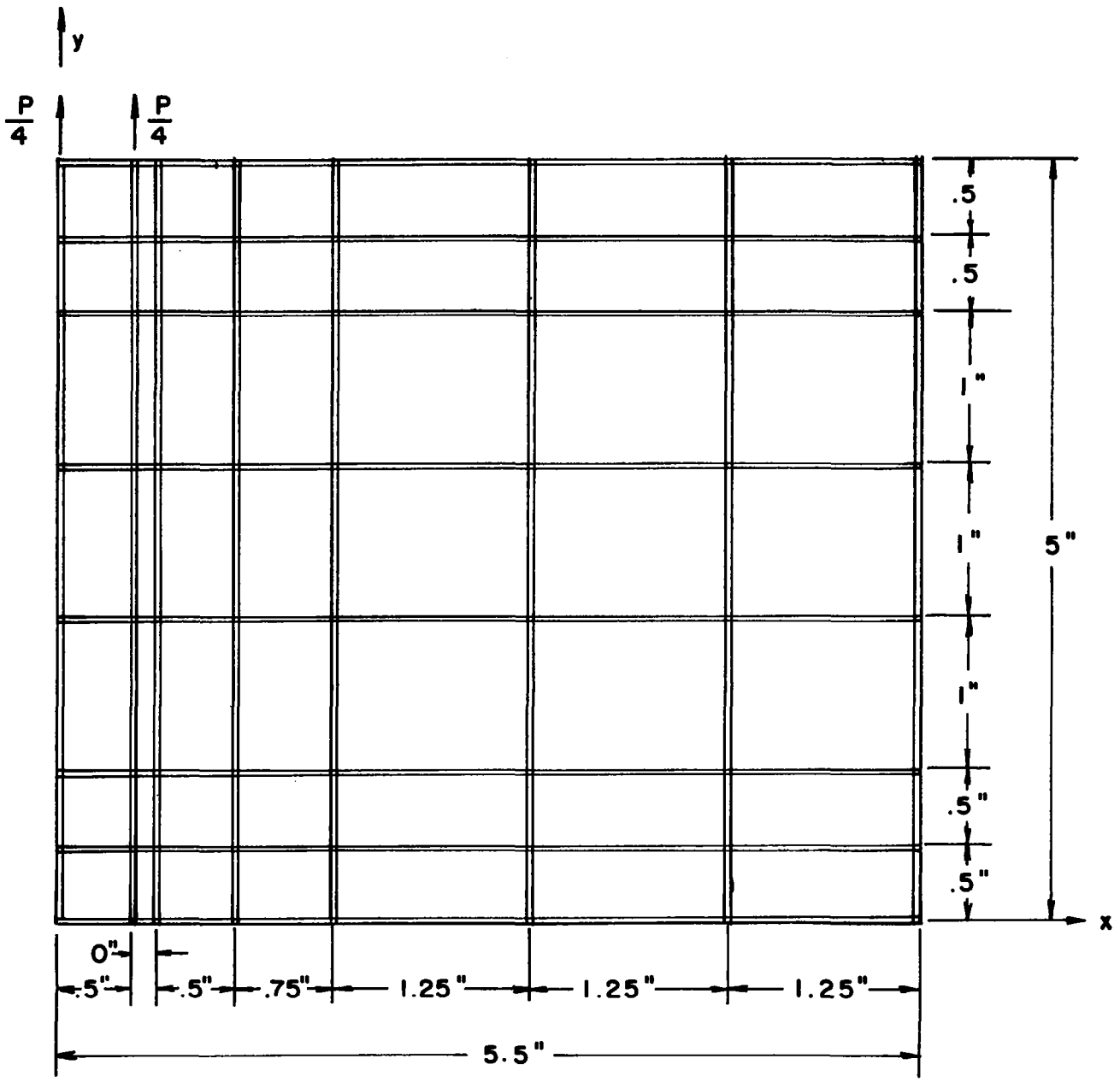

Fig. 4. DISCRETE-ELEMENT IDEALIZATION OF QUADRANT OF STIFFENED PANEL

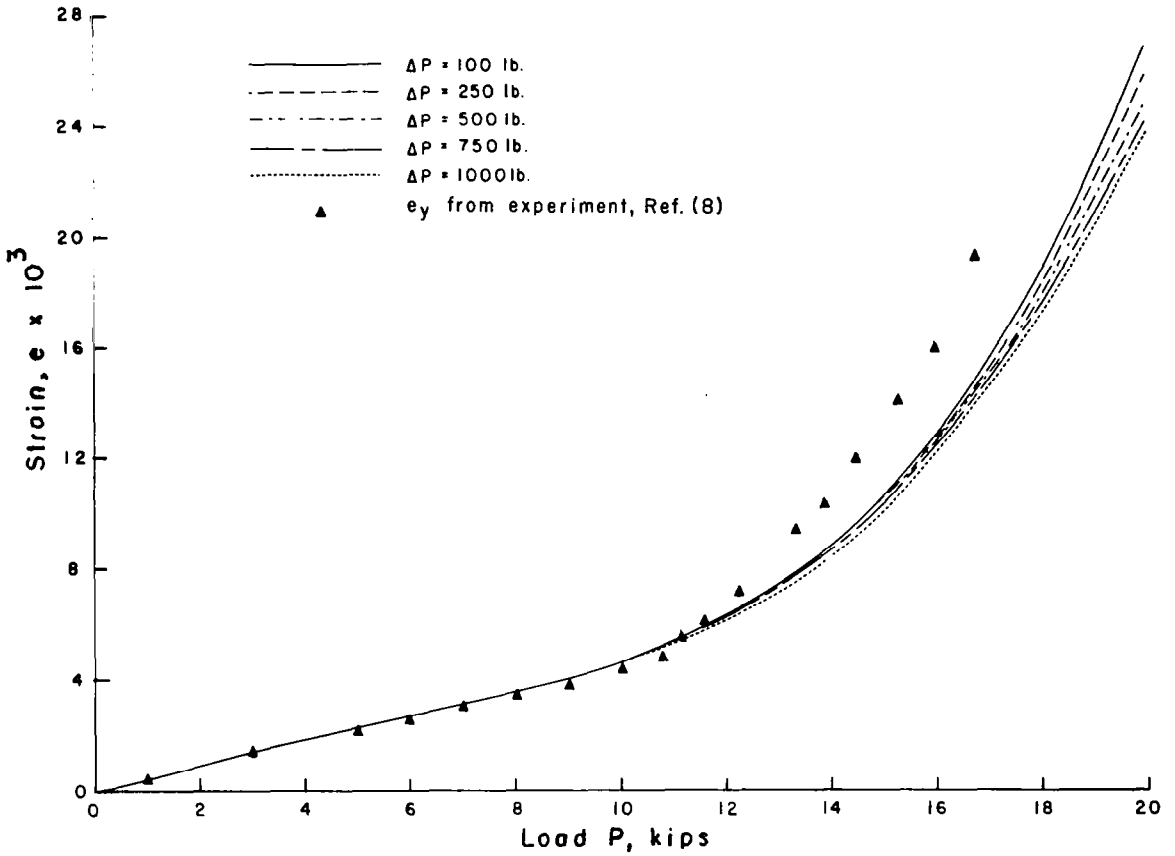

Fig.5 STIFFENED PANEL : LOAD vs STRAIN AT THE CENTER FOR VARIOUS LOAD INCREMENTS

(a) STRESS METHOD – STEPWISE LINEARIZATION PROCEDURE

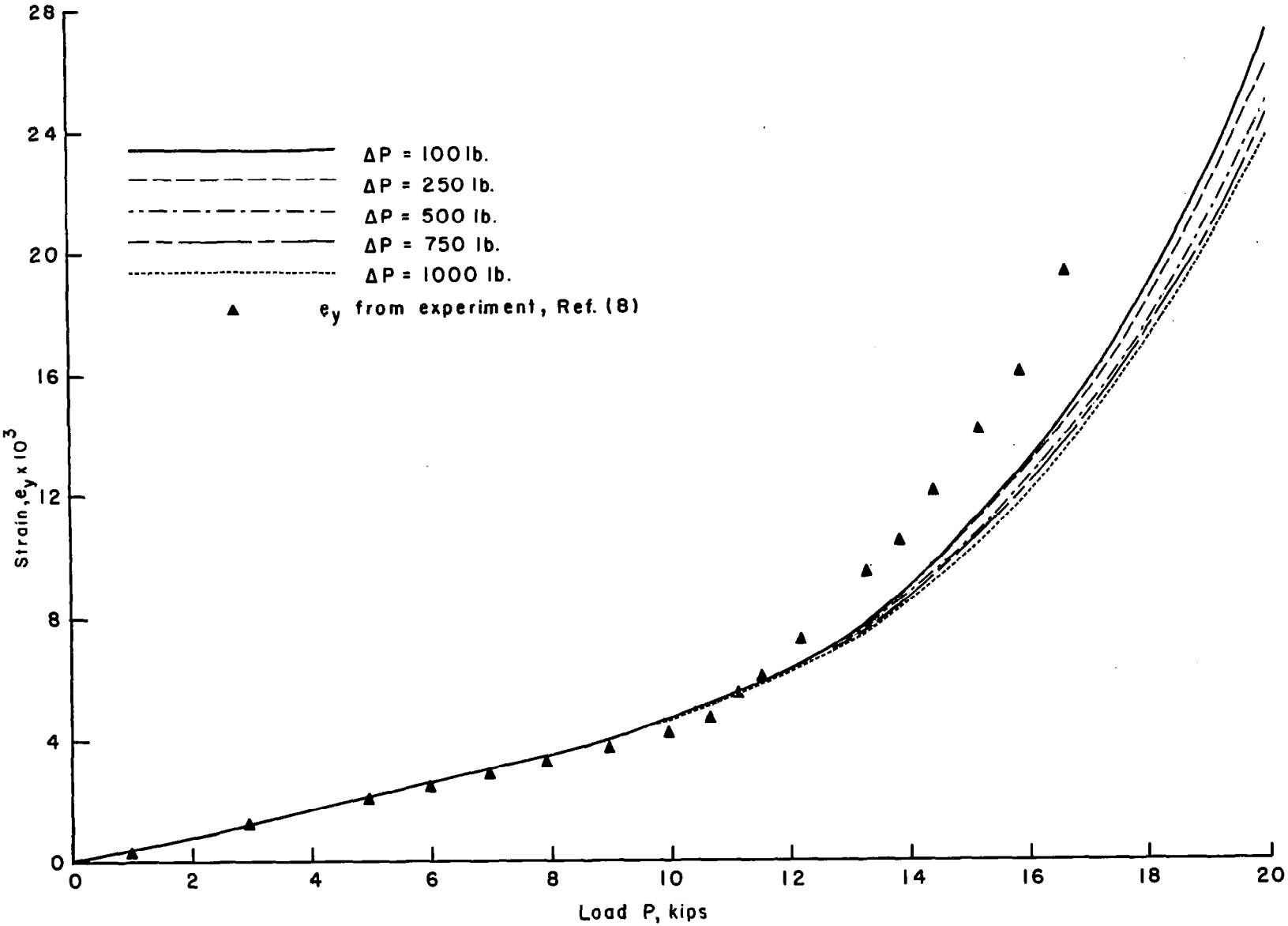

Fig. 5 (CONTINUED)

(b) STRAIN METHOD - STEPWISE LINEARIZATION PROCEDURE

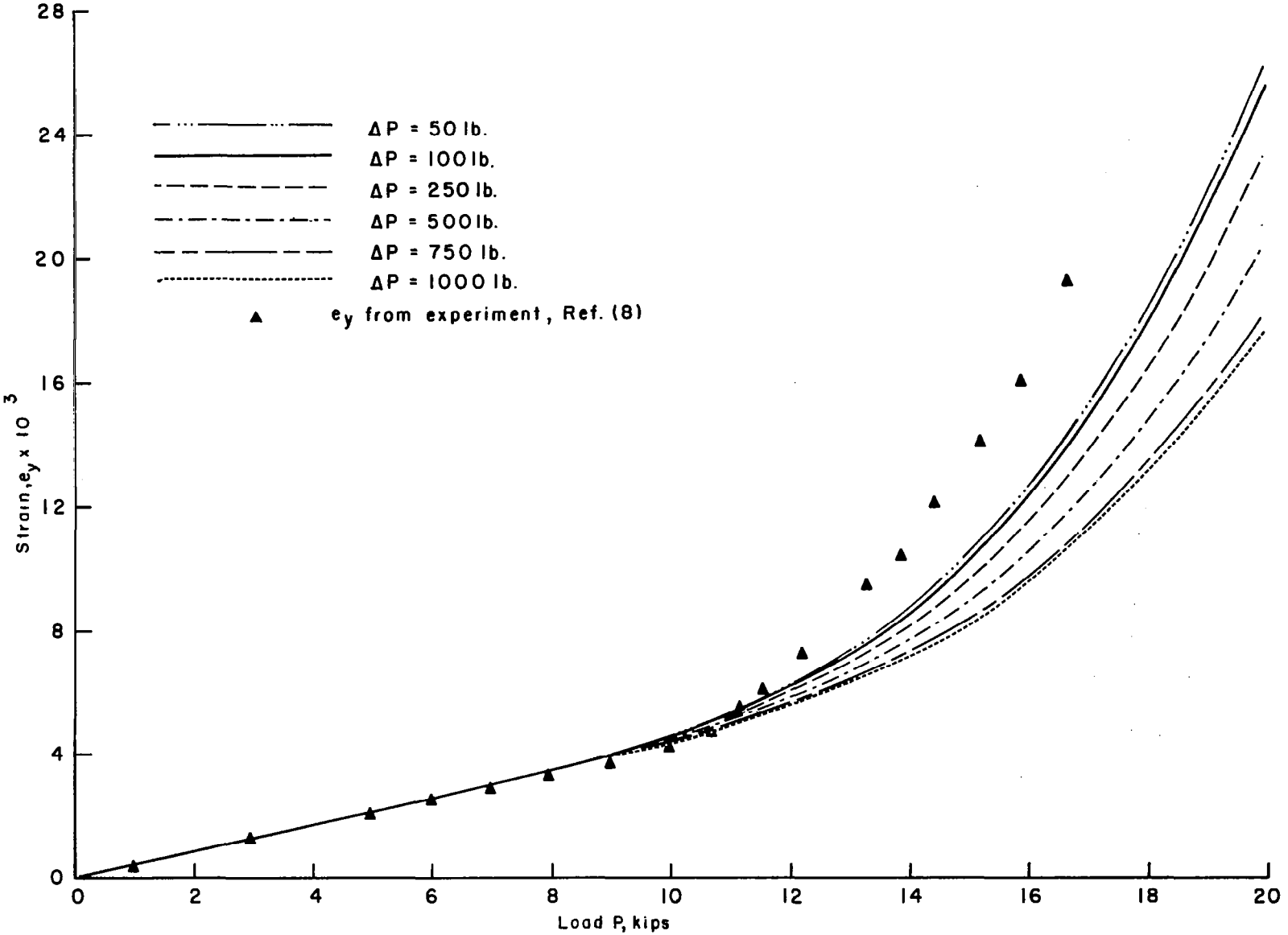

Fig. 5 (CONCLUDED)

(c) STRAIN METHOD - PREDICTOR PROCEDURE

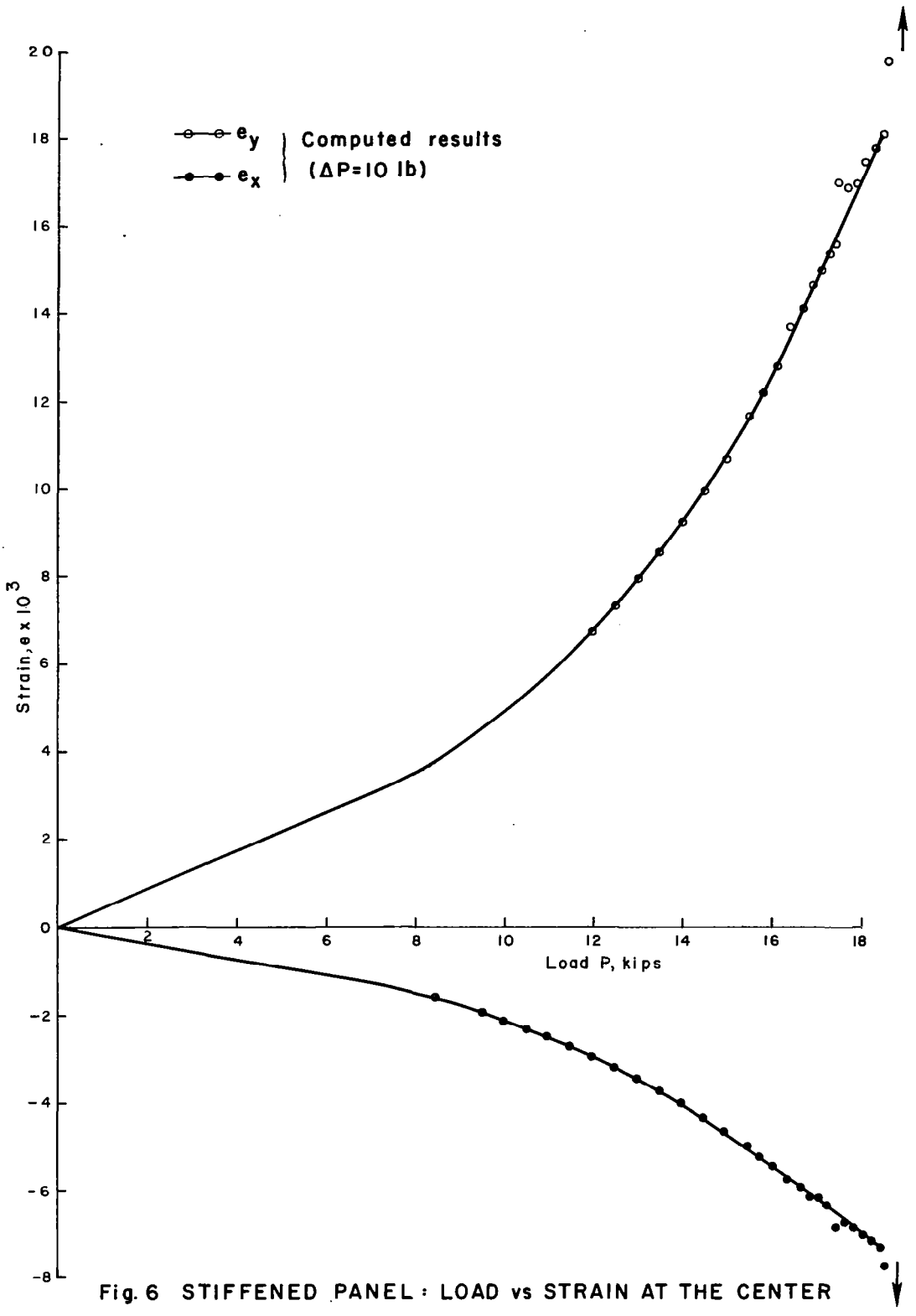

Fig. 6 STIFFENED PANEL : LOAD vs STRAIN AT THE CENTER FOR UNLIMITED STRAIN HARDENING. STRESS METHOD - PREDICTOR PROCEDURE

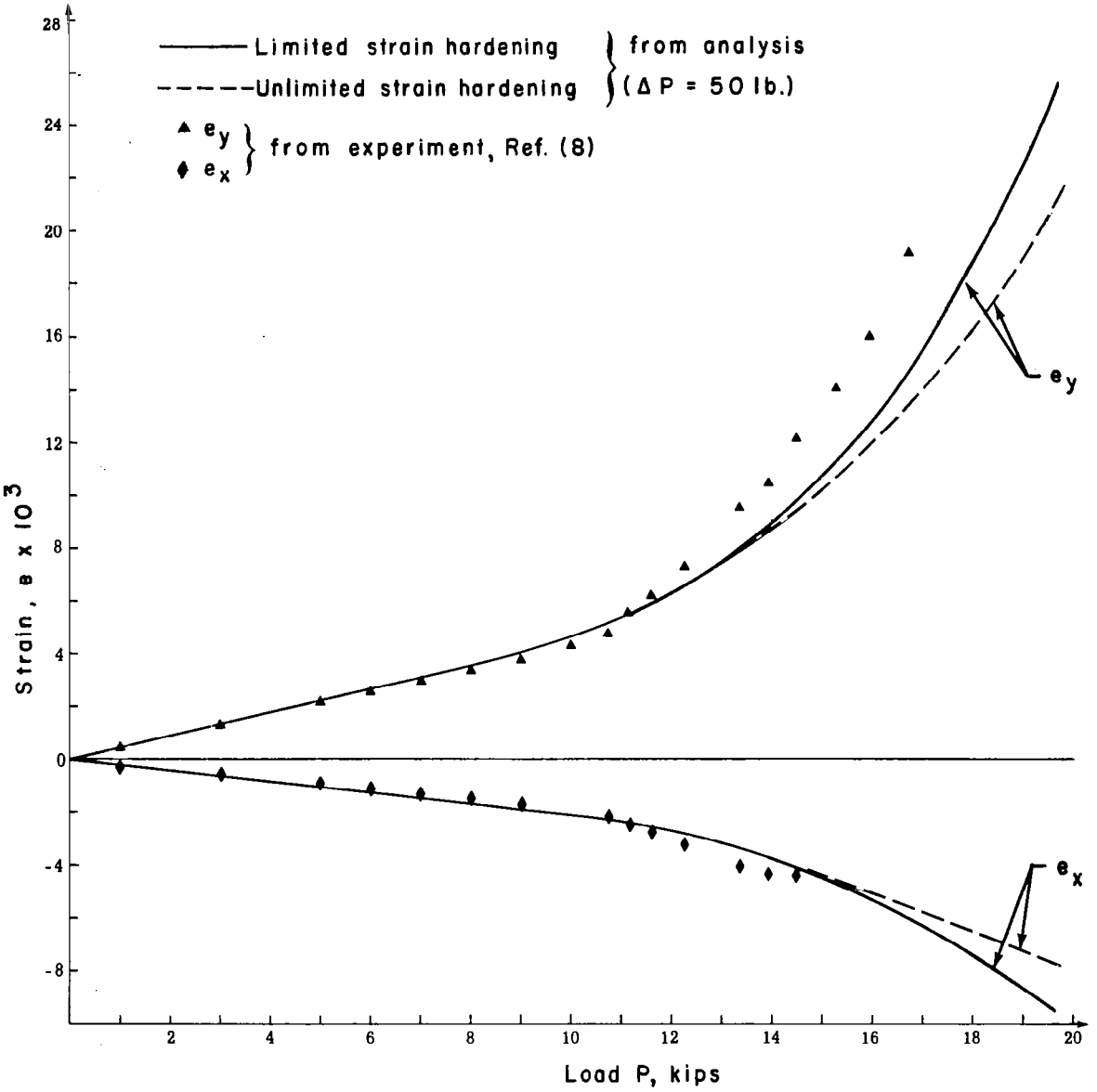

Fig. 7 STIFFENED PANEL: LOAD vs STRAIN AT THE CENTER FOR LIMITED AND UNLIMITED STRAIN HARDENING

(a) STRESS METHOD - STEPWISE LINEARIZATION PROCEDURE.

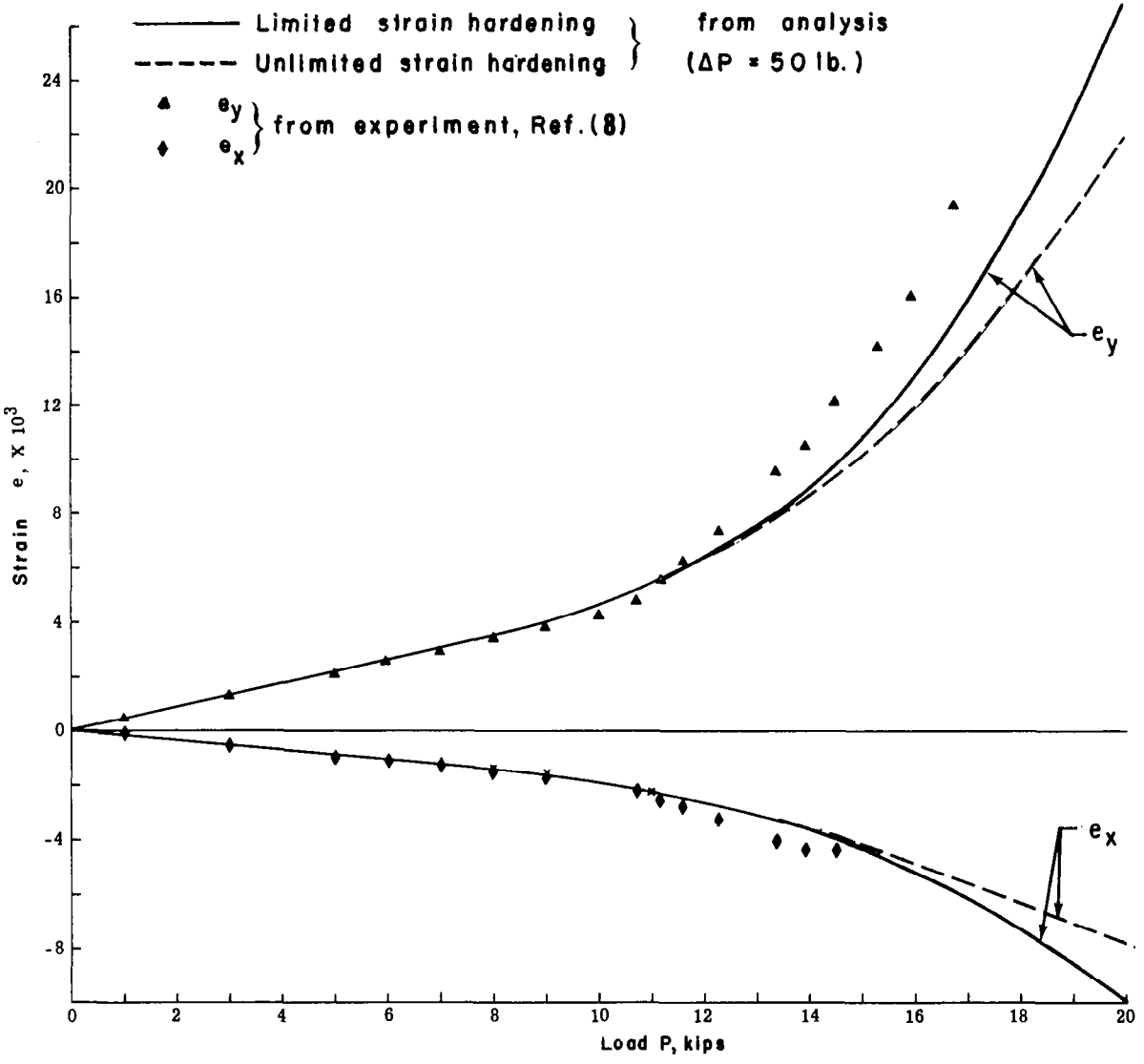

Fig. 7 (CONTINUED)

(b) STRAIN METHOD-STEPWISE LINEARIZATION PROCEDURE

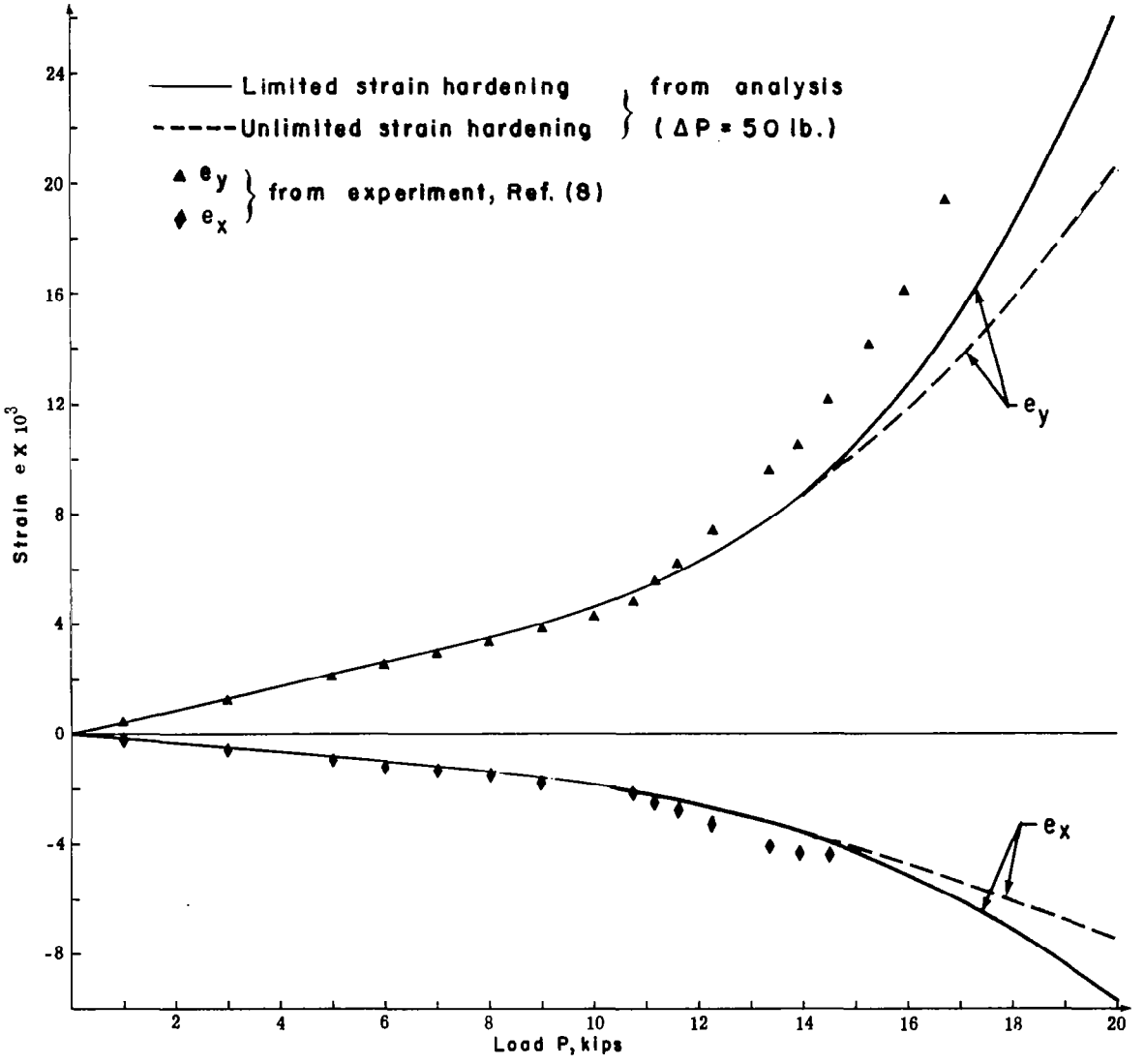

Fig. 7 (CONCLUDED)

(c) STRAIN METHOD - PREDICTOR PROCEDURE

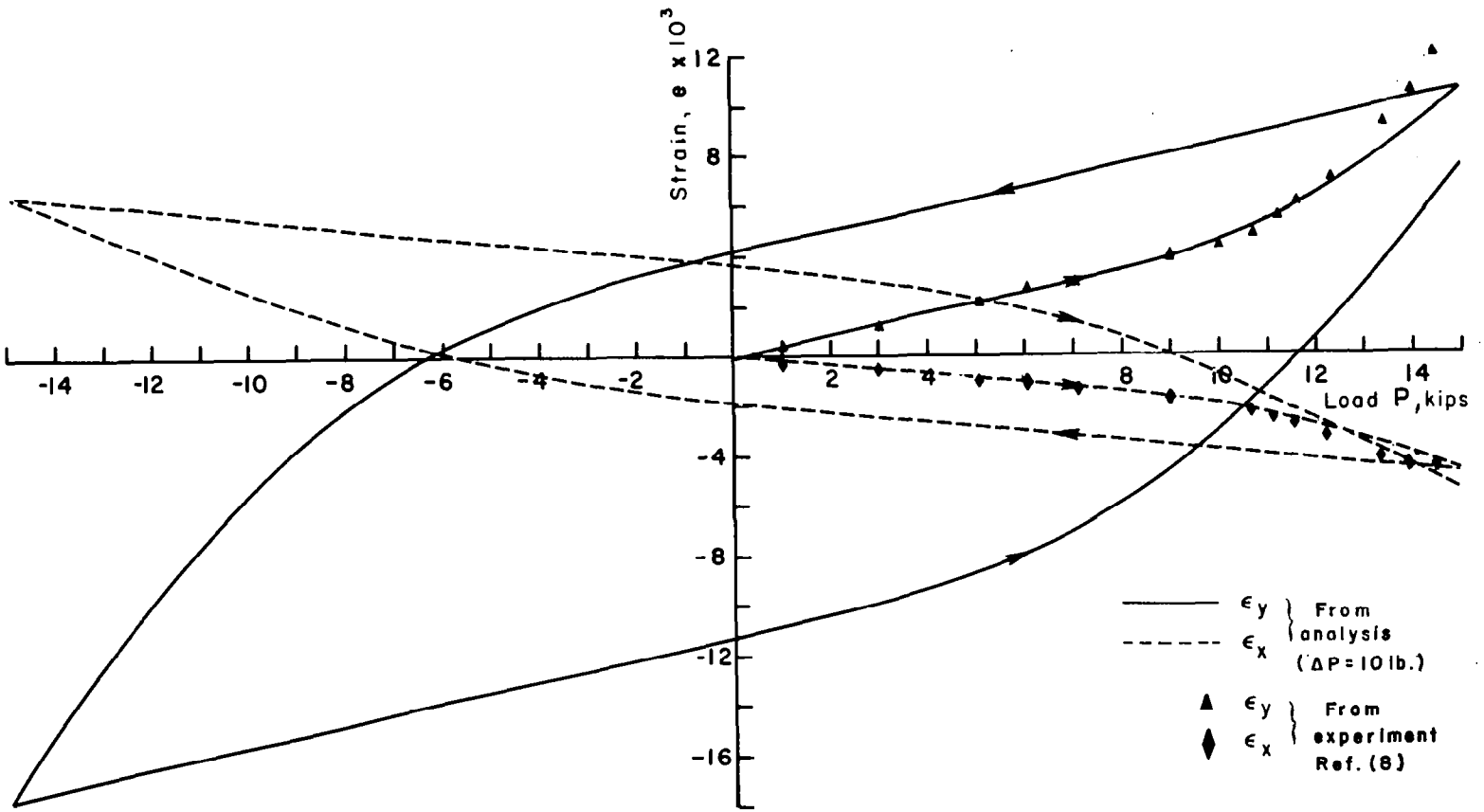

Fig. 8 STIFFENED PANEL: CYCLIC LOAD-STRAIN CURVES AT CENTER.
STRESS METHOD - PREDICTOR PROCEDURE

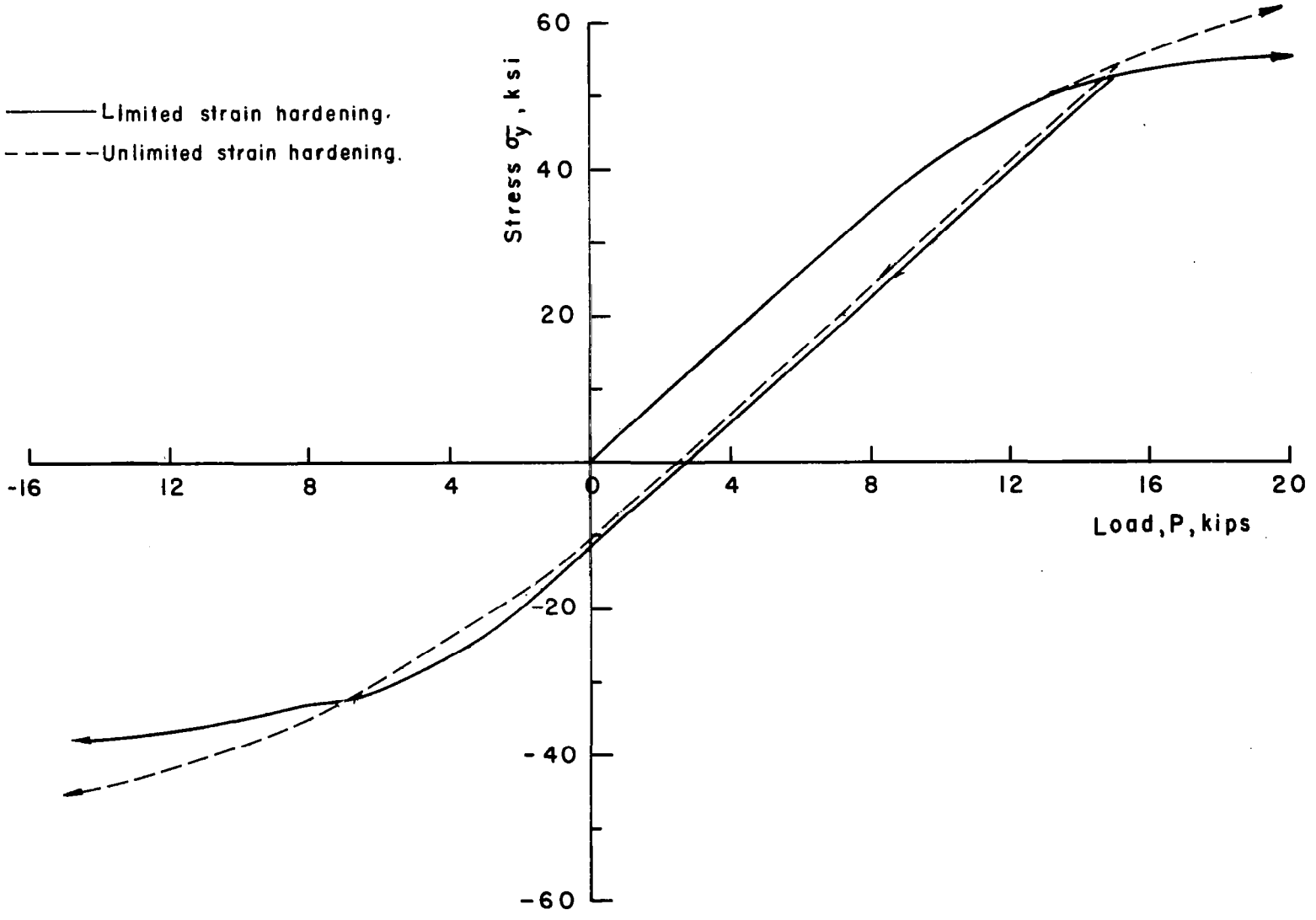

Fig. 9 STIFFENED PANEL: LOAD vs STRESS AT THE CENTER FOR LIMITED AND UNLIMITED STRAIN HARDENING
STRAIN METHOD - STEPWISE LINEARIZATION PROCEDURE ($\Delta P = 50$ lb.)

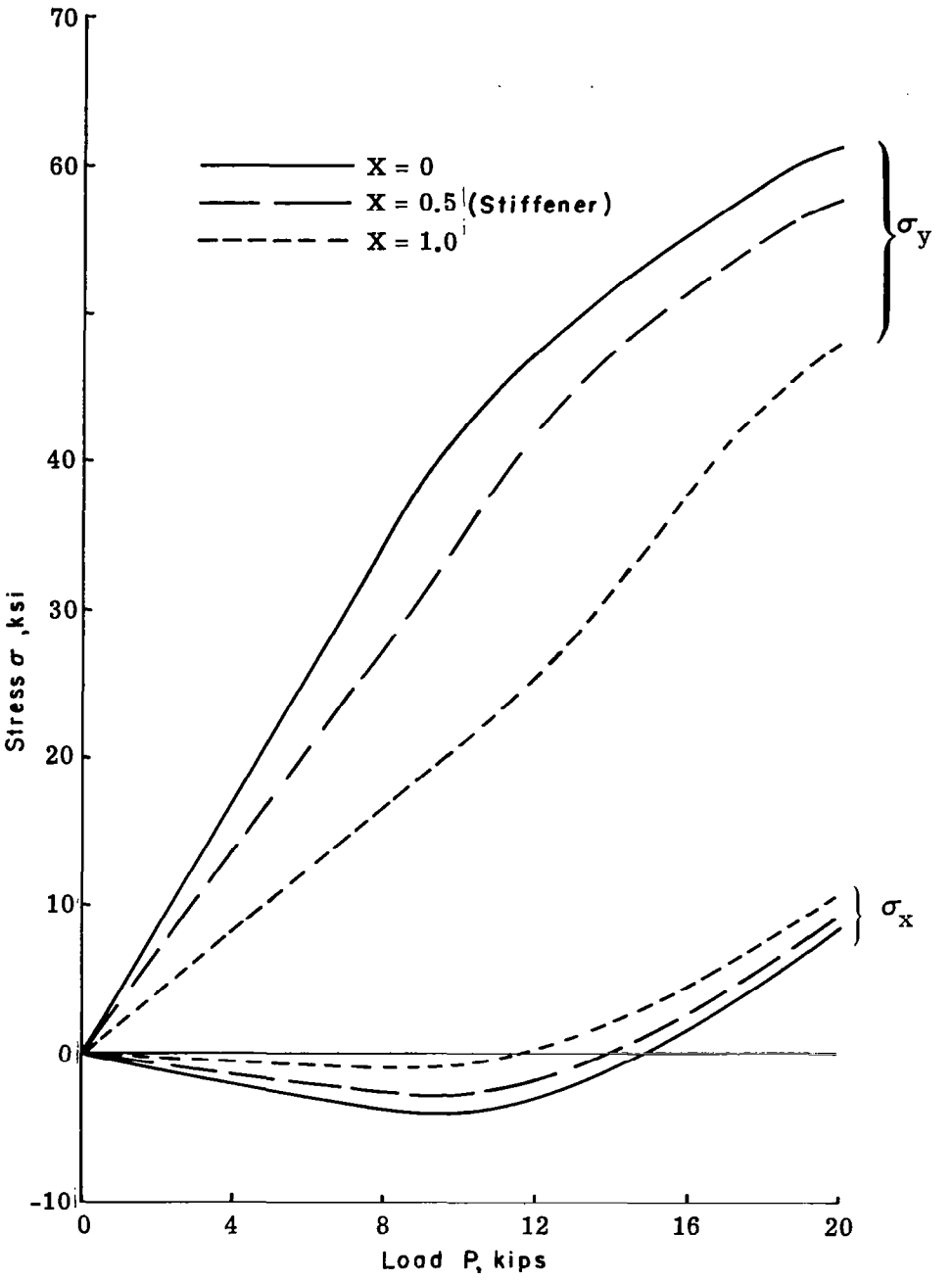

Fig. 10 STIFFENED PANEL: LOAD vs STRESS AT SEVERAL POINTS ALONG X-AXIS

(a) UNLIMITED STRAIN HARDENING; STRAIN METHOD - STEPWISE LINEARIZATION PROCEDURE ($\Delta P = 50$ lb)

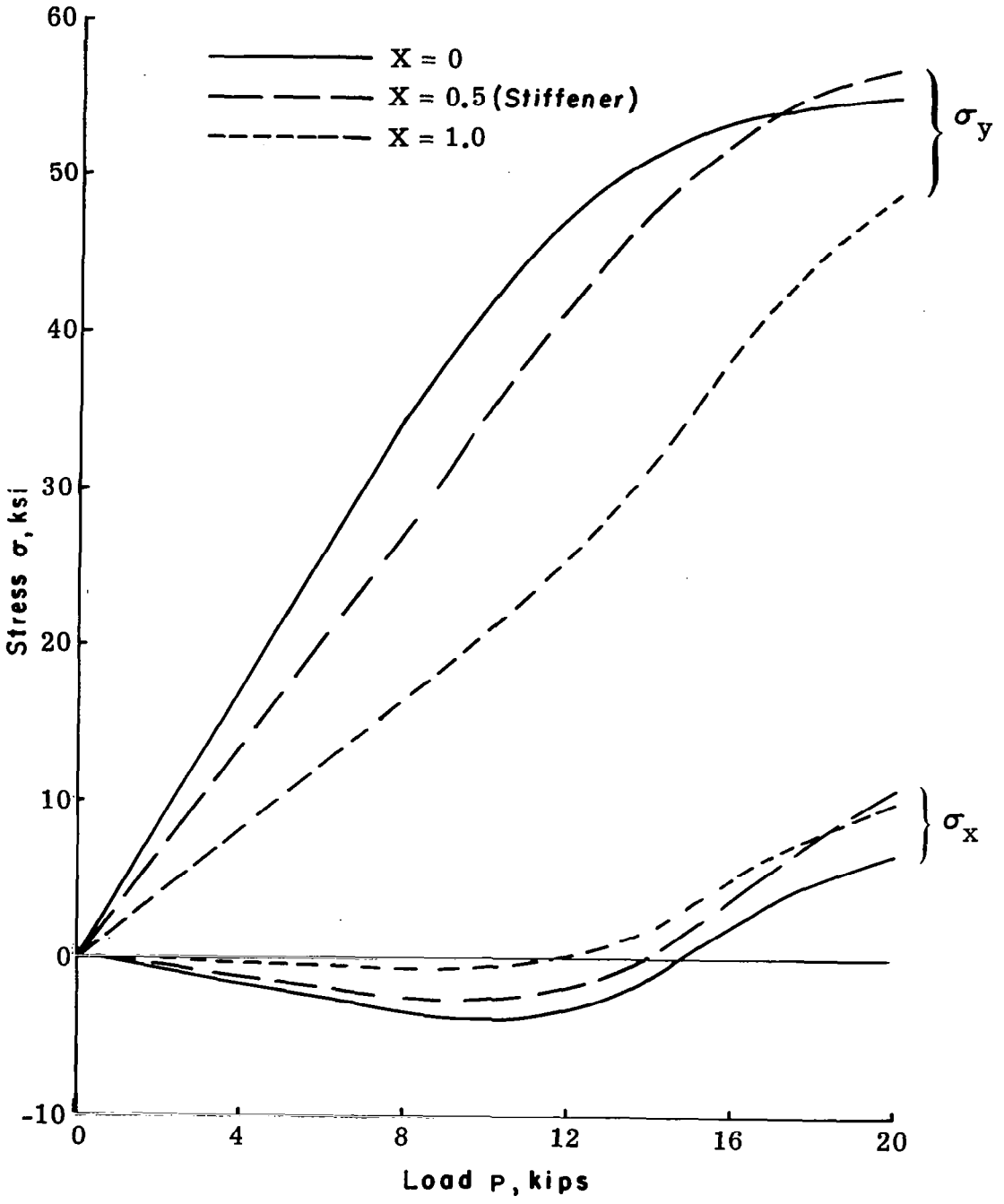

Fig. 10 (CONCLUDED)
(b) LIMITED STRAIN HARDENING
STRAIN METHOD - STEPWISE LINEARIZATION
PROCEDURE ($\Delta P = 50$ lb.)

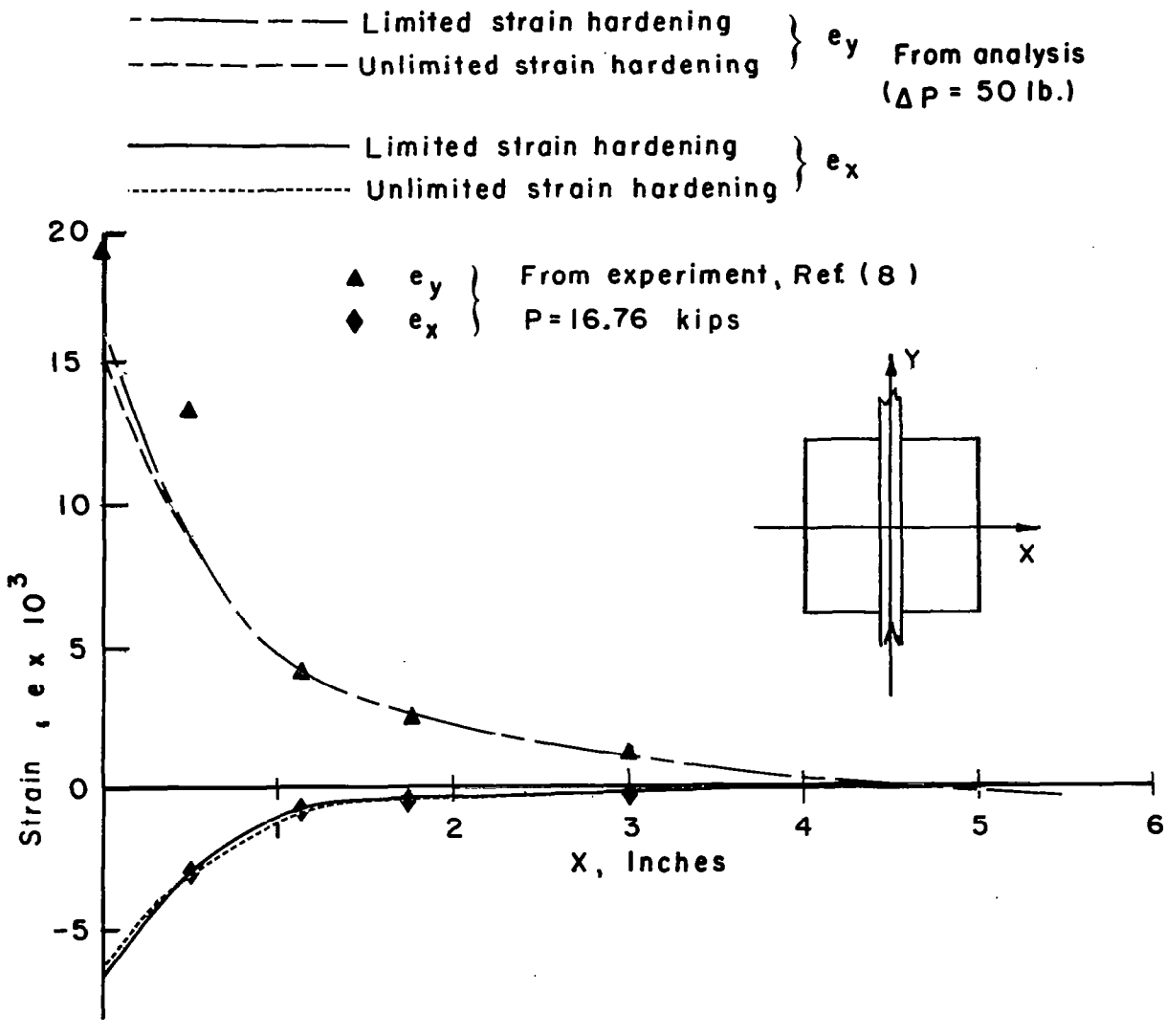

Fig. 11. STIFFENED PANEL: STRAIN DISTRIBUTION ALONG X-AXIS AT P = 16.66 kips
STRAIN METHOD-STEPWISE LINEARIZATION PROCEDURE
(ΔP = 50 lb.)

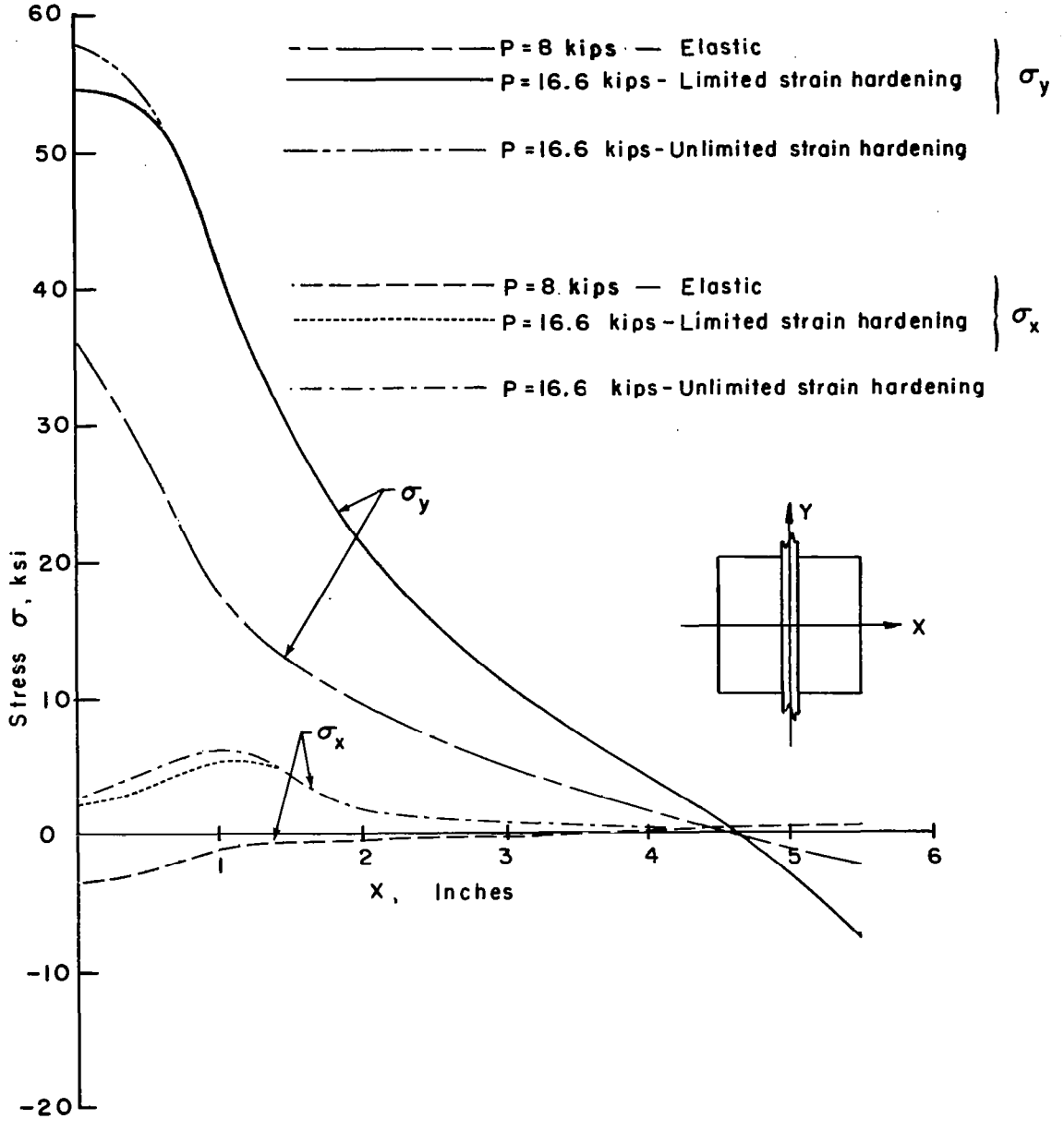

Fig. 12. STIFFENED PANEL: STRESS DISTRIBUTION ALONG X-AXIS AT TWO LOAD LEVELS
STRAIN METHOD-STEPWISE LINEARIZATION PROCEDURE
($\Delta P = 50$ lb.)

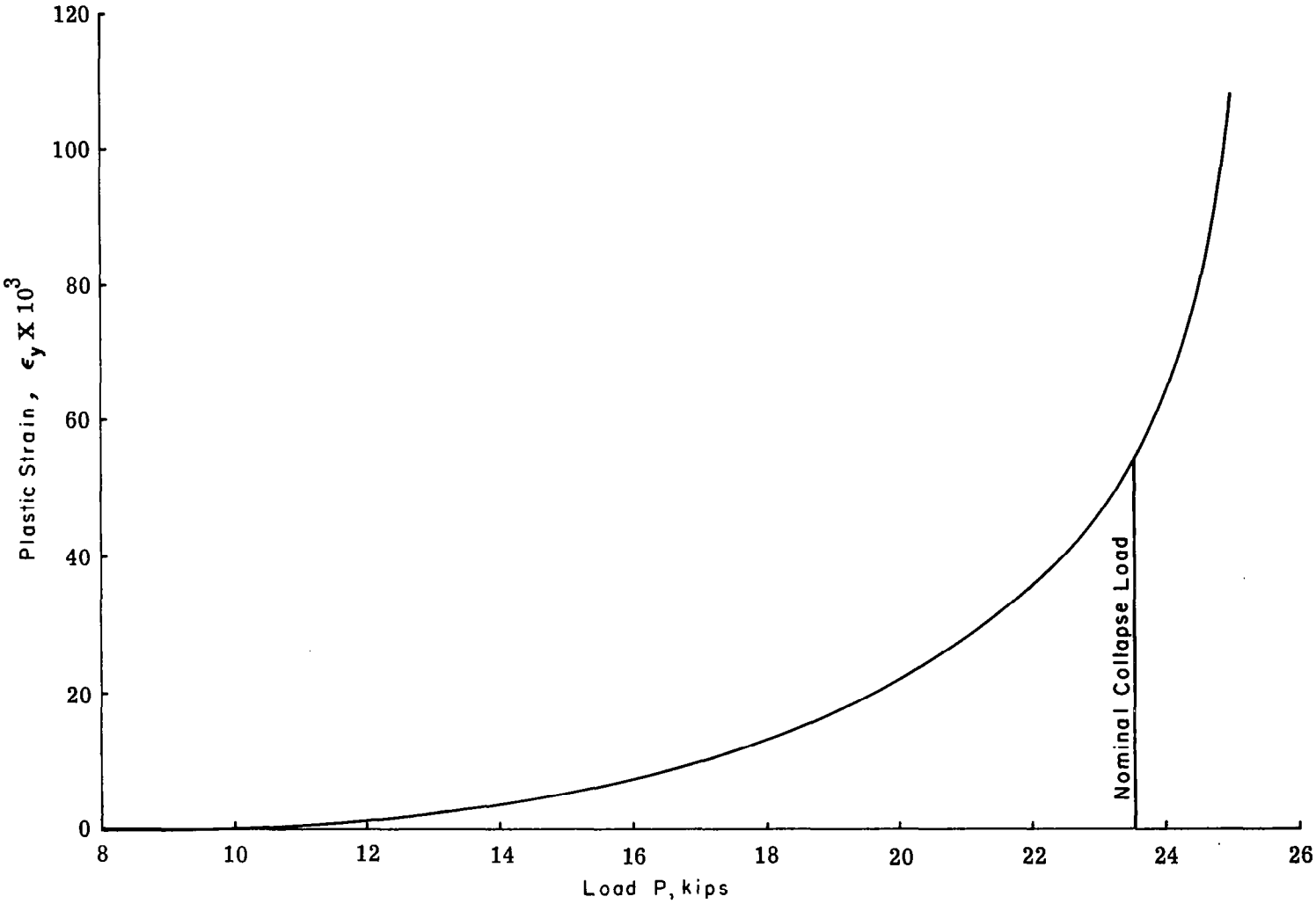

Fig. 13 STIFFENED PANEL: LOAD vs PLASTIC STRAIN AT THE CENTER
STRESS METHOD – STEPWISE LINEARIZATION PROCEDURE (ΔP = 50 lb)

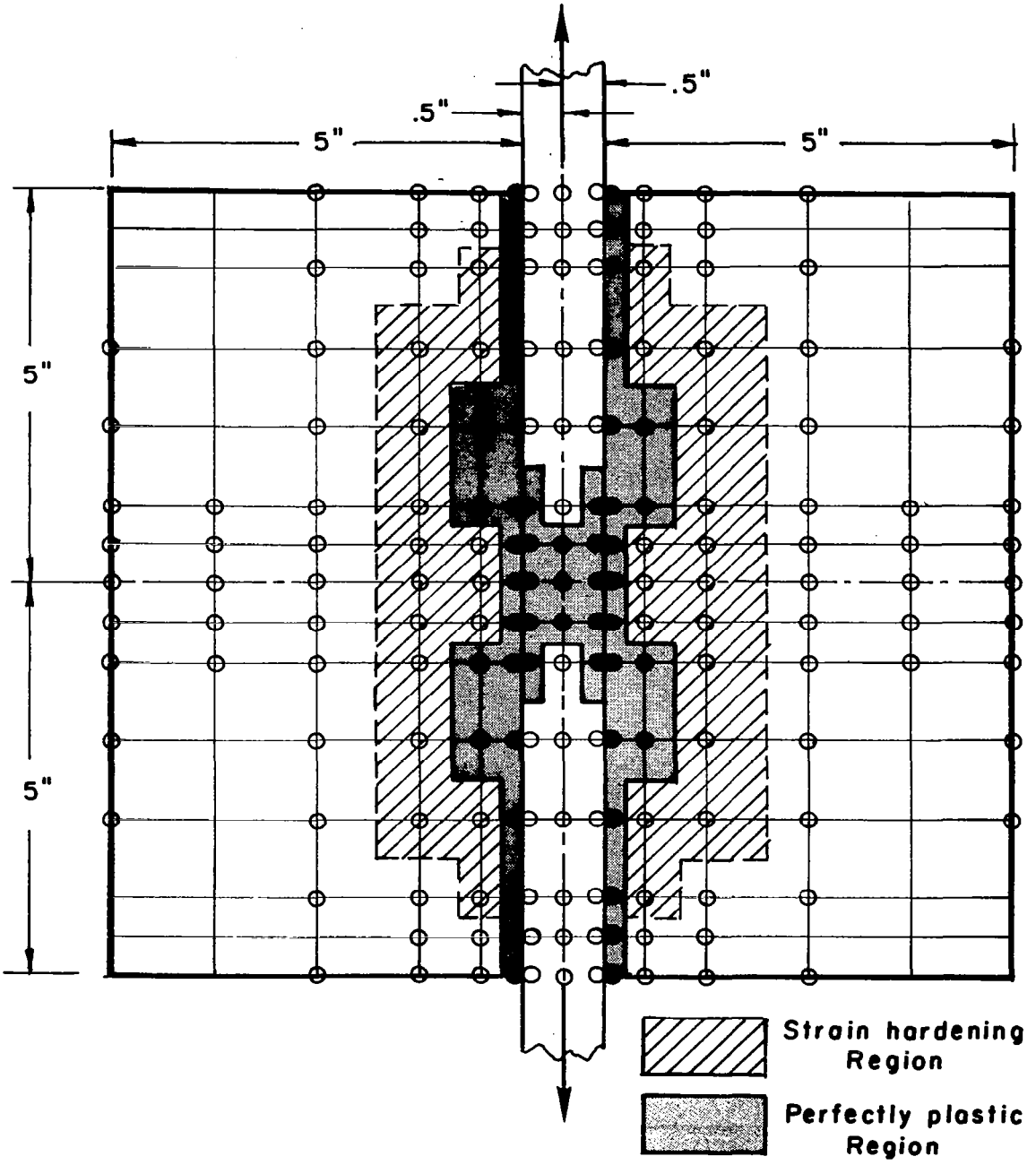

Fig. 14 STIFFENED PANEL: REGION OF PLASTICITY DEVELOPED AT P= 23.55 kips

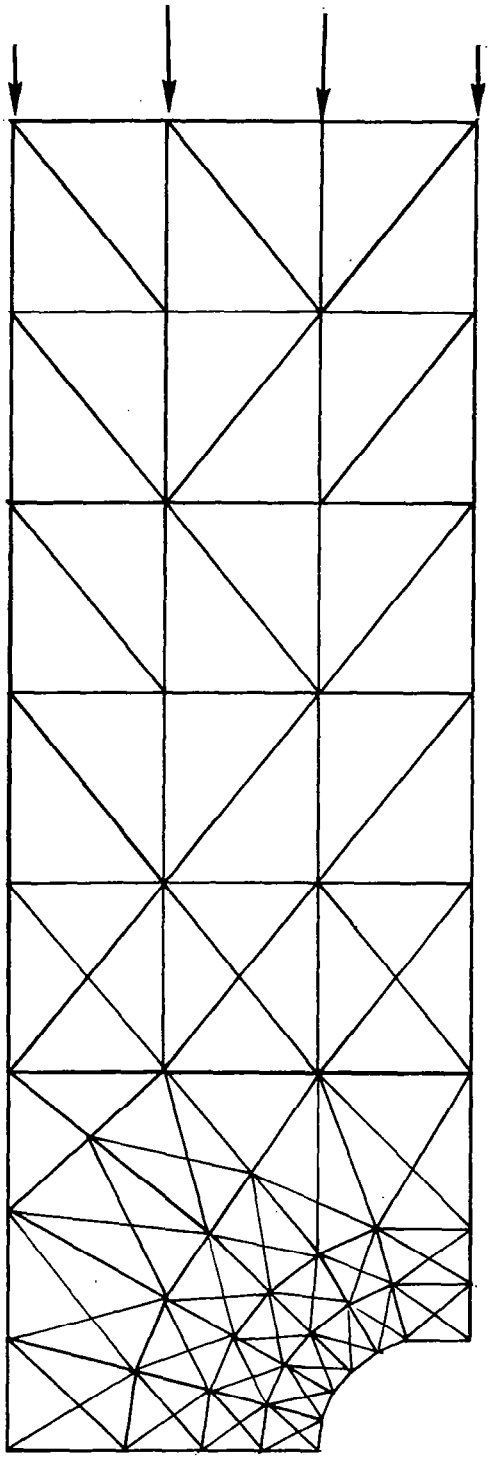

Fig. 15 DISCRETE-ELEMENT IDEALIZATION OF QUADRANT OF NOTCHED BAR

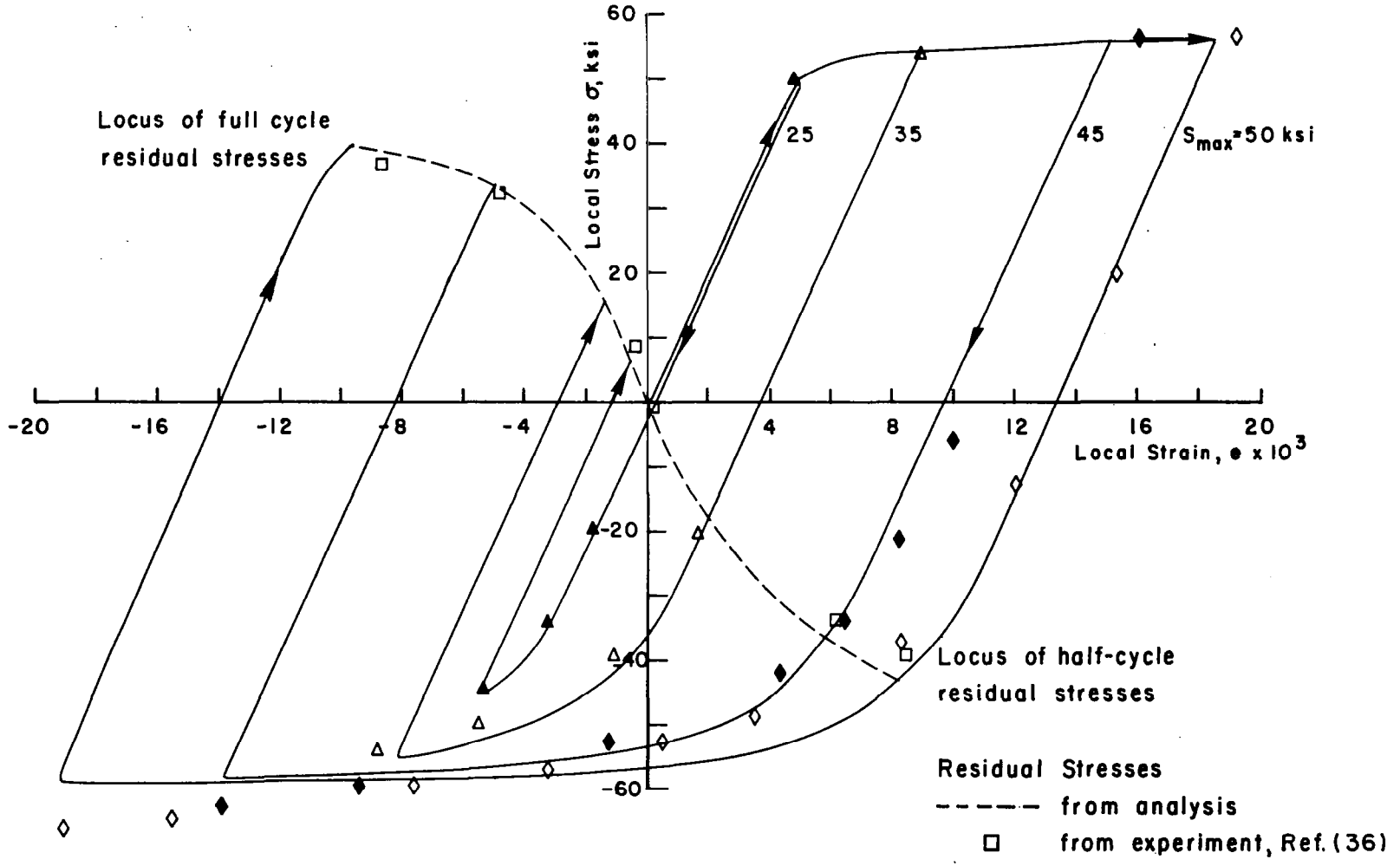

Fig. 16 NOTCHED BAR: LOCAL STRESS-STRAIN CURVES AT NOTCH ROOT FOR FIRST CYCLE OF REVERSED LOADING

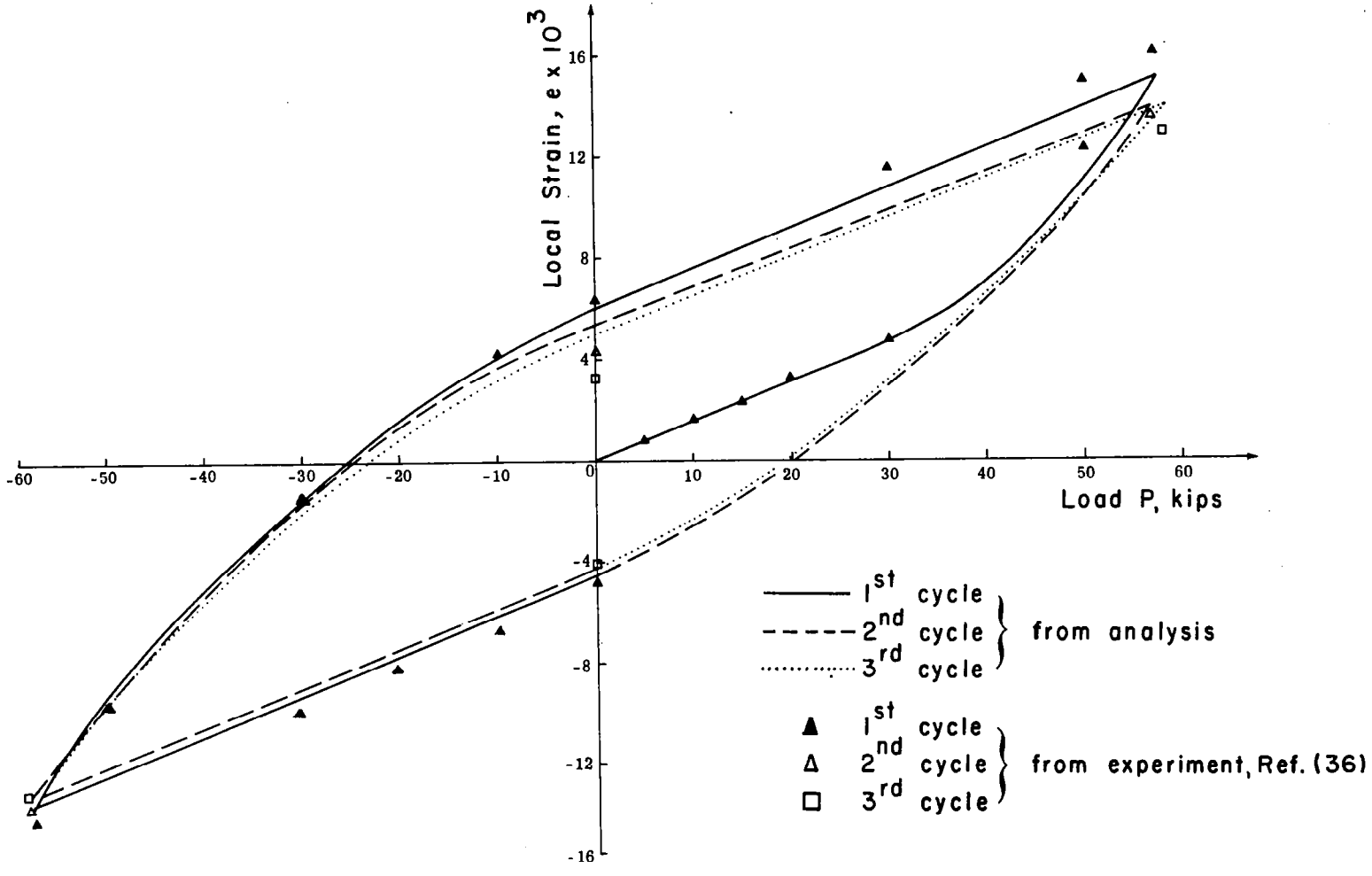

Fig. 17 NOTCHED BAR: THREE CYCLE LOAD-STRAIN CURVE AT NOTCH ROOT
(a) S_{max} = 45 ksi

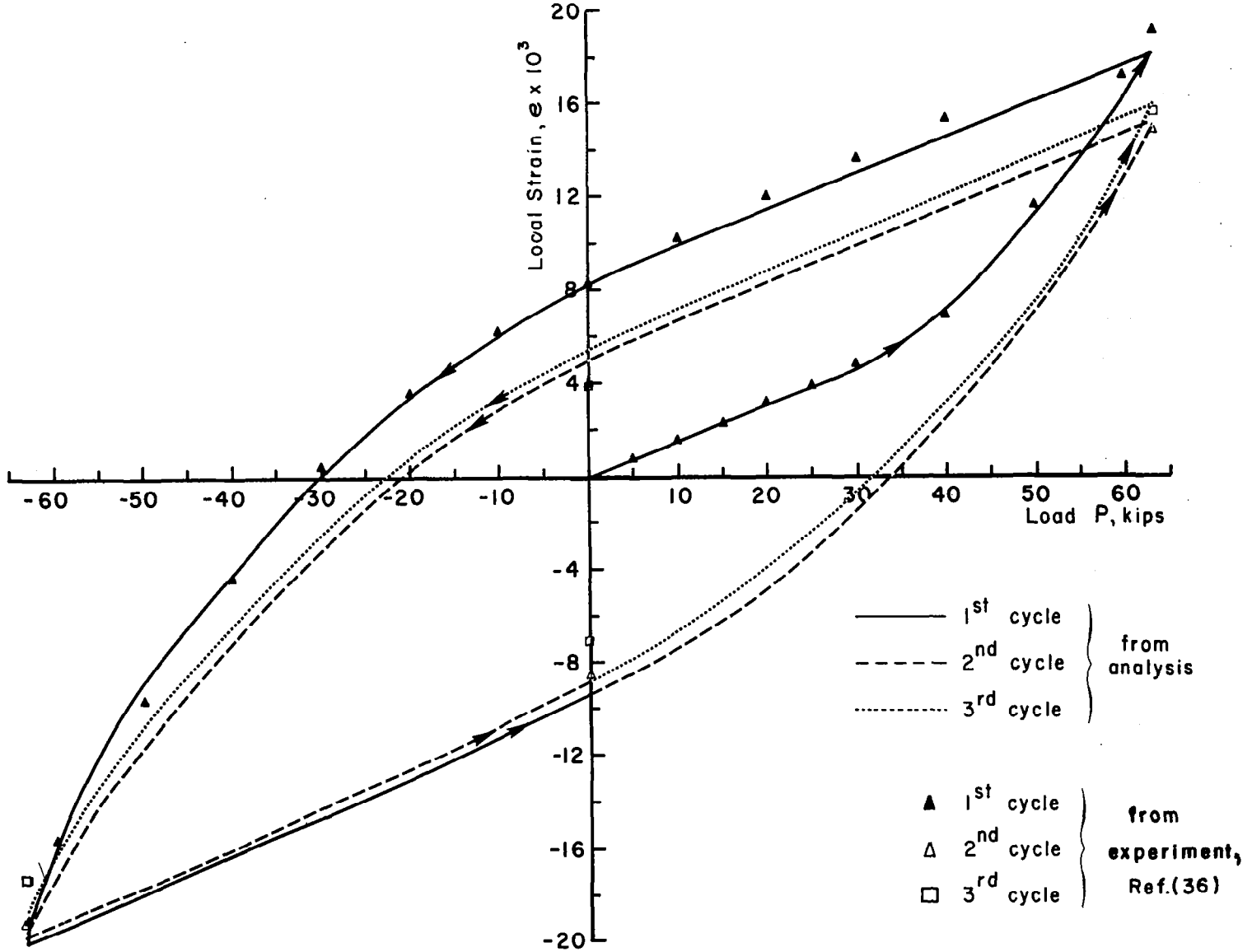

Fig. 17 (CONCLUDED)

(b) S_{max} = 50 KSI

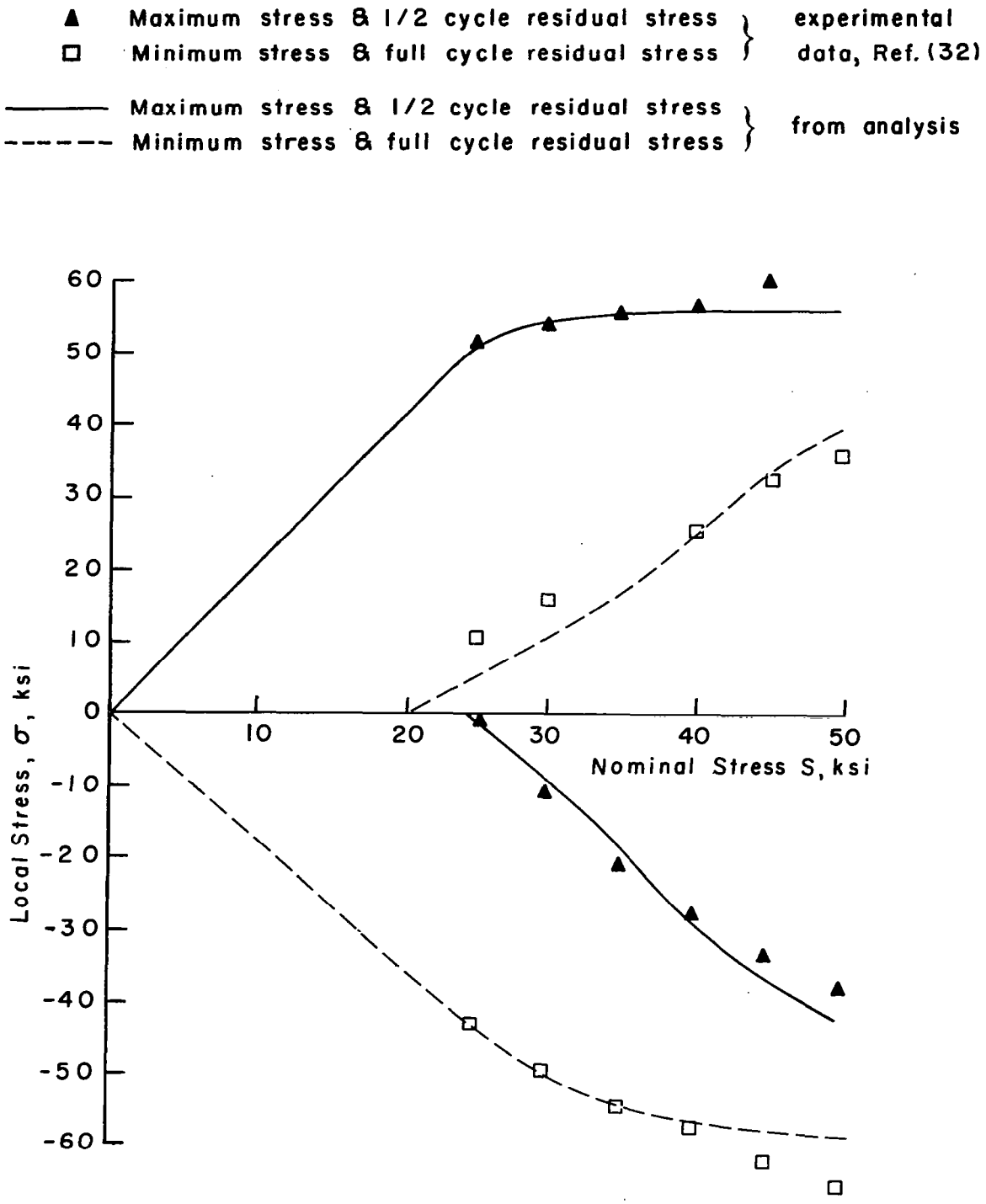

Fig. 18 NOTCHED BAR: FIRST CYCLE STRESSES AT NOTCH ROOT FOR REVERSED LOADING.

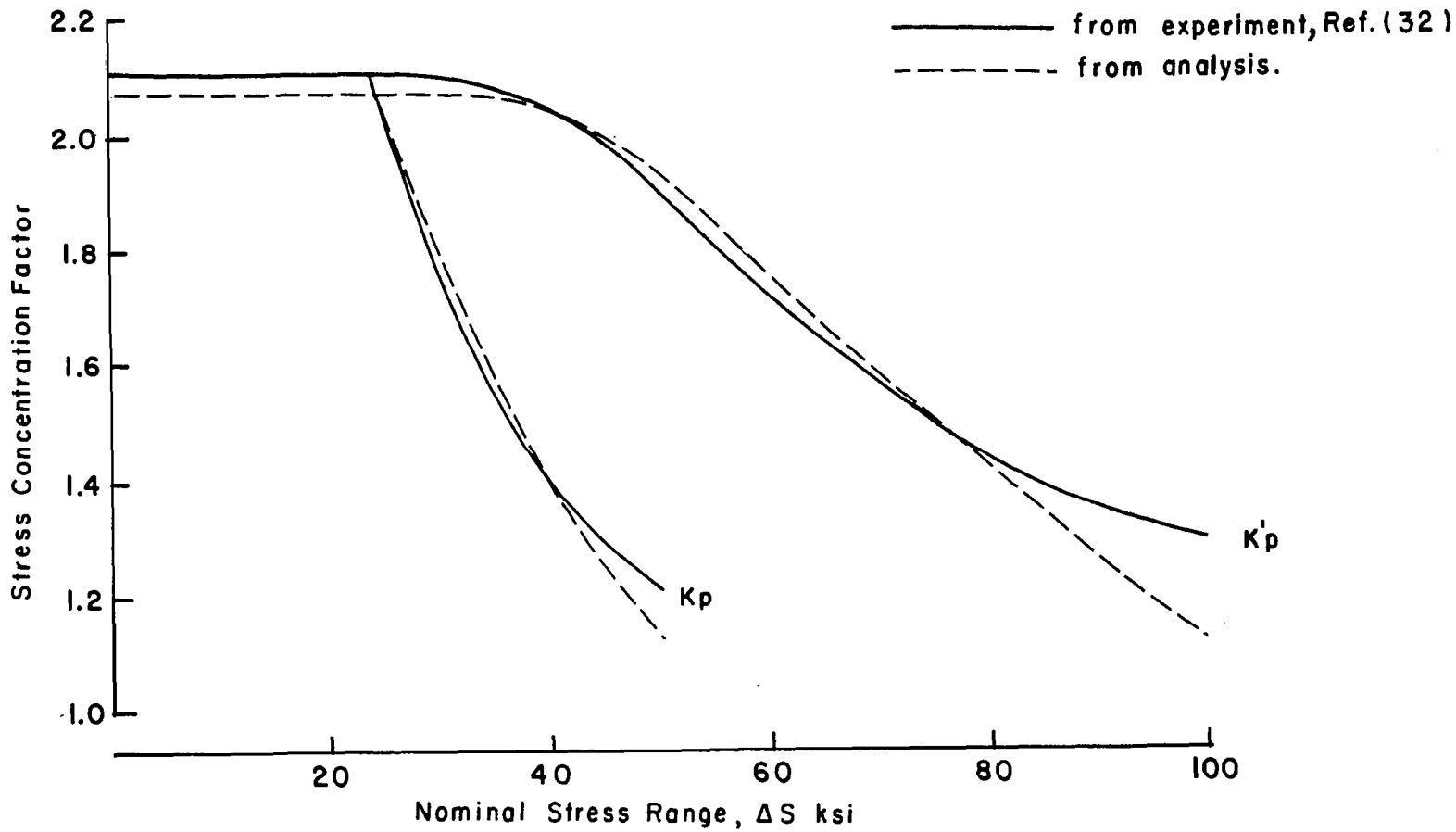

Fig. 19 NOTCHED BAR: PLASTIC STRESS CONCENTRATION FACTORS AT NOTCH ROOT vs. NOMINAL NET SECTION STRESS

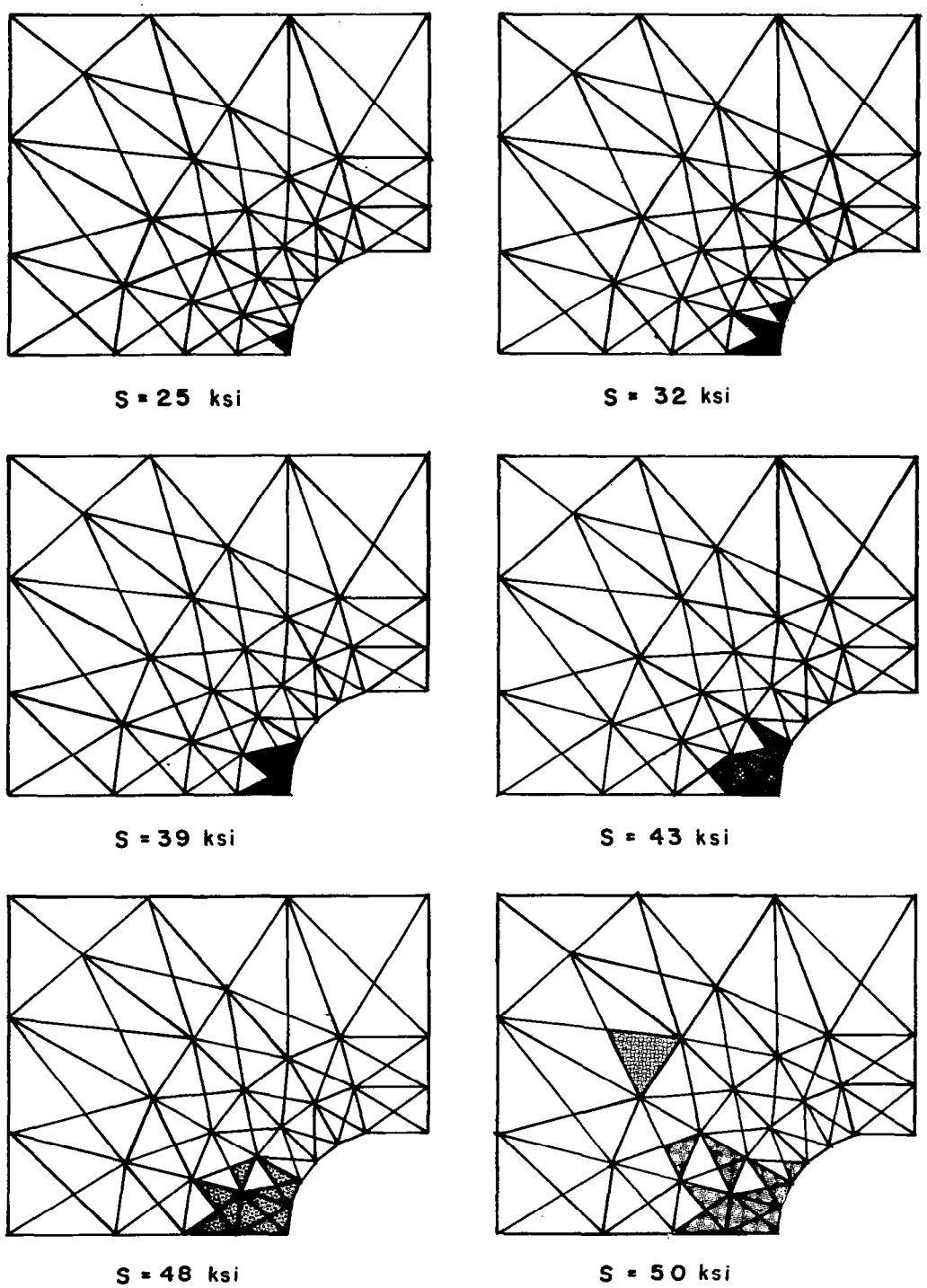

Fig. 20. NOTCHED BAR: DEVELOPMENT OF PLASTIC REGION (a) INITIAL TENSILE LOADING (S_{max}= 50 ksi)

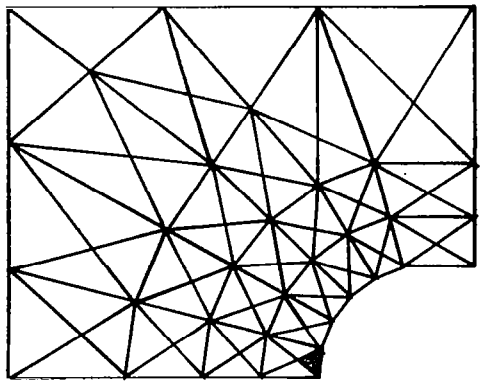

S = 7 ksi

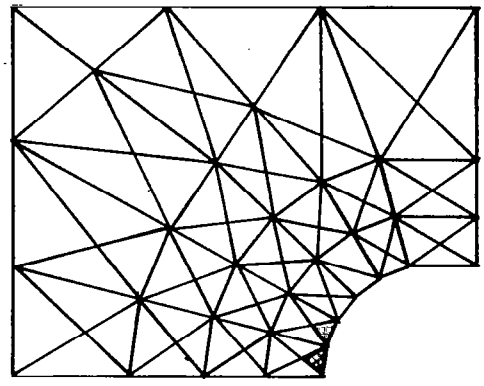

S = 5 ksi

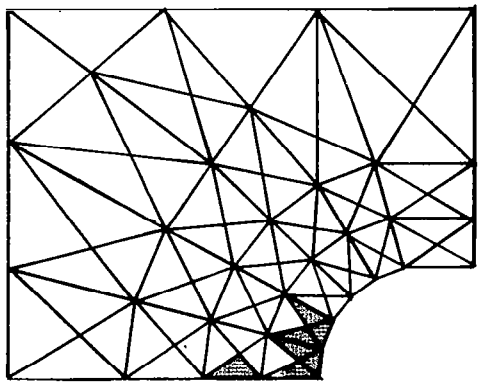

S = −16 ksi

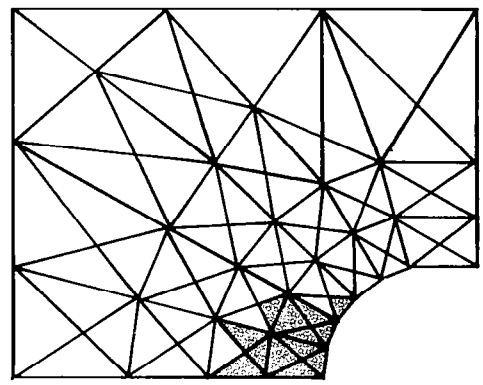

S = -28 ksi

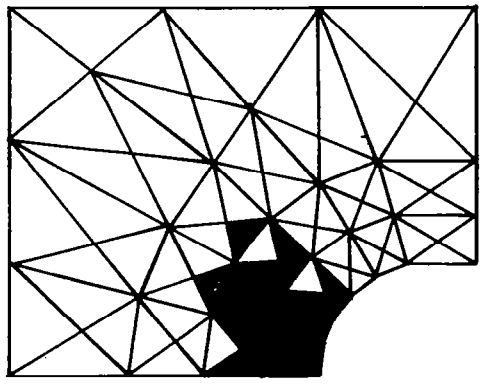

S = −38 ksi

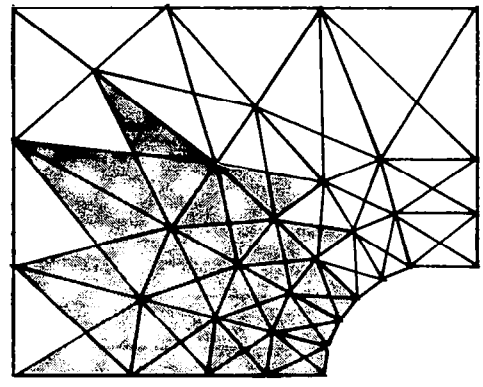

S = −50 ksi

Fig. 20 (CONCLUDED)
(b) UNLOADING and REVERSED LOADING (S_{min}=-50 KSI)

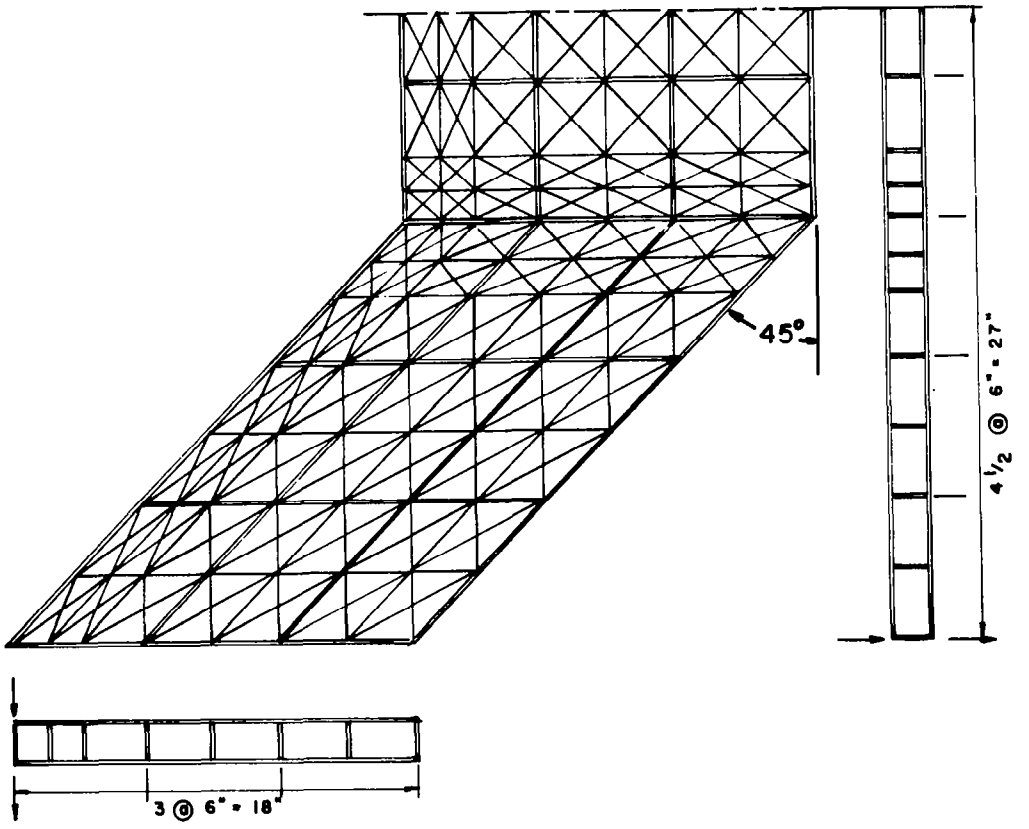

Fig. 21 , DISCRETE-ELEMENT IDEALIZATION OF SWEPT MULTICELL BOX BEAM.

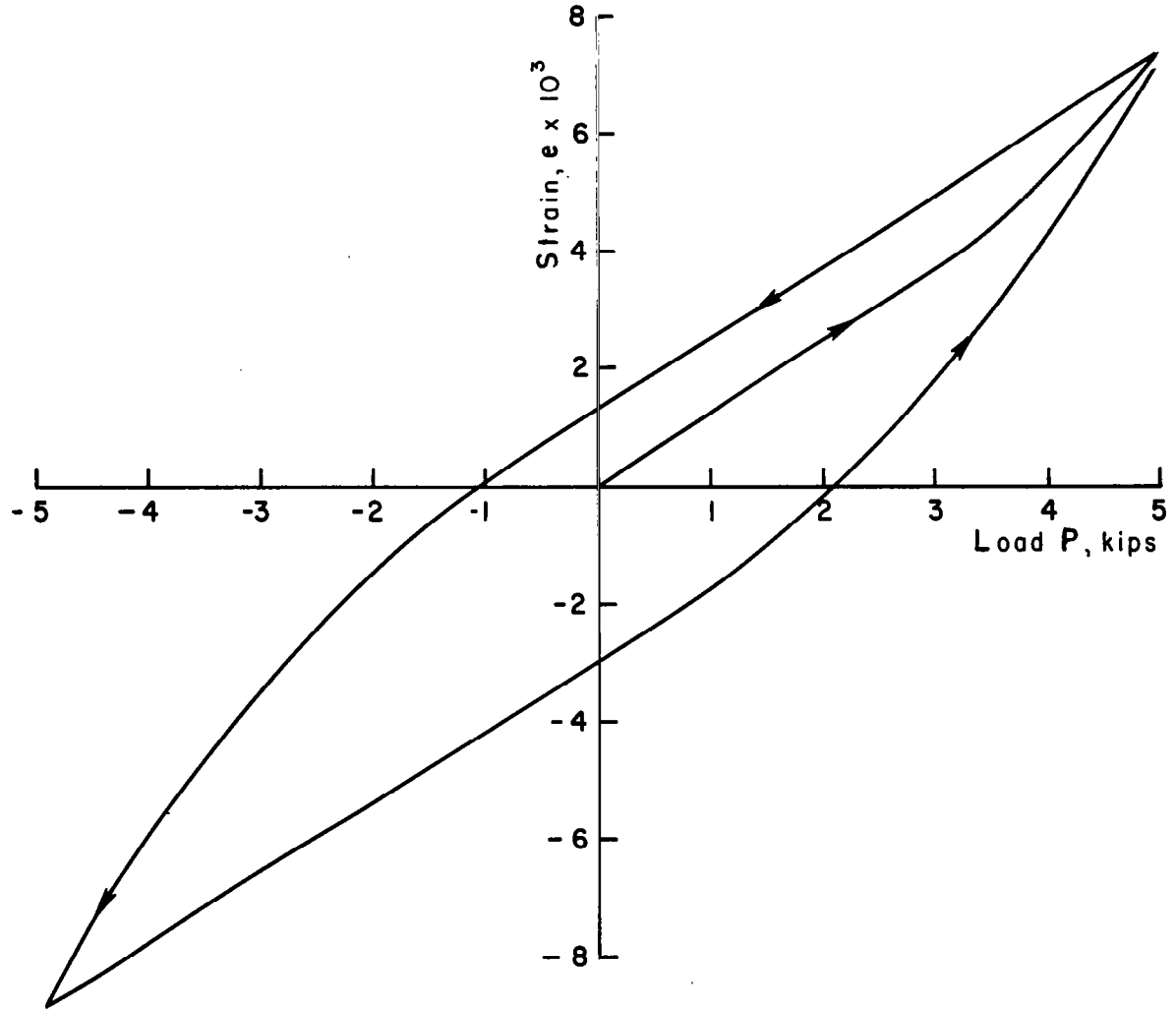

Fig.22 SWEPT BOX BEAM: CYCLIC LOAD vs. STRAIN AT ROOT OF TRAILING EDGE OF SWEPT PORTION.
STRESS METHOD - STEPWISE LINERIZATION PROCEDURE ($\Delta P = 50$ lb.)

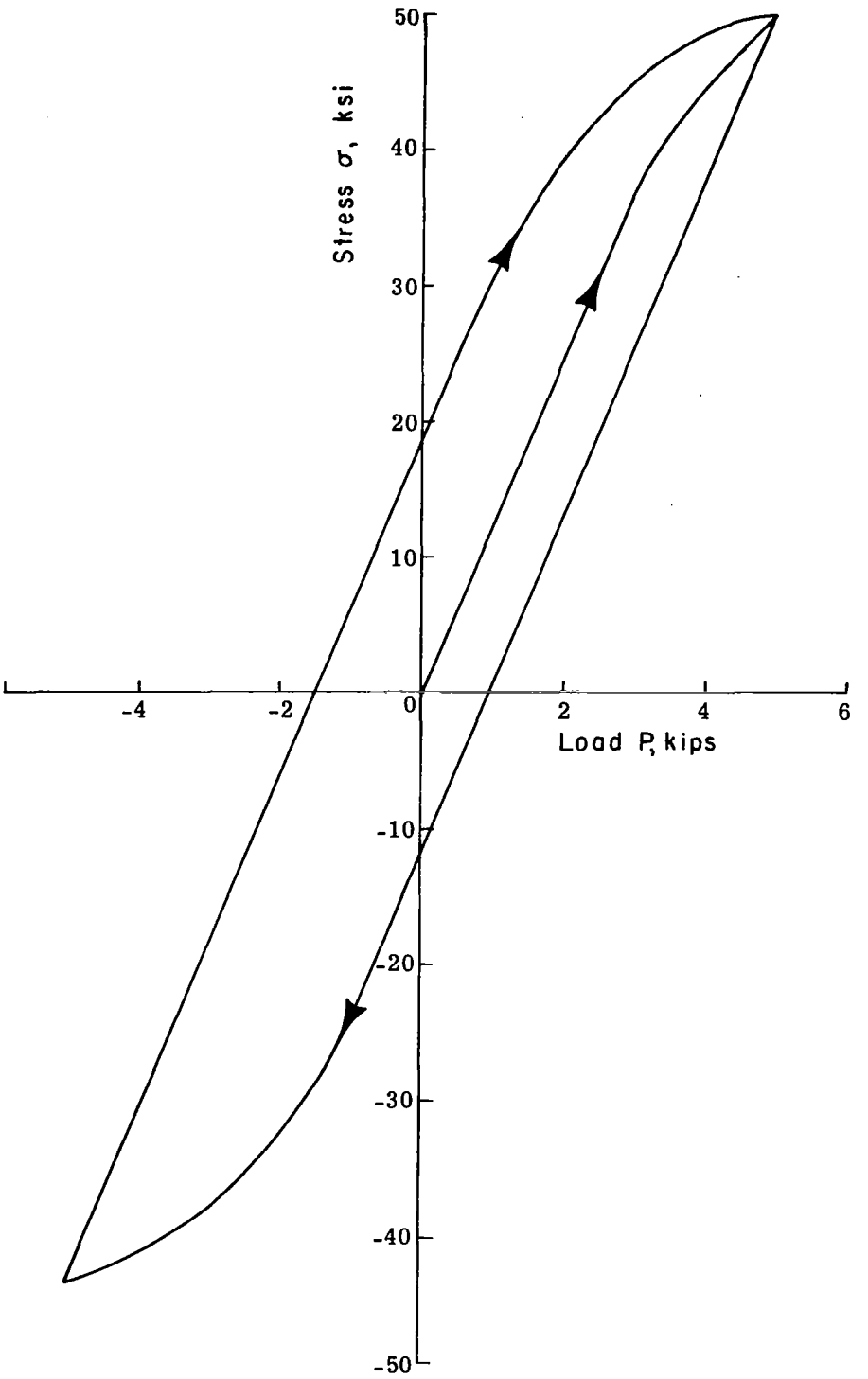

Fig.23 SWEPT BOX BEAM CYCLIC LOAD vs. STRESS AT ROOT OF TRAILING EDGE OF SWEPT PORTION
STRESS METHOD - STEPWISE LINEARIZATION PROCEDURE ($\Delta P = 50$ lb.)

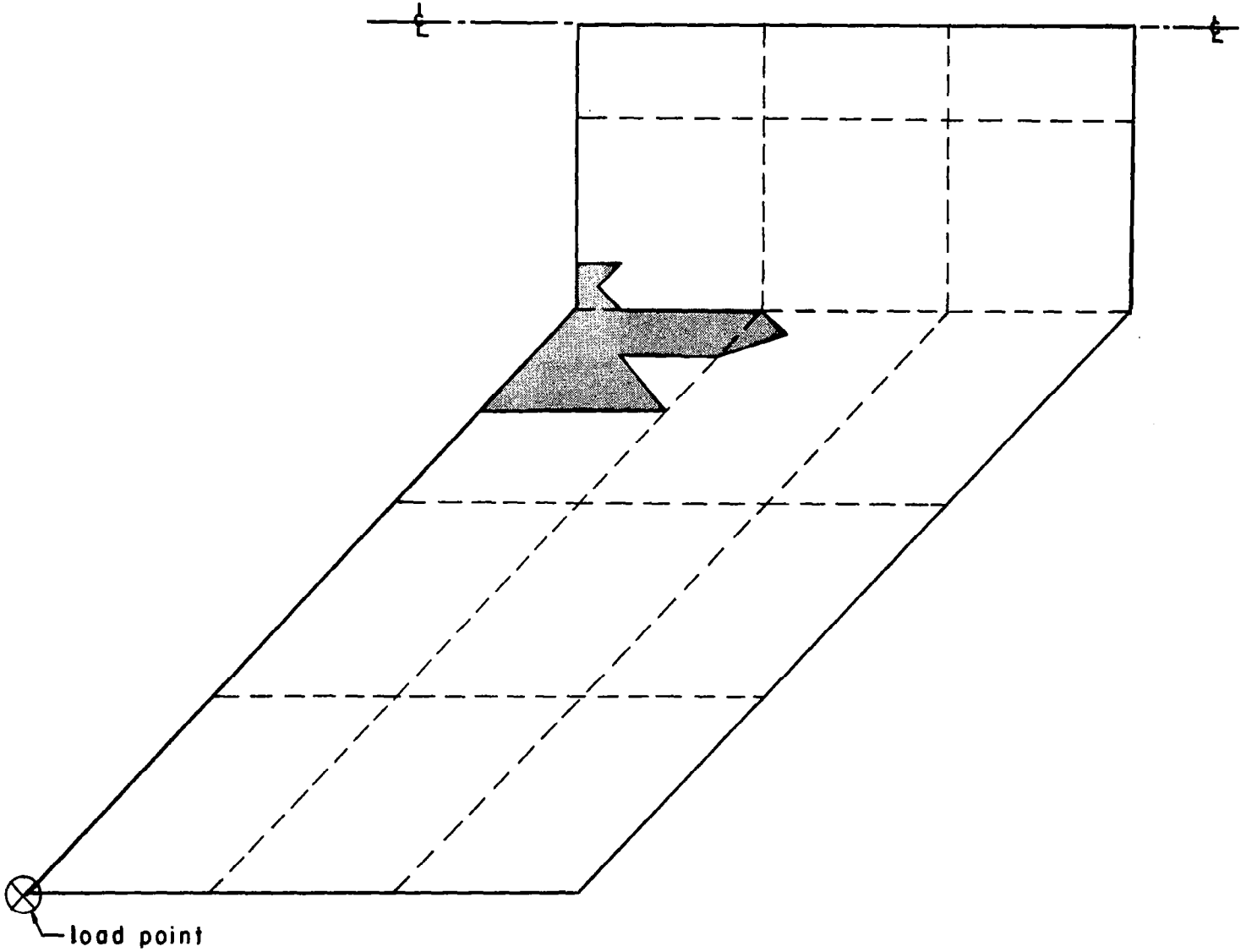

Fig.24 SWEPT BOX BEAM: REGION OF PLASTICITY DEVELOPED AT P = 5.5 kips

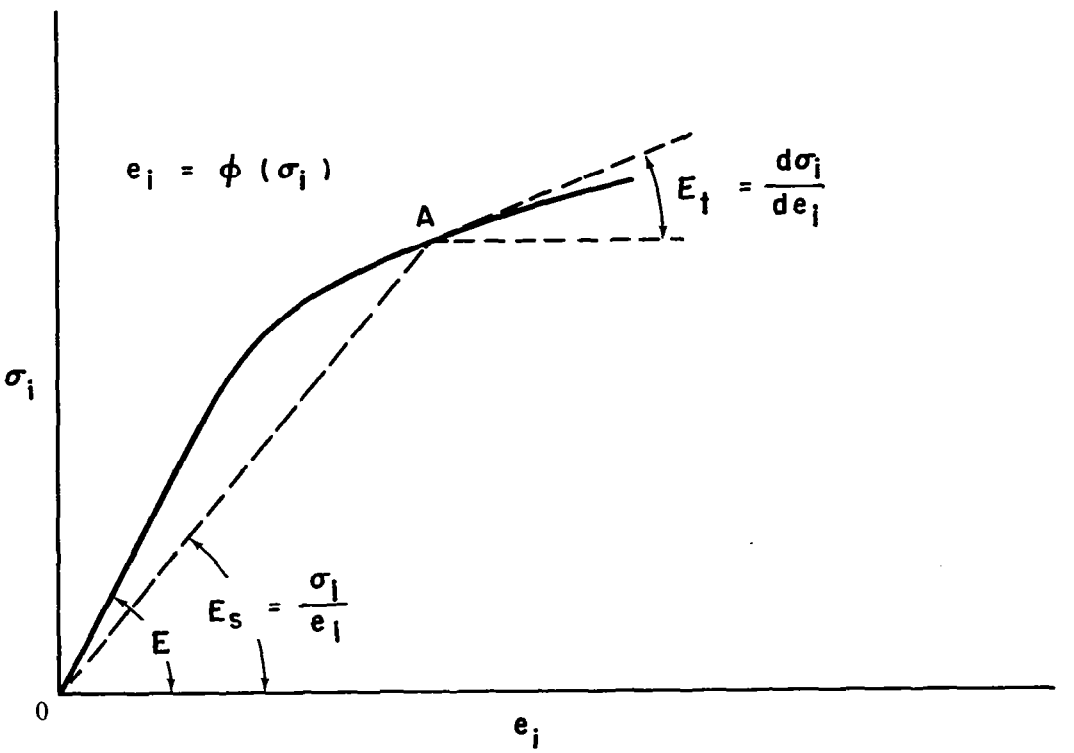

Fig. 25 TYPICAL EFFECTIVE STRESS-STRAIN CURVE.

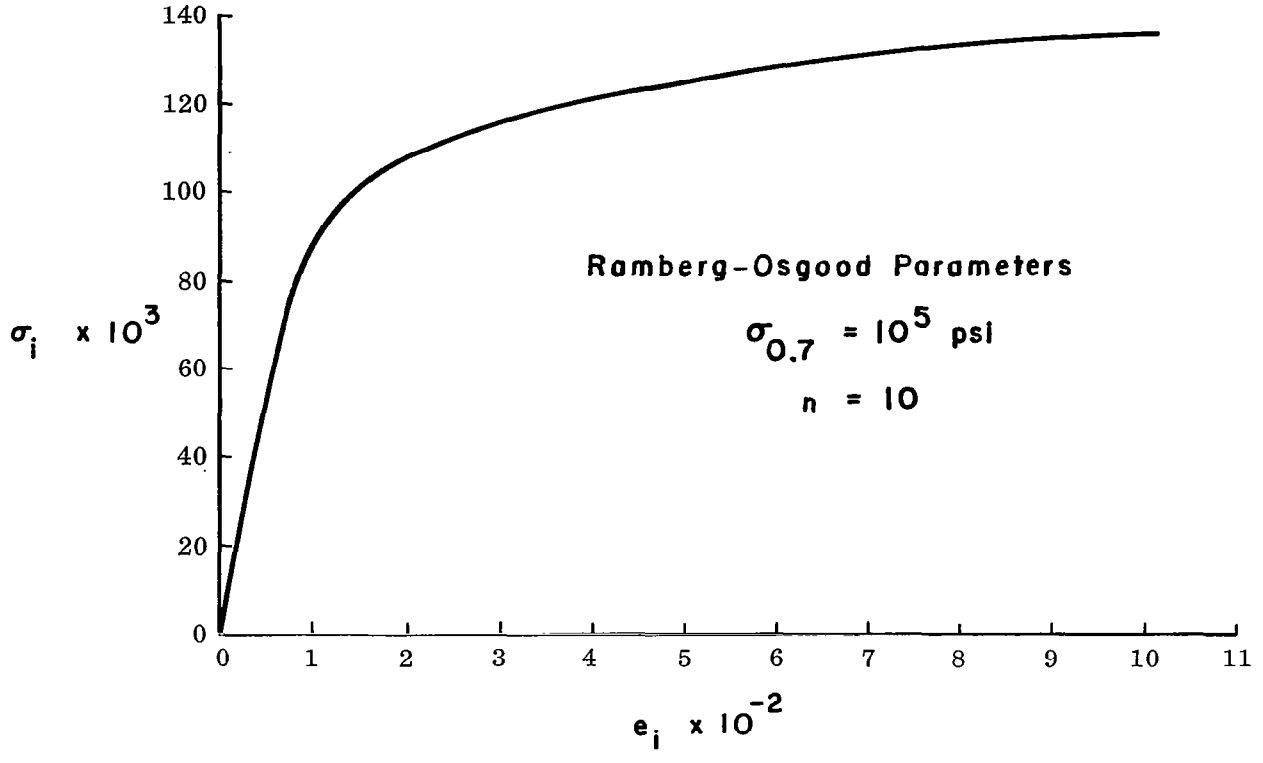

Fig. 26 EFFECTIVE STRESS vs EFFECTIVE STRAIN CURVE BASED ON THE RAMBERG-OSGOOD REPRESENTATION.

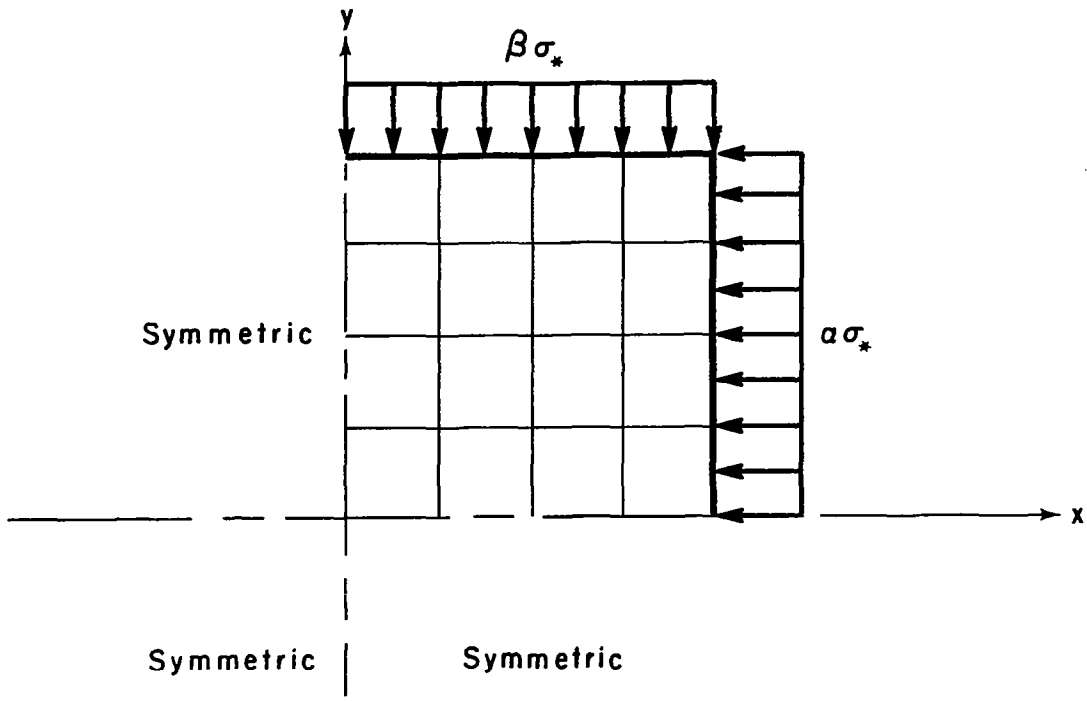

Fig. 27a IDEALIZATION USED FOR THE CASES SHOWN IN TABLE 2.

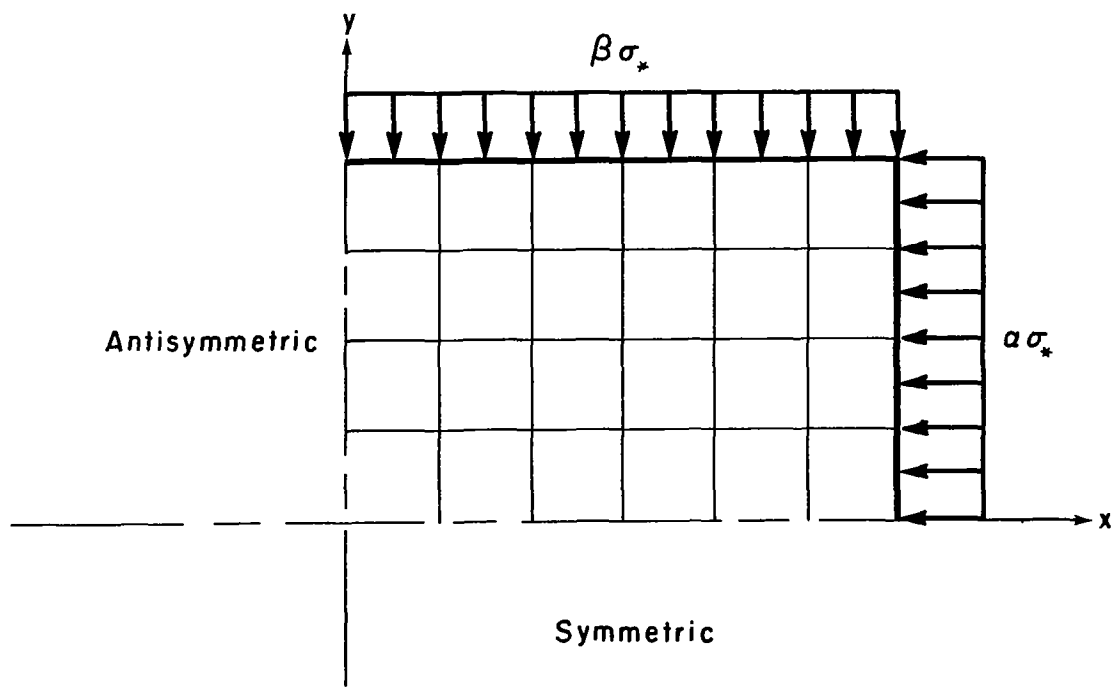

Fig. 27b IDEALIZATION USED FOR THE CASES SHOWN IN TABLE 3.

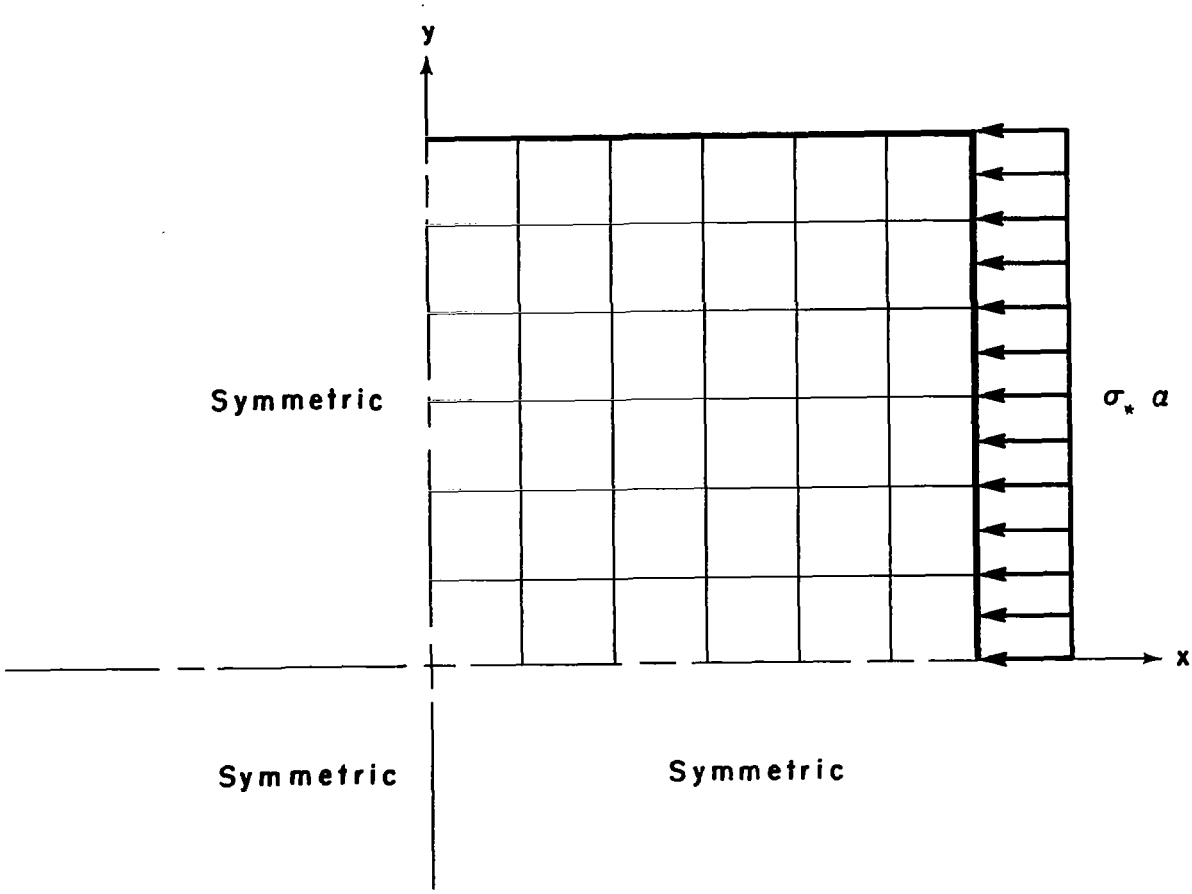

Fig. 28 IDEALIZATION FOR A CLAMPED SQUARE PLATE WITH A UNIFORM COMPRESSIVE LOAD ON TWO OPPOSITE EDGES.

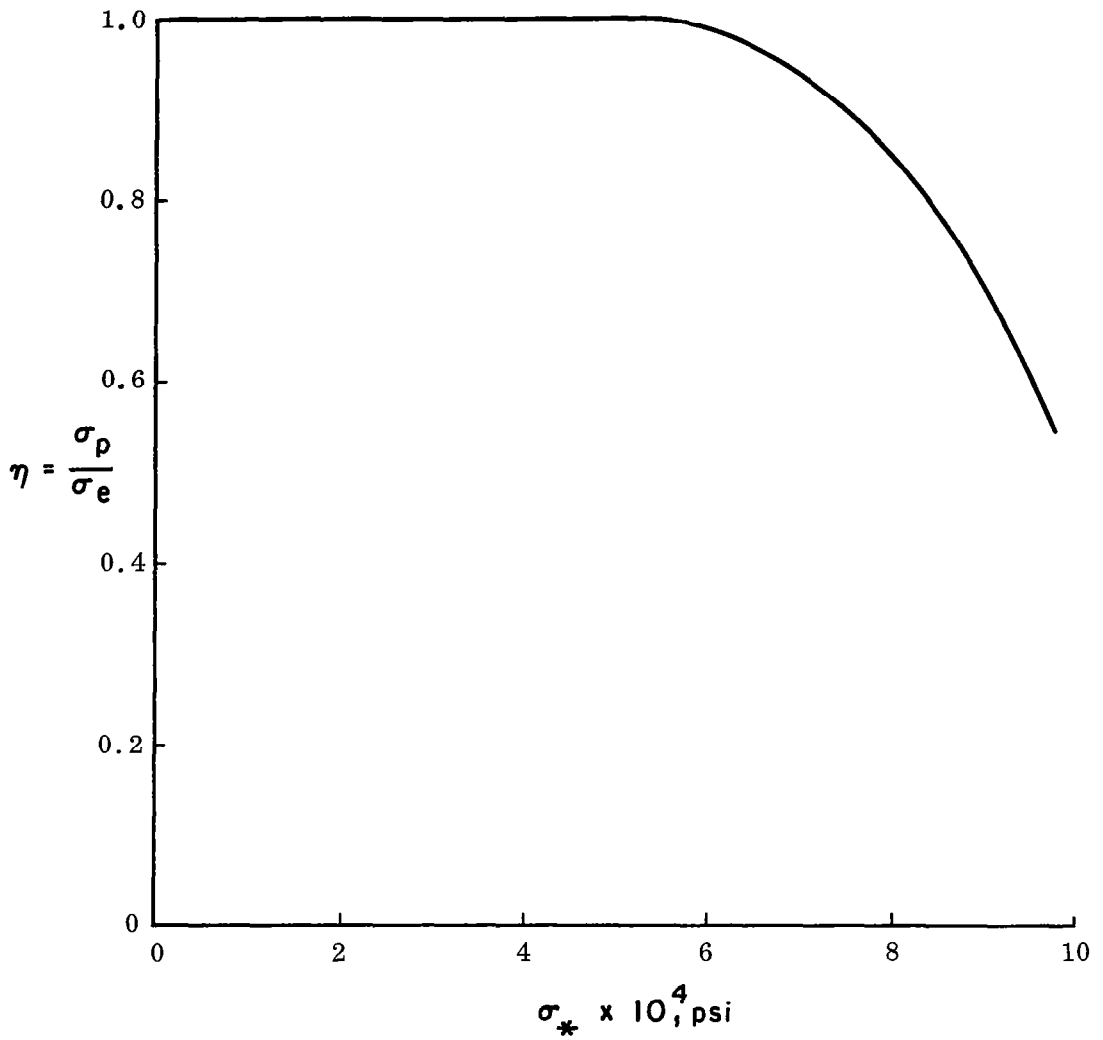

Fig. 29 PLASTICITY REDUCTION FACTOR FOR A CLAMPED SQUARE PLATE WITH A UNIFORM COMPRESSIVE LOAD ON TWO OPPOSITE EDGES.

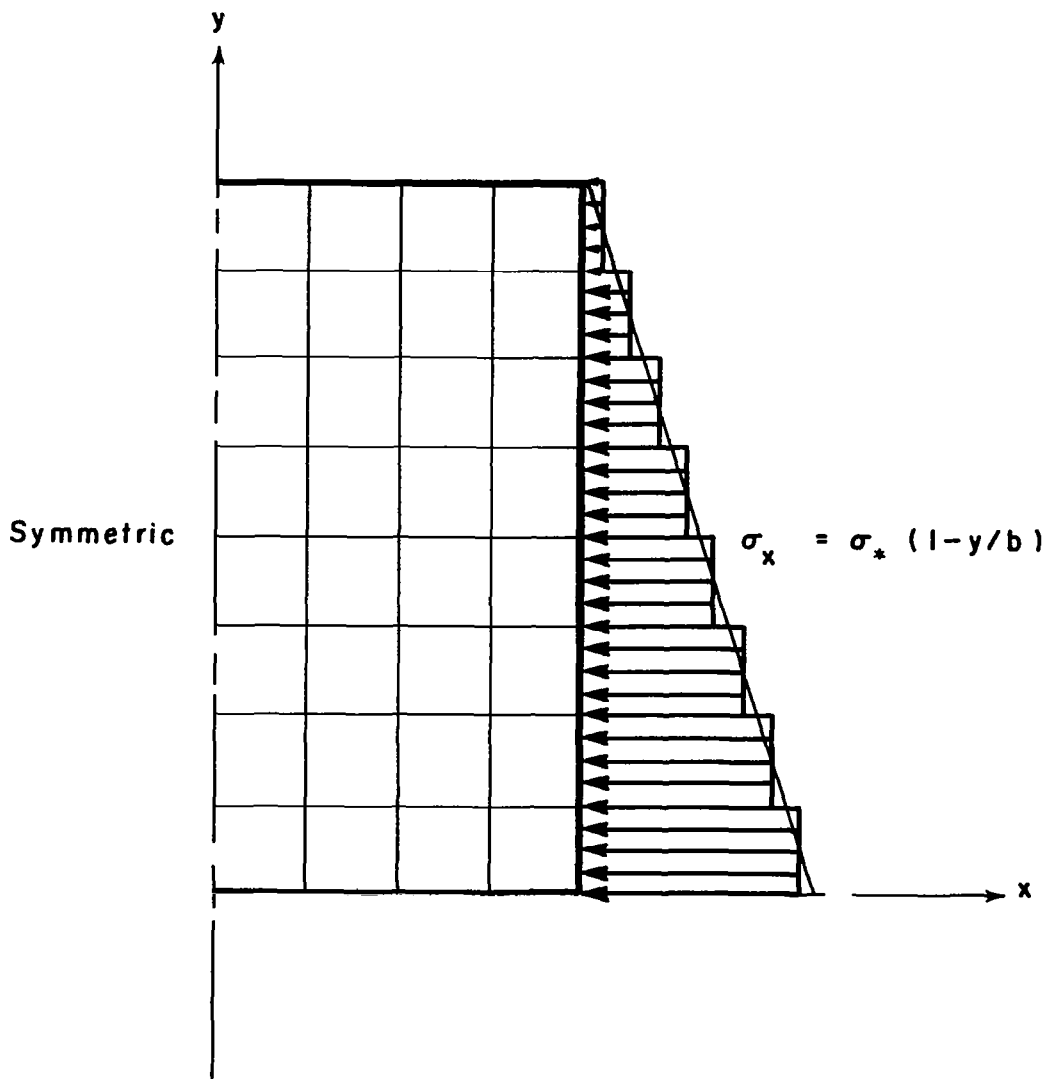

Fig. 30 IDEALIZATION FOR SIMPLY-SUPPORTED SQUARE PLATE WITH A TRIANGULAR COMPRESSIVE EDGE LOAD.

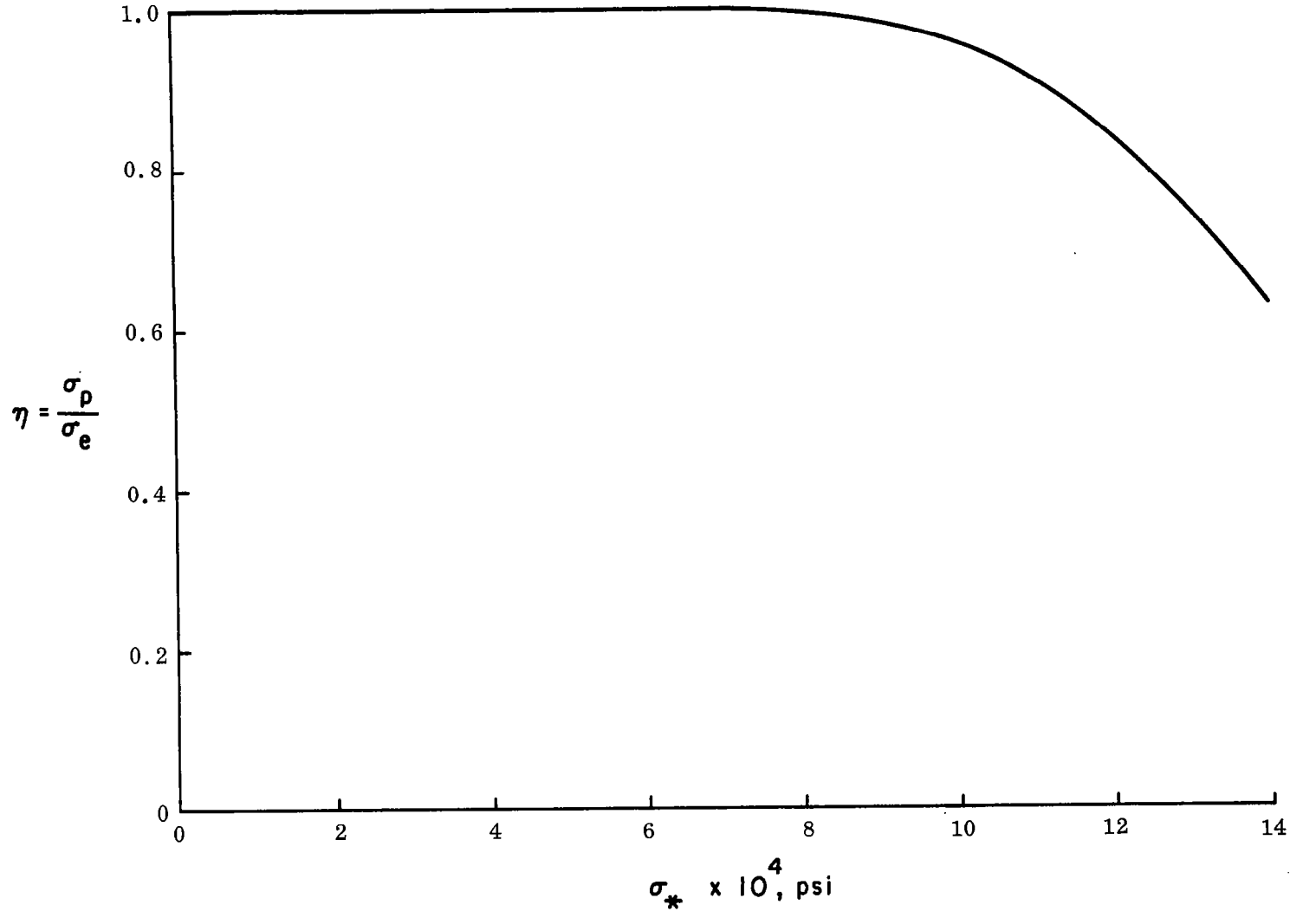

Fig. 31 PLASTICITY REDUCTION FACTOR FOR A SIMPLY-SUPPORTED SQUARE PLATE WITH A TRIANGULAR COMPRESSIVE LOAD ON TWO OPPOSITE EDGES.

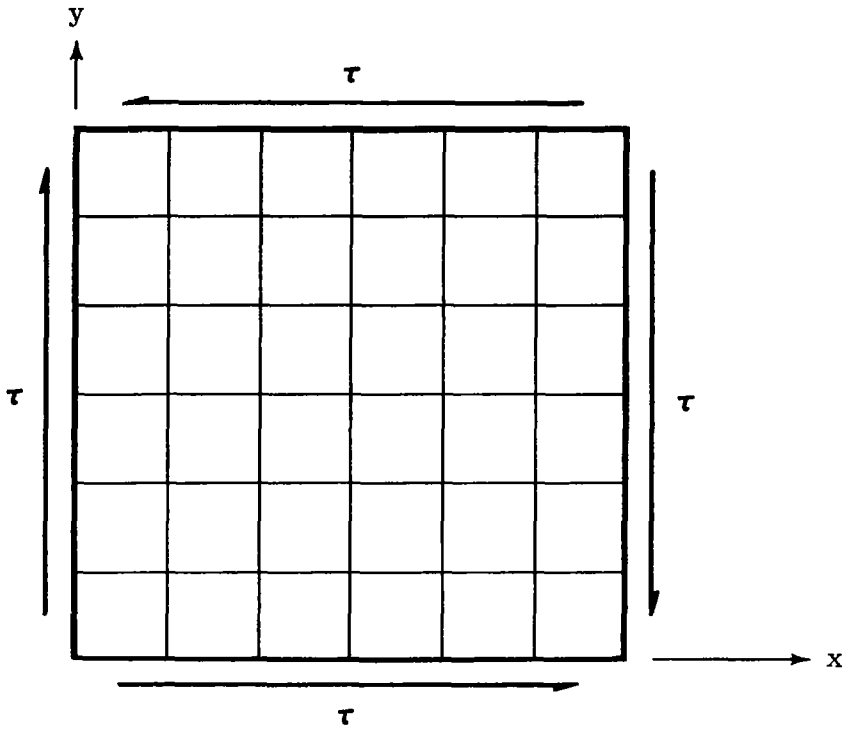

Fig. 32 IDEALIZATION FOR A SIMPLY-SUPPORTED SQUARE PLATE WITH A UNIFORM EDGE SHEAR LOAD.

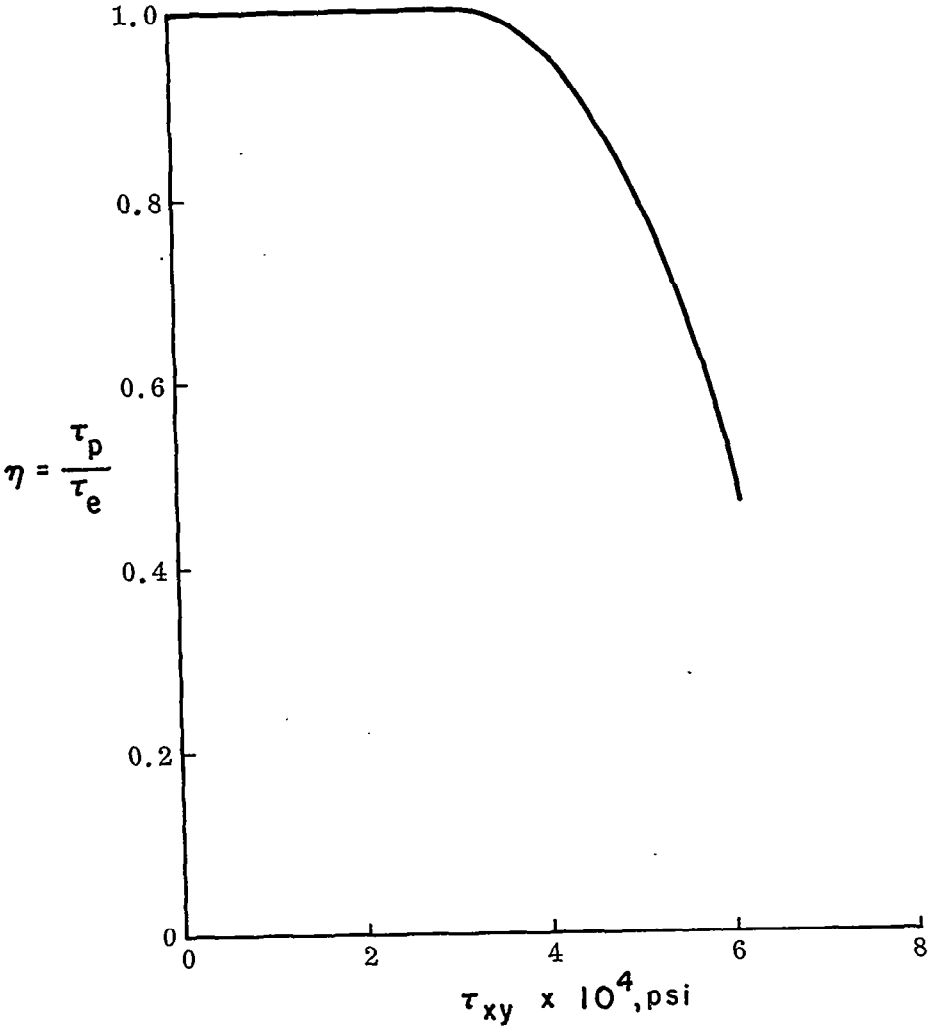

Fig. 33 PLASTICITY REDUCTION FACTOR FOR A SIMPLY-SUPPORTED SQUARE PLATE WITH A UNIFORM EDGE SHEAR LOAD.

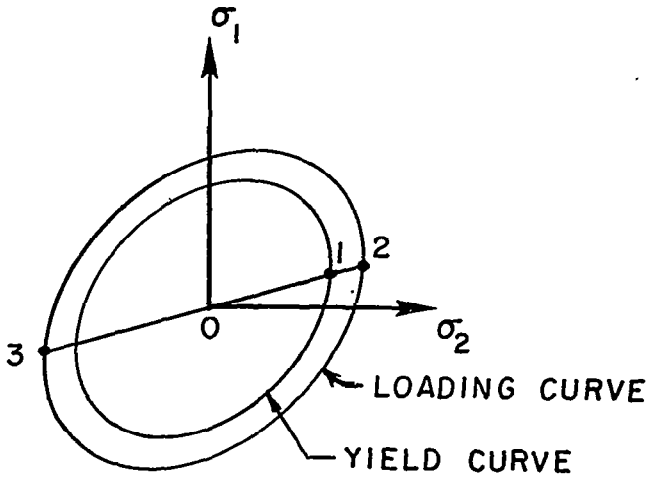

Fig.34 ISOTROPIC HARDENING

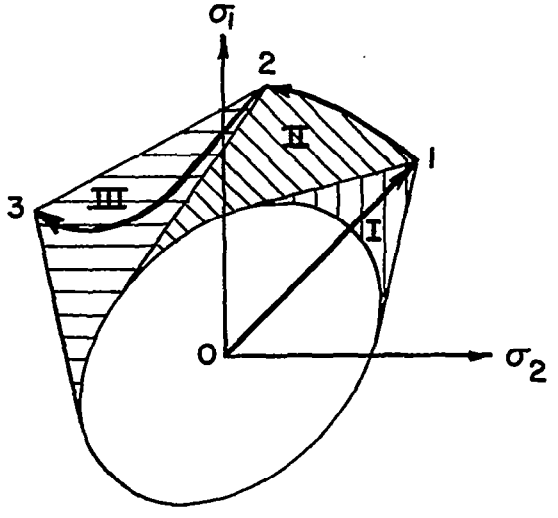

Fig.35 SLIP THEORY HARDENING

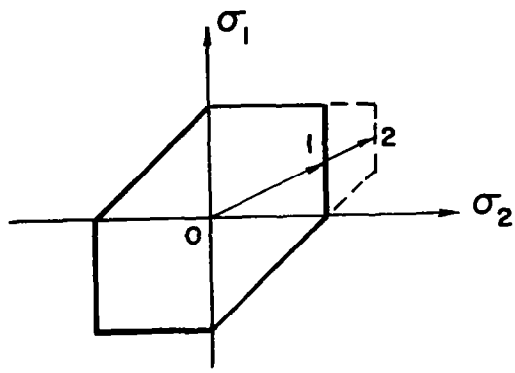

(a) INDEPENDENT LOADING SURFACES

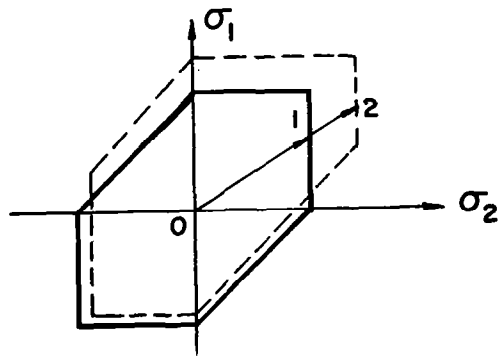

(b) INTERDEPENDENT LOADING SURFACES

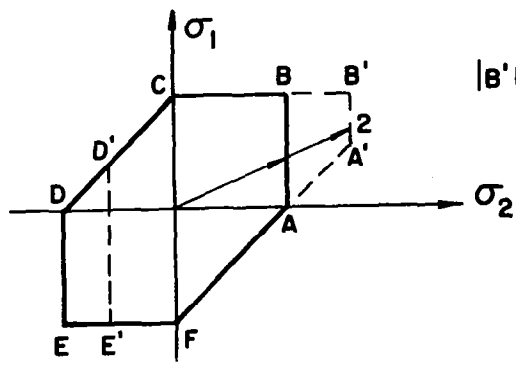

(c) SPECIAL CASE OF (b) (From Ref. 14)

Fig. 36 PIECEWISE LINEAR HARDENING

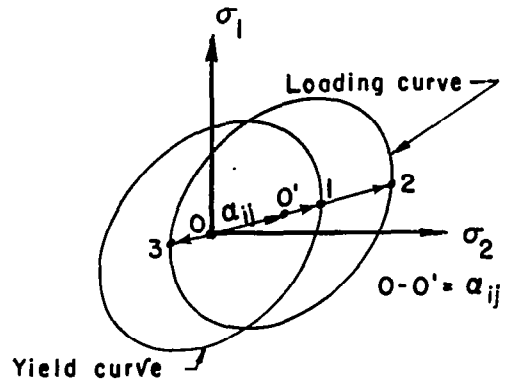

Fig.37 KINEMATIC HARDENING

$da_{ij}^{(P)}$: Prager's kinematic hardening

$da_{ij}^{(Z)}$: Ziegler's modification.

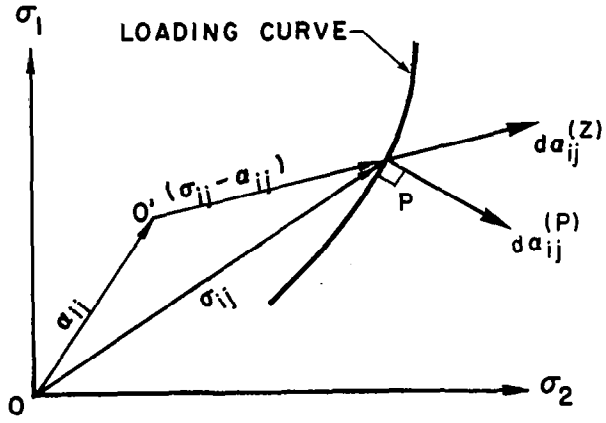

Fig.38 COMPARISON OF PRAGER'S RULE WITH ZIEGLER'S MODIFICATION

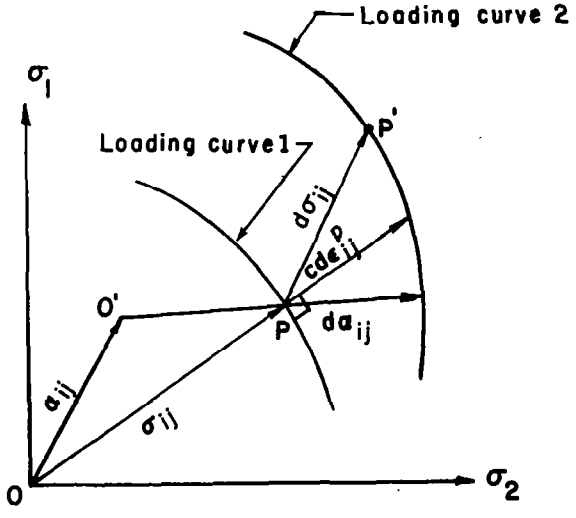

Fig.39 HARDENING RULE AND FLOW LAW FOR WORK-HARDENING MATERIAL USING ZIEGLER'S MODIFICATION

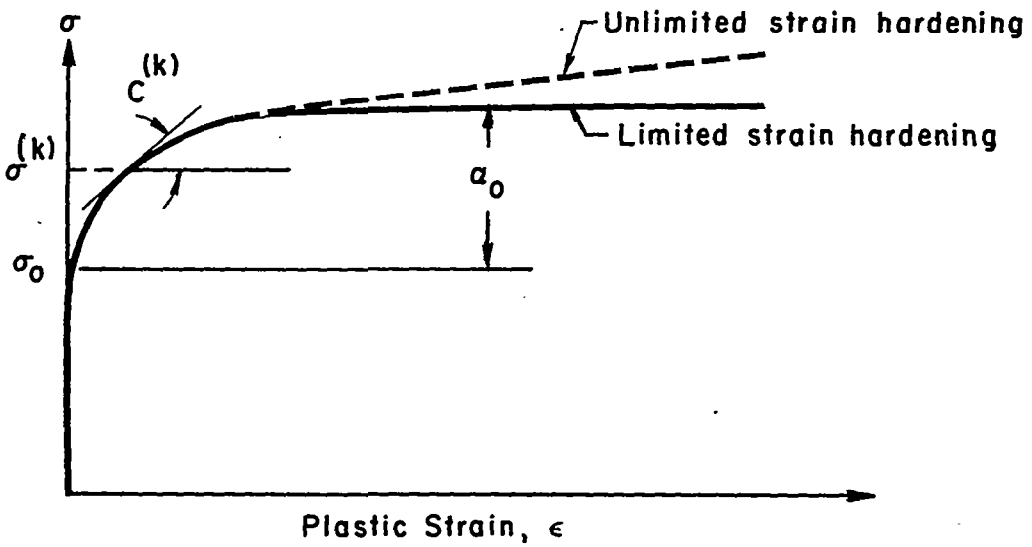

Fig. 40 TYPICAL UNIAXIAL STRESS vs PLASTIC STRAIN CURVE

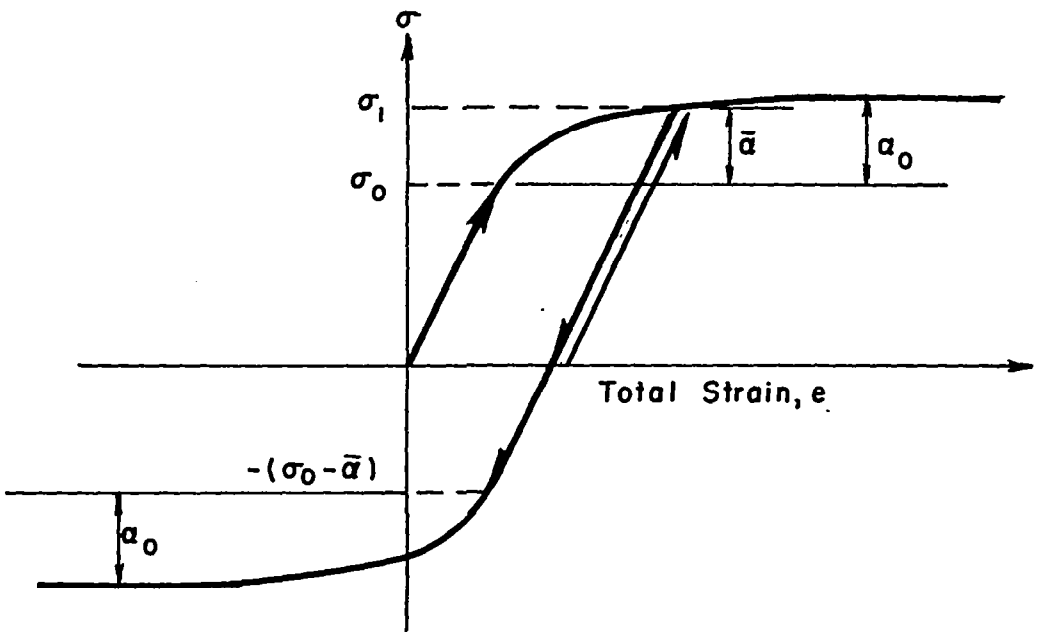

Fig. 41 ASSUMED CYCLIC STRESS-STRAIN BEHAVIOR FOR LIMITED STRAIN HARDENING

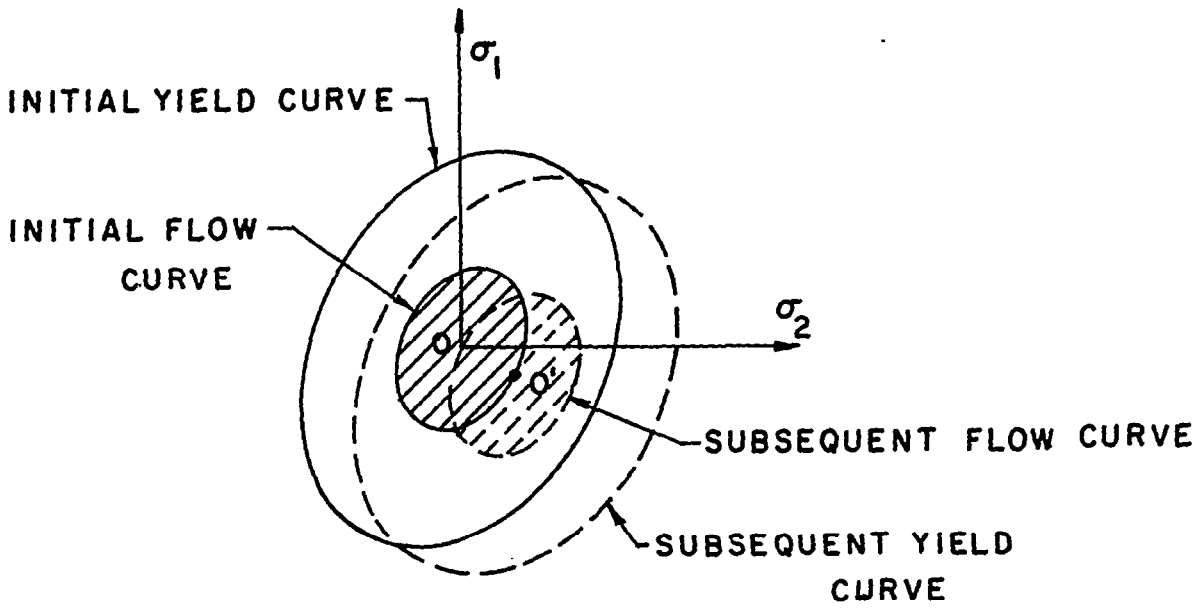

Fig.42 INITIAL AND SUBSEQUENT YIELD AND FLOW CURVES

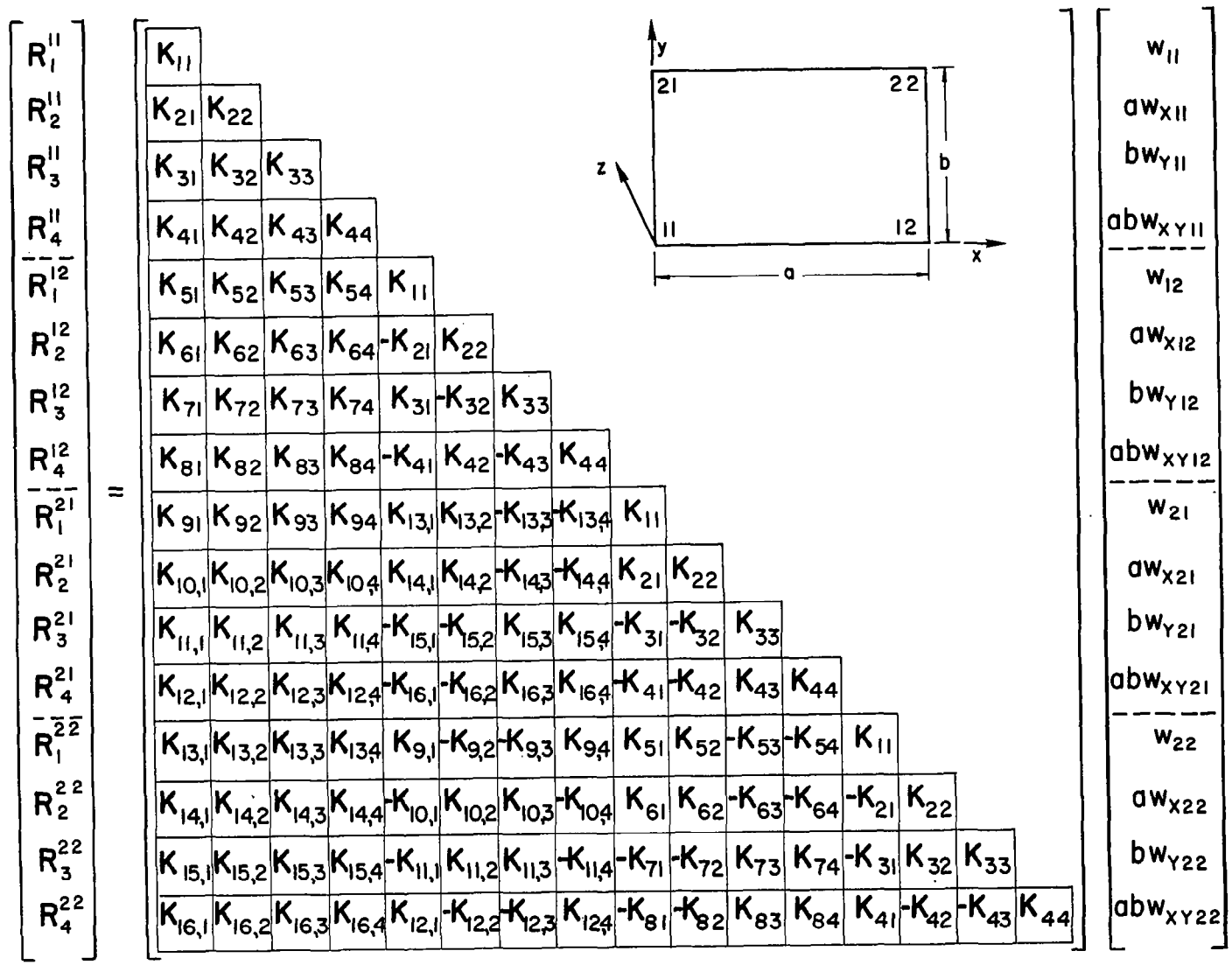

Fig. 43 a. ARRANGEMENT OF THE STIFFNESS MATRICES (PATTERN USED WITH COMPONENT PARTS MULTIPLIED BY C_1, C_5, $\bar{C}_3$, $\tilde{C}_3$, σ_x, σ_y)

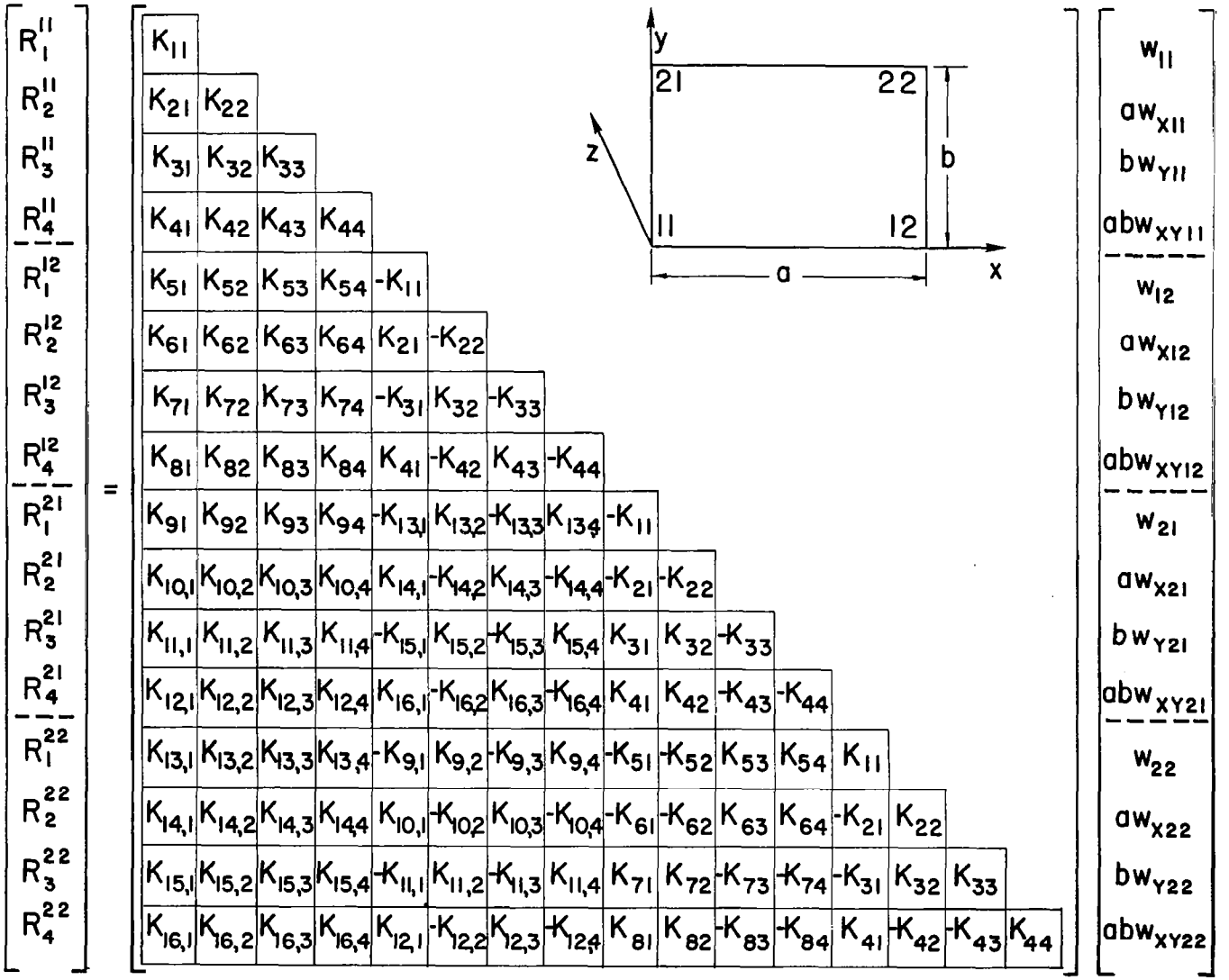

Fig. 43 b. ARRANGEMENT OF THE STIFFNESS MATRICES (PATTERN USED WITH COMPONENT PARTS MULTIPLIED BY C_2 , C_4 , τ_{xy})

$K_{C_1} =$

156	78	22	11
78	52	11	22/3
22	11	4	2
1	22/3	2	4/3
-156	-78	-22	-11
78	26	11	11/3
-22	-11	-4	-2
11	11/3	2	2/3
54	27	13	13/2
27	18	13/2	13/3
-13	-13/2	-3	-3/2
-13/2	-13/3	-3/2	-1
-54	-27	-13	-13/2
27	9	13/2	13/6
13	13/2	3	3/2
-13/2	-13/6	-3/2	-1/2

$K_{C_5} =$

156	22	78	11
22	4	11	2
78	11	52	22/3
11	2	22/3	4/3
54	13	27	13/2
-13	-3	-13/2	-3/2
27	13/2	18	13/3
-13/2	-3/2	-13/3	-1
-156	-22	-78	-11
-22	-4	-11	-2
78	11	26	11/3
11	2	11/3	2/3
-54	-13	-27	-13/2
13	3	13/2	3/2
27	13/2	9	13/6
-13/2	-3/2	-13/6	-1/2

$K_{\bar{C}_3} =$

36	3	3	.25
3	4	.25	1/3
3	.25	4	1/3
.25	1/3	1/3	4/9
-36	-3	-3	-.25
3	-1	.25	-1/12
-3	-.25	-4	-1/3
.25	-1/12	1/3	-1/9
-36	-3	-3	-.25
-3	-4	-.25	-1/3
3	.25	-1	-1/12
.25	1/3	-1/12	-1/9
36	3	3	.25
-3	1	-.25	1/12
-3	-.25	1	1/12
.25	-1/12	-1/12	1/36

Fig. 44a FIRST FOUR COLUMNS OF THE BENDING STIFFNESS MATRIX (COMPONENT PARTS MULTIPLIED BY $C_1, C_2, \bar{C}_3$)

$K_{\tilde{C}_3} =$

36	18	18	11/4
18	4	61/4	2
18	61/4	4	2
11/4	2	2	4/9
-36	-3	-18	-1.5
3	-1	1.5	-.5
-18	-1.5	-4	-1/3
1.5	-.5	1/3	-1/9
-36	-18	-3	-1.5
-18	-4	-1.5	-1/3
3	1.5	-1	-.5
1.5	1/3	-.5	-1/9
36	3	3	.25
-3	1	-.25	1/12
-3	-.25	1	1/12
.25	-1/12	-1/12	1/36

$K_{C_2} =$

0	0	0	.1
0	-.25	-.1	0
0	-.1	0	0
.1	0	0	0
0	0	0	-.1
0	0	.1	.05
0	.1	0	0
-.1	-.05	0	0
0	-.5	0	-.1
.5	0	.1	0
0	.1	0	1/60
-.1	0	-1/60	0
0	.5	0	.1
-.5	-.25	-.1	-.05
0	-.1	0	-1/60
.1	.05	1/60	1/120

$K_{C_4} =$

0	0	0	.1
0	0	-.1	0
0	-.1	-.25	0
.1	0	0	0
0	0	-.5	-.1
0	0	.1	1/60
.5	.1	0	0
-.1	-1/60	0	0
0	0	0	-.1
0	0	.1	0
0	.1	0	.05
-.1	0	-.05	0
0	0	.5	.1
0	0	-.1	-1/60
-.5	-.1	-.25	-.05
.1	1/60	.05	1/120

Fig. 44 b FIRST FOUR COLUMNS OF THE BENDING STIFFNESS MATRIX
(COMPONENT PARTS MULTIPLIED BY $\tilde{C}_3, C_2, C_4$)

K_{mx} =

1872	156	264	22
156	208	22	88/3
264	22	48	4
22	88/3	4	16/3
-1872	-156	-264	-22
156	-52	22	-22/3
-264	-22	-48	-4
22	-22/3	4	-4/3
648	54	156	13
54	72	13	52/3
-156	-13	-36	-3
-13	-52/3	-3	-4
-648	-54	-156	-13
54	-18	13	-13/3
156	13	36	3
-13	13/3	-3	1

K_{my} =

1872	264	156	22
264	48	22	4
156	22	208	88/3
22	4	88/3	16/3
648	156	54	13
-156	-36	-13	-3
54	13	72	52/3
-13	-3	-52/3	-4
-1872	-264	-156	-22
-264	-48	-22	-4
156	22	-52	-22/3
22	4	-22/3	-4/3
-648	-156	-54	-13
156	36	13	3
54	13	-18	-13/3
-13	-3	13/3	1

K_{mxy} =

150	0	0	-6
0	0	6	0
0	6	0	0
-6	0	0	0
0	0	30	6
0	0	-6	-1
-30	-6	0	0
6	1	0	0
0	30	0	6
-30	0	-6	0
0	-6	0	-1
6	0	1	0
-150	-30	-30	-6
30	5	6	1
30	6	5	1
-6	-1	-1	-1/6

Fig. 45 FIRST FOUR COLUMNS OF THE COMPONENT PARTS OF THE INITIAL STRESS STIFFNESS MATRIX.

NASA-Langley, 1967 —— 32 CR-803